RESPONSE TO REVIEWER 1

Minor and Technical Comments

Abstract, first sentence. You need to tell the reader what "EB" is and what the model does before launching into a discussion of its implementation. Like this: "The Maxwell Elasto-Brittle (EB) model uses a sea-ice rheology that allows tensile stress... blah blah [one sentence about the model]. This paper presents a first implementation of the..."

This sentence is now added to the abstract: " This continuum model, called Maxwell-Elasto Brittle (Maxwell-EB), is based on an Maxwell constitutive law, a progressive damage mechanism that is coupled to both the elastic modulus and apparent viscosity of the ice cover and to a Mohr-Coulomb damage criterion that allows for pure (uniaxial and biaxial) tensile strength."

Abstract, lines 6-8. This sentence is a bit awkward. I suggest: "In agreement with observations, the model captures the propagation of damage..." etc. (and delete "are all represented" at the end of the sentence).

Agreed: we made the suggested modifications.

Abstract, last sentence. "weakening of the ice cover" and "shorter lifespan of ice bridges" – over what time period? You should add something like "in the 2000s relative to the 1980s and 1990s". And then "with implications in terms of increased ice export" – say that this would be expected because sea ice is expected to continue thinning in the future. In fact, maybe this is a positive feedback on the loss of ice: as it weakens, it drains from the Arctic faster, which weakens it further.

We are not specific about a time period for these two processes in the abstract because they have not been deduced to occur at the exact same time: the weakening of the ice cover estimated by *Gimbert et. al. 2012b* occurred over the period 2002-2008 relative to the period 1979-2001 while the shorter lifespan of ice bridges reported by *Barber et al., 2001* occurred in the 1990s relative to the 1980s (see section 5.1.3). The formulation used in the abstract reflects the aim of the experiments presented here, where is to relate in a general sense a mechanical weakening of the ice cover to a shorter lifespan (or absence) of ice bridges and increased ice export, i.e., not to reproduce a trend in the lifespan of ice bridges observed in recent years. Moreover, we do not believe that speculating about a future ice thinning is relevant at this point in the paper: actually, the numerical experiments presented here aim to relate a shorter lifespan of ice bridges and increased ice export to a *genuine mechanical weakening* of the ice cover, i.e., a weakening that is *independent* of a decrease in ice thickness. Mentioning an expected thinning of the ice cover in future years in the abstract would turn the attention away from this important point.

Page 1, line 15. "expenses" should be "expanses"

Page 1, line 21. "May 2005" should be July 2010.

Page 2, line 12. Change "allowed demonstrating" to "demonstrated"

Page 2, lines 18-20. "shorter lifespan of ice arches" and "increased ice export" – over what time period?

Here we added the reference time period for the mechanical weakening reported by *Gimbert et. al. 2012b.* To clarify the point made in the response to your earlier comment, we modified this sentence as follow: "we also discuss how the mechanical weakening of the ice cover estimated over the period 2002-2008 relative to the period 1979-2001 (*Gimbert et al., 2012b*) can be linked to a shorter lifespan of ice arches and consequently, to an increased ice export through Nares Strait".

Figure 1. The dates on the images are in the format DAY-MONTH-YEAR. Is that standard for The Cryosphere? It might confuse U.S. readers, who often use MONTH-DAY-YEAR.

Yes, DAY-MONTH-YEAR is a standard for the *European* Geosciences Union.

Figure 1, caption. Put "(MODIS)" before the word "reflectance", not after.

Page 4, line 10. 0.32 degrees is not 4-10 km.

There was a word missing there: 0.32 degrees *of longitude* is indeed equivalent to 4 km in the Lincoln Sea and 10 km in Baffin Bay (taken from *Rasmussen et al., 2010,* page 163: "The model horizontal grid has a longitudinal grid size of 0.32° resulting in a grid size ranging from 4 km in the Lincoln Sea to 10 km in the Baffin Bay"). We now remove the mention to degrees and give the resolution in kilometres only to avoid any confusion.

Page 4, lines 21-24. For the statement about the sea-ice thickness PDF you can cite: Lindsay, R. W. 2013. Unified Sea Ice Thickness Cli- mate Data Record, 1975-2012. Boulder, Colorado USA: National Snow and Ice Data Center. http://dx.doi.org/10.7265/N5D50JXV. Web site: http://nsidc.org/data/docs/noaa/g10006-unified-sea-ice/

Thank you for this reference.

Page 5, line 3. Change "pioneer" to "pioneering"

Page 5, line 9. "dubiously" – Why it is dubious to base the modelling framework on energy conservation?

Basing the estimation of the strength of the ice cover, i.e., equating deformational work to the sinks of energy that are taken into account in this framework is dubious in the sense that all of these sinks are very hard to estimate, and do not account for other processes such as ice crushing, buckling, frictional contacts between ice blocks in the rubble pile, etc. However, we agree that the use of the adjective "dubious" is unnecessary and nonobjective. We rephrase this passage in an clearer and more objective manner as follow:

"The relation between the redistribution process and the strength of the ice (often characterized by a pressure, *P*) in this modelling framework is based on energy conservation principles : the deformational work is equated to the work done in building ridges, which is partitioned between potential energy changes (*Thorndike et al., 1975*), the frictional dissipation in ridging (*Rothrock, 1975*) and dissipation in shearing deformation (*Pritchard, 1981*), all of which are very hard to estimate. This theory does not take into account other mechanisms such as crushing, buckling, flexural breakage, inelastic contacts and frictional sliding contacts between rubble ice blocks (*Hopkins, 1998*)."

Page 5, line 18. There is an error in the citation of Hibler's 1980 paper. William D. Hibler III should be "Hibler", not "III". Also on page 23, line 10, the author is Hibler, not III.

Yes, thank you for catching this.

Page 5, line 19. "sensible" should be "sensitive"

Page 6, line 5. Instead of "recall", better to write "review"

Page 6, line 7. Instead of "passage", I think "connection" is the intended meaning

You are right, "passage" might not be the right word: we changed it for transition.

Page 6, line 9. After "elastic modulus" write "(E)" because it is used three lines later in the definition of lambda.

Page 6, equations (1) and (2) – you need to say that "mu" is the internal friction coefficient.

Yes, thank you.

Page 6, lines 27-28. About healing: healing allows the level of damage to DECREASE – more healing, less damage. But the damage parameter d INCREASES as healing increases (d=1 is undamaged). So you have to be careful when describing healing. Verbally, healing means a SMALLER AMOUNT of damage. But numerically, healing means a LARGER VALUE of d.

The formulation in lines 27-28 is correct: the *level of damage*, *d*, has been introduced in lines 15 and 16. It is not employed the same as "damage". Here it is specified that the *level of damage* re-increases at most to the (numerical) value of 1.

Here I add "the level of damage *variable*" to make the distinction clearer.

Page 7, Figure 2, caption. Several things: – It is awkward to have complicated equations in the caption. Furthermore, the components sigma11, sigma12, and sigma22 are not used anywhere else in the paper, so I think it would be OK to delete the equations entirely. Otherwise, they should probably go in the main text. That's just a suggestion, there is nothing wrong with the current presentation. – Second sentence: "The thin solid lines represent the damage criterion in the case of C=0." To make this clearer, consider: "The thin solid lines radiating from the origin represent the damage criterion in the case of no cohesion (C=0)." – What is the shaded region in the figure?

Agreed: the equations are now removed. We also included your comment about the cohesion. The shaded region is also removed: it has actually no meaning relative to the simulation results presented here.

Page 8, line 7. Change "assimilated to" to "simulated as"

OK

Page 8, line 27. I think max[0,(1-A)] should be max[0,A-1]. This is supposed to describe "the excess concentration" when A > 1. If A > 1 then max[0,1-A] = 0, which doesn't make sense. The excess concentration should be max[0,A-1].

Yes, thank you very much for catching this: this is a typing mistake and the right form is indeed given in Eq. 6.

Page 9, equation 7. This equation doesn't make sense either. When A > 1, h+ = 0. I think this equation should be h+ = max[0,A-1]h.

Yes, the same mistake was repeated there. We however insist on the fact that this term is implemented in the correct form (h+ = max[0,A-1]h) in the code (see response to reviewer's 2 comment).

Page 9, line 18. Change "of being" to "to be". Change "sturdy" to "steady" Page 9, line 19. Capitalize "Lincoln Sea"

Page 10, line 27. Acceleration and advection terms are neglected in equation 3. Does this mean the solution is steady state, with no time dependence?

No: in the originally submitted version of the paper, the acceleration and advection term were neglected only in the momentum equation. The time derivatives and advection of all other variables (σ, h, A, C, d) were accounted for. Hence the solution was therefore not steady state. However, as mentioned in our response to reviewer 2, and as expected from a dimensional analysis of the momentum equation (see *Dansereau et al., 2016*, section 4.1.4), including the advection and acceleration terms in the momentum equation does not affect the results and conclusions of this paper. In the corrected version of the paper, both terms are included in all simulations (which needed to be run again due to an error in the thickness redistribution scheme, see our response to reviewer 2). This does not impact the results.

Page 11, Figure 3 caption. Delete the first "(a)" because the caption later refers to (a) and (b).

Page 11, line 11. "quenched disorder" – this needs a reference.

You are right, and more precision was needed on this point. This paragraph is now modified and this sentence is added after line 15 : "In all simulations, the disorder introduced in the field of cohesion is quenched (*Hermann and Roux, 1990*): it is set once, at the beginning of each simulation, and is passively advected with the ice flow".

Page 11, line 16. Beaufort SEA. Also, Weiss et al (2007) is cited in connection with Figure 8(a), but the figure caption cites Weiss and Schulson (2009).

Weiss et al., 2007 are cited in connection with the in-situ stress measurements in the Beaufort Sea, but figure 8(a) does show figure 13(a) from *Weiss and Schulson, 2009* (which presents the same measurements as in *Weiss et al., 2007*, figure 2A, but with the convention that compressive stresses are positive, as in the present paper). The reference to *Weiss and Schulson, 2009*, is now added in line 16 to make the connection to figure 8(a).

Page 12, line 10. Delete "the upstream part of", so the sentence reads, "...prescribed on GAMMAin and GAMMAout..."

Page 12, lines 14-15. "The equations of motion... Galerkin methods are used to handle advective processes" – but the advection terms in equation 3 are neglected. So I don't understand this. Does it refer to advection in equations 4 and 5?

The advection of ice momentum only is neglected here. All other variables are advected with the ice flow.

Page 14, line 2. "deformation rates" – I think this should be "high deformation rates"

Yes, thank you.

Page 14, line 3. "downstream of the channel" should be "downstream of the constriction"

No: here we precise "in the interior" of the channel, hence downstream of the constriction point, and "downstream of the channel", i.e., of the opening point.

Page 14, Figure 4. This figure should be bigger, so that it fills the full width of the page. It's a bit difficult to see the peaks of wind stress in panel (a) – bigger would be better.

Agreed: this figure is now resized.

Page 15, line 23. I think "Fig 4b and 4c" should be "Fig 5b and 5c" Page 15, line 27. I think "Fig 4b" should be "Fig 5b"

Thank you for catching this.

Page 16, line 24. The text says "Weiss et al (2007)" but the Figure 8 caption says "Weiss and Schulson (2009)"

We changed the reference there to *Weiss and Schulson, 2009*.

Page 18, line 2. "ice landfast" should be "landfast ice"

Page 18, line 8-9. How does the ice become weaker without thinning? Is it because the ice strength is temperature-dependent, so increasing the temperature would make it weaker? Is it because the composition of the ice could change, such as increased salinity?

Here, the mechanical weakening refers to a more fragmented/fractured ice cover (*Gimbert et al., 2012b*), and so (as mentioned by reviewer 3) an evolution towards smaller and different shape (more circular) ice floes. This point is now made clearer in section 5.1.2 (page 17, line 12, see response to reviewer 3). We neglect temperature and salinity effects.

Page 23, line 10. The first author is Hibler, W.D. III Page 25, line 27. Weiss and Dansereau 2016 – is the DOI correct?

Page 26, Figure 5 caption. At the end of the last sentence, "red arrows on (a)" should be "red arrows on 4(a)"

Page 27, Figure 6 caption. Delete the first "(a)" because the caption later refers to (a) and (b).

Page 29, Figure 8 caption. Delete the first "(a)". Capitalize "Beaufort Sea" C5

Page 31, Figure 10 caption: – line 2: "is of 10" should be "is 10" – lines 5 and 6: "insert" should be "inset"

I recommend deleting these two sentences: "The tail of the distribution..." and "The temporal evolution..." because the last sentence of the caption explains the same thing as these sentences.

Agreed, these sentences are removed.

Page 31, Figure 11 caption:

- **line 2: "is of 10" should be "is 10"**
- **line 5: "insert" should be "inset"**

Agreed, and the repetitions mentioned in your previous comment were also removed from this caption.

Please note: I have not flagged all the minor grammatical corrections that should be made by an editor, for example:

Page 9, line 10. "is of 100%" – delete "of" Page 9, line 26. such AN ice bridge Page 10, line 8. "in Cartesian" should be "to Cartesian" Page 10, line 9. Delete "is" Page 11, line 8. employed IN the simulations Page 11, line 12. "by randomly by" – delete second "by" ...and so on...

RESPONSE TO REVIEWER 2

Major comments:

These major comments are also addressed through the response to your other minor comments, below.

There are many statements that require more discussion and clarification. In some places strong statements are made that not supported by the results of the model simulations. These statements need either be toned down, or sufficient evidence should be provided (which is probably not possible without additional experiments, especially when reference to VP models is made.)

We stress the point that no direct comparison was made between the present Maxwell-EB and VP/EVP model simulations. This is further discussed in the responses to minor comments.

For instance, the impact of the simplified model equations, geometry, wind forcing and no thermodynamics is discussed too little, especially when comparing to observations made outside of a channel. The model set-up for the analysis of PDFs of ice thickness facilitates ridging with a high amount of coastal boundaries, low cohesion parameter and strong wind forcing (and a presumably wrong source term in Equation (7)), which is not further discussed.

We have addressed issues with the thickness distribution in the revised version of the paper. These issues are discussed in the responses below. The PDFs of ice thickness produced are not the result of a "low cohesion" (see our response to your comments about cohesion below : there is no physical or observational basis to claim that the value of cohesion used for these particular simulation are "low), nor of the amount of coastal boundaries (as idealized simulations have also been used). The strong wind forcing used here has the effect of redistributing the ice thickness starting from a uniform ice cover in a shorter amount of time. A lower wind forcing gives similar results over a longer time.

In the experiments with reduced mechanical strength a comparison to observations would be even possible: Are a collapse of ice bridges and no flow storage observed in the recent years?

As mentioned in the paper, the absence of stable ice bridges in Nares Strait was indeed observed in the year (September to August) 2006/2007. For that year, *Kwok et al., 2010* estimated an annual ice areal and volume flux equivalent to twice their average value over the 1997 to 2009 period. For the same year, *Ryan et al., 2017* observed the maximum of the median ice draft (measured across Kennedy channel, upstream Kane Basin) over the 2003 to 2012 period. *Munchow et al., 2016* reported that the ice arch between Kane Basin and Smith Sound failed to form in the winters 2006/07, 2007/08, and 2009/10, and collapsed after less than 2 months in 2008/09. They estimated an increase of 45% of the volume flux, of 69% of the ocean freshwater flux and of 46% of the freshwater flux through Nares Strait over the 2007-2009 period relative to the 2003-2006 period, during which a stable arch did form at that location. We now add references to the recent studies of *Ryan et al., 2017* and *Munchow et al., 2016* in the text (section 5.1.3).

A direct comparison of the model simulations to the ice area or volume flux estimated for instance by *Kwok et al., 2010* is not trivial: it would require at least the knowledge of the temporal and spatial evolution of the wind forcing (and perhaps of ocean currents) as well as of the coverage and thickness of ice over Nares Strait over that time period. In the absence of these informations, we compared time series of the meridional component of the simulated ice drift velocity averaged across the constriction point between Kane Basin and Smith Sound for different ice cohesion scenarios to illustrate the impact of ice strength on the simulated outflow.

Especially, regarding the comparison to VP-models more caution is required. If no reference VP simulation is performed, the differences of the referred studies need to be considered, as most of the studies do not agree in resolution or region used in the experiments presented here. For example, it is not clear, if VP models at the same resolution would not lead to the same type of "ridging" behavior; as long as it is not clear, it shouldn't be claimed. The detailed overview which points need further discussion are listed below in the minor comments.

2 EVP studies were mentioned (*Dumont and Gratton, 2009* and *Rasmussen et al., 2010*), in the context of simulating ice bridges, not ridges, and the resolutions of their simulations are indeed comparable to the one used here, at least in the case of *Dumont et al., 2009*. As mentioned in the response to a later comment, the Maxwell-EB model produce similar results at lower resolutions. Moreover, as discussed below, we insist on the fact that no direct comparison was made here between the Maxwell-EB and VP/EVP model simulations.

Again, we insist on the fact that it was not claimed in the original version of the paper that the VP model couldn't reproduce the same type of "ridging". What was stated is that the Maxwell-EB model can reproduce characteristics of the observed ice thickness distribution with a very simple redistribution scheme. As mentioned in the response to your later comment, *rheologies* and *thickness redistribution schemes,* are *distinct* components of a sea ice model.

In Section 3, a sea-ice model using the Maxwell-EB rheology is outlined. However, due to the reference to individual equations in Dansereau, et al. (2015) the readability is reduced. A summary of the model equations cited from Dansereau et al. (2015) in an appendix would assist the reader. In addition, if you would include the simplifications that are made in your experiments into the model description, it is directly clear to the reader what equations are solved in your model. For example, the full momentum equations are given

in Equation (3); one can easily miss the fact that many terms are not solved for (p10, l.26-27). Here the reduced equations could replace Equation (3), since this is all that is used in the manuscript.

We completely agree on the need for more information about the equations and numerical scheme. We now include a detailed description of both in an Appendix. We further comment on the simplifications to the equations which are listed in the paper (p. 10, lines 26 to 29) here:

- *No thermodynamics coupling.* The present implementation of the Maxwell-EB rheology is not coupled to a thermodynamics model. The goal of these numerical experiments is to investigate its dynamical behaviour. Including thermodynamics processes would complicate this investigation. Simulations are analyzed over a short time-period (3 days maximum). This point is now made clearer in section 4. In terms of referring to previous VP (EVP) simulations at comparable resolution, this simplification is justified as thermodynamic processes were also neglected in the study of *Dumont et al., 2009*.

- *No Coriolis acceleration and ocean tilt terms.* As mentioned in section 4, second and third paragraphs, forcing conditions are made as simple as possible to facilitate the analysis of the dynamical behaviour of the model. Hence the ocean is at rest and the wind forcing is uniform over the channel in both the idealized and realistic cases. The Coriolis term is neglected with the intention to retain symmetry in the forcing conditions. Because the Coriolis acceleration plus sea surface tilt term is smaller in magnitude than the air and water drag and rheology terms (*Steele et al., 1997*) this is not expected to have a significant impact on the results. Note that *Dumont et al., 2009* also neglected the Coriolis acceleration in the idealized case. Also, in the realistic case, the ocean in *Dumont et al., 2009* is initially static.

- *No acceleration and advection term in the momentum equation.* Scaling analysis show that these terms are small (see *Dansereau et al., 2016*, section 4.1.4) Most sea ice models now include the $\partial v/\partial \tau$ term, however the advection term is still neglected in a number of, if not most, sea ice and ice-ocean coupled models (e.g., LIM3, FESIM/FESOM, ...). Additional simulations have shown that including both terms in the momentum equation does not affect the simulation results reported here. To correct the error made in the thickness redistribution scheme (see your later comment), all simulations needed to be run again for the resubmission of the paper. Both the acceleration and the advection terms are included in the corrected version of the model used to perform these simulations. The results are in all aspects very similar to the previously reported results such that all the conclusions of the paper remain unchanged.

We corrected the reported spelling and structure mistakes and respond to your minor comments below.

Minor comments:

page 1,l.7: "in" -> into page 1,l.8: "Strait" -> strait page 1,l.9: "different dynamical behaviours" -> various dynamical behaviour

page 2, l.26: "to" -> and?

page 2, l.32: "This rheological framework typically does not account for (uniaxial or biaxial) tensile strength." Not quite true, there is uniaxial tensile strength in Hibler elliptical yield curve (see your figure 2), but there's usually no isotropic/biaxial tensile strength; adding tensile strength is another option for the VP model and has been used to improve simulations of land fast ice (Lemieux et al 2016, Olason, 2016). Could be mentioned in this context, too.

As shown on figure 2, there is no uniaxial tensile strength in Hibler's elliptical yield curve. Instead, there is only *biaxial tensile-compressive strength* (accounted by the portion of the curve in the second and fourth quadrants, see stress state 2, Fig. 2). Uniaxial tensile strength is represented on Fig. 2 by stress state number 1 : $\sigma_1 < 0$ and $\sigma_2 = 0$ (or the inverse, by symmetry with the $\sigma_1 = \sigma_2$ axis). Biaxial tensile strength implies resistance of the material for $\sigma_1 < 0$ *and* $\sigma_2 < 0$. This state of stress is now represented schematically as stress state number 0 on figure 2.

Thank you for these references. We are aware that the elliptical yield curve has been modified especially in the context of modelling landfast ice, which has been related to the phenomenon of arching between islands. However, as both these papers are really concerned with the phenomenon of landfast ice, and landfast ice is also influenced by other phenomenon such as the grounding of keels, we beleive that including these reference at this point in the paper (in the discussion of the phenomenon of ice bridges, in particular in Nares Strait) would take the reader away the main point, which is that we are testing a new rheology on the basis of its capacity to represent the phenomenon of arching.

page 2, l. 30-32: Dumont also used EVP

Thanks for catching this. This is now corrected.

page 4, l. 13-14: That's a speculation. It would be nicer to actually show that this can work or not work with

VP models at high resolution (better than 4km grid spacing).

"It is not clear" is not speculation. We however remove the work "better" in this sentence, which indeed implies a comparison to VP models.

page 4, l.13: ". . .(e.g., see Fig. 1b and Sodhi,1977)" wrong citation

page 4, l.20: Section 2.2 "Ice ridges". First paragraph is relevant for the following analysis of the ice thickness distribution. The last three paragraphs can be shortened or discarded, as neither a VP-model nor an ITD is used later on.

We do not agree with this comment: this discussion of ice thickness redistribution schemes is relevant and necessary to interpret the results discussed in this paper. We also stress the fact the thickness distribution scheme is a component *independent* of the rheological framework implemented in a sea ice model. VP rheology models actually use both the schemes described here. The only sentence that discusses the VP model in these paragraphs is the following:

"Nevertheless, it is still unclear to this day if, when incorporated in viscous-plastic type models, either of the two-level scheme or the multi-categories scheme, even when tuned, is able to reproduce the form of tail of the PDFs calculated from Arctic sea ice thickness measurements (e.g., *Flato et al., 1995)*."

This statement refers to a 22 years-old paper. Other more recent VP or EVP model studies in which an ice *thickness distribution* was represented (otherwise only thickness fields are discussed) were not found, which adds to the fact that the point made in this sentence "is still unclear". We however agree that the mention of VP models here is unnecessary since *the goal of the paper is to demonstrate that the Maxwell-EB model, with a very simple redistribution scheme, is capable of reproducing the exponential tail of the ice thickness distribution*. We therefore remove this sentence and add another one at the end of this section to stress this later point.

page 5, l.17: wrong citation, I guess Hibler, 1980 is meant? page 5, l.19: "badly" -> poorly

page 6, l. 5: "details" -> detail

page 6, l. 5: "recall" -> repeat?

We changed it for "review", as suggested by reviewer 1.

page 6, l.15: This definition is unfortunate and unintuitive. 0 should be "undamaged" (zero damage) and 1 should "completely damaged" if d is called "damage". d feels more like "integrity" for the material, but it's just terminology . . .

Indeed, in solid mechanics conventions d in this case would have the meaning of "continuity". However, this just terminology that helped us simplify the writing of some equations while developing the model. As this is the definition included in the paper describing the Maxwell-EB rheology (*Dansereau et al., 2016*) we do not modify it in the present paper.

page 6, l. 22: Isn't Equation (2) t = 2C[(μ2 + 1)1/2 + μ] 1 ? At least in Danserau et al. (2016) Equation (7),(8) and (10) are not consistent and I guess the exponent -1 is missing in Equation (10).

You are right: thank you for catching this. This is also a mistake in *Dansereau et al., 2016*. Here we correct this mistake and write σ_t as it is implemented in the code, that is, $\sigma_t = -\sigma_c/q$, and add the definition of q, the slope of the damage criterion. We also add a footnote to report the mistake made in *Dansereau et al., 2016,* Eq. 10.

page 6, l. 27-28: Unclear, if it represents refreezing of leads, how can it be independent of pure thermodynamics, please explain/rewrite/elaborate

You are right, this formulation is confusing. Healing is "distinct" but not "independent" from thermodynamics processes, as obviously, in a coupled dynamic-thermodynamic model, the rate of healing should depend on the air and ocean temperature. In the present, uncoupled, implementation of the model, it is constant. What was meant is that, on a modelling point of view, healing is not the same process as thermodynamic growth because it allows the level of damage variable to increase *at most* to its undamaged value ($d = 1$) and does *not* allow the mean ice thickness nor the ice concentration to increase. The sentence is rephrased as "This mechanism is distinct from pure thermodynamic growth (...)" and the reader is referred to *Dansereau et al., 2016* for more precision about healing.

page 8, l.9: Equation (3); Please also state the simplified version of the equation that is actually used by the model, to prevent misunderstandings.

This is now incorporated in the Appendix, together with the description of the numerical scheme.

page 8, l. 21-22: Mechanical redistribution in your formulations is represented by the divergence term, see next comment about Equation (7).

We address this point in the response to your next comment, below.

page 9, l. 1, Equation (7) That is wrong: h is defined as the mean thickness (per grid cell area), so something like a volume of ice in the cell. The ice volume does not change if A > 1 is reset to A = 1, but the (mean) thickness of the thick ice hthick = h/A is increased, and there is no extra contribution to Sh. (See also Schulkes (1995), JGR.) This should be corrected in the text and also in the model, if the model actually implements this extra (spurious) tendency in Equation (4).

There was indeed an error made in the redistribution scheme, which lied in the fact that for A > 1, *h* could increase both through convergence and through the prescribed redistribution (equation 7). To correct this mistake, we have modified the parameterization as follow: the thickness of thick ice, $h_{thick} = h/A$, is advected passively with the flow for $A < 1$. This means that under convergent motion, there is no ridging if $A < 1$, but the ice volume (h) can effectively increase if the ice concentration over a grid cell increases. If $A > 1$over a given grid cell, it is reset to $A = 1$, and the mean ice thickness, h, (equal to the thickness of thick ice when $A = 1$) is increased (equation 7): hence the ice volume in that grid cell increases.

As mentioned in this section, in the present implementation of the model we seek to account for mechanical redistribution of the ice thickness in the simplest possible manner, so that to test the input of the rheological framework, i.e., its representation of ice deformation, on the thickness distribution. *In Schulkes et al., 1995* the divergence term is weighted as a function of *A*. In the ice concentration equation, this term is penalized as *A* increases from 0 to 1 and is zero for $A = 1$. Conversely, in the thickness equation, it is penalized as *A* decreases from 1 to 0 and is zero for $A = 0$. As opposed to the scheme presented in *Schulkes et al.,1995,* we do not suppose ice ridging occur for $A < 1$ and assume ice riding occurs only for $A \geq 1$. This avoids using any weighting/penalty function based on sea ice concentration, which would imply introducing additional parameters and which is not well constrained by observations.

Our approach is therefore simpler and more similar to that of *Hibler 1979*, in which the adjustment to the conservation equations for *A* and *h* occurs abruptly when and where $A = 1$, as discussed by *Schulkes, 1995*. For $A < 1$, our scheme is equivalent to that of Hibler 1979. For $A \geq 1$, the schemes differ. Our approach is as follow: the same differential equation is still solved for *A*, with a manual adjustment to $A = 1$, and ice thickness is adjusted for the excess ice concentration. This redistribution scheme conserves the ice volume and, compared to the Hibler 1979 scheme, has the advantage of not creating any spurious oscillations in the solution (which happened due to the abrupt change in the differential equations at $A = 1$, see *Schulkes et al., 1995*).

In correcting the paper, we have also addressed some issues with the presentation of the conservation equations for *A* and *h* and thickness redistribution scheme in the original version of the paper.

- First, the reference to *Hibler, 1979* for the parameterization of the ice thickness redistribution was a mistake. We drop the reference to *Lietaer et al., 2008* (who seem to have made the same error as we initially did with their redistribution scheme based on *h*). We also drop the reference to *Thompson et al., 1988*, as we suspect their redistribution scheme might also not be coherent.
- As pointed out by reviewer 1, there is a typo in equation (7), also found in the text (p. 8, line 27), and the right form, now corrected, reads:

  $h^+ = \max[0, (A-1)]\, h$.

  This is the formulation used in the code, hence this typo does not impact the results reported here.
- As pointed out by reviewer 3, there was also a typo in the equation appearing on line 18, page 19. The correct expression, implemented in the model, is $\nabla \cdot (h\,u) = u \cdot \nabla\, h + h \nabla \cdot u$
- The adjustment on the excess ice concentration and associated redistribution of ice thickness (given by equation 7) is made a second numerical step, after solving the conservation equation for the ice thickness. This was discussed on page 13, lines 12 and 13, but this might not have been clear in the original version of the paper because the numerical scheme was not described in details. The inclusion of the appendix now clarifies this point.

The model simulations presented in the newly submitted version of the paper have all been corrected for this error in the thickness redistribution scheme. This correction has no significant effect on the reported results. The simulated ice thickness is somewhat lower than in the previous simulations, as expected from the removal of the extra growing tendency on *h*. However, both the PDF of the mean ice thickness in the idealized and realistic case show a similar shape and evolution, such that the main conclusions drawn form these numerical experiments remain unchanged.

page 9, l. 4-5, Equation (8) and (9): Just for clarity, a dependence on the thickness as in Hibler (1979) is not needed, as the internal stress is used in the momentum equation?

Yes, this is right. We now add a mention to this effect when introducing the form of the momentum equation solved in the simulations (A1) in the Appendix. The mechanical parameters (E, η, C) are intrinsic properties of the ice cover, as a material, and are independent of its thickness. For instance, E is an elastic modulus (Nm^{-2}), not a rigidity of the ice plate (Nm^{-1}). In particular, the fact that C is independent of ice thickness is important here as the contribution from thickness and cohesion to the strength of the ice cover are differentiated (in section 5.1.3).

page 9, l. 8: "widely" -> is widely page 9, l. 22: "(Kwok et al., 2010))" -> (Kwok et al., 2010)

page 10, l.11: "northerly, wind stress" -> not sure about this: northerly winds, but the stress is acting towards the south, should be made clearer I think.

This sentence and the next are rephrased as: "Consistent with observations of orographic channelling, an along-channel, i.e., southward, wind stress, τ_a is applied. The stress is spatially uniform and increased steadily between (...)".

page 10, l.24: "transport of the cohesion, C" there are no sources and sinks of cohesion? How realistic is that? Please comment and elaborate the cohesion equation in Dansereau et al. (2016), this is not discussed.

There is no sources or sinks of cohesion in the model. The field of cohesion is set at t = 0, i.e., as other initial conditions, and is advected passively with the flow. As discussed on page 12, lines 3 to 12, for ice entering the channel through open boundaries, the cohesion is set over each model element as it is set for the initial conditions, that is, by drawing a value randomly from a given uniform distribution.

As mentioned in our response to your previous comment, the cohesion is an intrinsic property of the material which sets its mechanical strength (its resistance to pure shear). Here C is a grid-cell averaged quantity and is allowed to vary locally to represent the natural homogeneity/heterogeneity of the material (various defects of different scales, for instance brine pockets at the small scale or the presence of different types of ice, e.g, a mixture of first year and older floes, smaller and larger floes, etc., at large scales). A comment to this effect in now added at the end line 24, p. 10. The noise introduced on C could alternatively be applied to another mechanical parameter, for instance, the elastic modulus (*Amitrano et al., 1999 and others*).

As this property is independent of ice thickness, there is no source of C due to ice thinning/thickening. In progressive damage models, cohesion could be made to depend on the level of damage. Simulations have shown that this causes an even more extreme localization of the deformation and damage in a material (*Lucas Girard*, *Ph.D. thesis*). We cannot think of other sources or sinks of cohesion.

The cohesion equation (a transport equation) is now included in the appendix and referred to in the text.

page 10, l.32: What is the reference for the Young's modulus? Same as for the Poisson's ratio?

The value of the Young's modulus (0.585 GPa here) is of the same order of that used by *Girard et al., 2011* (0.35 GPa) and implies with an elastic shear wave speed of 500 ms^{-1}, consistent with that reported by *Marsan et al., 2011* (440 ms^{-1}). These references have been added in the text. Estimates of the Young's modulus are highly variables. The value used here is close to the lower bound of the range of reported value. Using a higher value (2.34 GPa), consistent with a shear wave speed of 1000 ms^{-1} and on the order of in-situ seismic measurements as reported by *Timco and Weeks, 2010* (between 1.7 and 9.1 GPa, with higher values for low brine volumes, i.e., fresher ice) however does not change the mechanical behaviour of the model. This has been verified in the context of the present channel flow simulations. As mentioned in our response to your later comment, a higher value of E_0 allows stable ice bridges to form in the channel for somewhat lower values of cohesion than the ones reported here. The exact values of E_0 and C to employ in the model at a given spatial resolution are therefore not strictly constrained.

page 11, l.5-8: The physical role of healing is unclear and needs to be explained better. It is clearly connected to the thermodynamics (in contrast to earlier statements in the manuscript) . . . Please elaborate . . .

Healing is linked to the level of damage of the ice cover, d, which represents the density of cracks/leads within a model grid cell and the impact of these features on the sea ice rheology. In the present model, this variable is independent of the ice concentration, A. Healing represents the refreezing within these cracks/leads and allows a damaged ice cover to recover at most its undamaged mechanical strength. As explained in the response to your earlier comment, healing is theoretically not independent from thermodynamics, as the rate of healing should depend on the difference in temperature between the atmosphere above and that of the ocean below. In the present model, healing is not coupled to a thermodynamics component and the healing rate is constant in both space and time.

Because of the absence of thermodynamic-dynamic coupling in the present model, d can increase locally due to healing, but the ice concentration, A, is not allowed to re-increase by the same process. Where the ice cover is highly fragmented but dense (high concentration), allowing the ice to heal without re-increasing the ice concentration is physically sound. However, where the ice concentration drops such that mechanical interactions (i.e., the rheology term) becomes insignificant, this absence of thermodynamic-

dynamic coupling leads to a situation where d can re-increase up to its undamaged value (1), but A can drop to 0, representing open water.

To deal with this unphysical situation, in the present simulations we impose a cutoff on healing when and where $A < 0.75$, which essentially occurs when the ice detaches from a bridge or a coast. As when $A < 0.75$, the rheology term in the momentum equation becomes negligible and the ice is in a free drift state, no matter the value of d, we find that imposing this cutoff and its specific value of A has no significant impact on the simulated dynamics.

This point is now clarified on page 11.

page 12, l.7: "location of ice bridges is not prescribed" only through the random field of cohesion (the spatial pattern should be shown somewhere). I would like to see simulations with uniform cohesion; the model geometry should be irregular enough to make the model develop ice bridges, etc.

We do not agree with this comment. As explained in the text, the field of cohesion is *random*, hence, by definition, there are no spatial correlations introduced by the field of C in the model. Cohesion therefore does not prescribe the location of ice leads and bridges, only the mechanical behaviour of the model and the domain geometry does. A sentence is added to stress this point in the last paragraph of page 11. Simulations, both idealized and realistic, started from different fields of C, set as described on page 11, line 10 to page 12, line 2, have indeed been performed, and have reproduced the same location of the ice bridge.

The disorder introduced in the field of cohesion causes the *progressive failure* of the ice cover, *even under homogeneous forcing conditions* (see *Dansereau et al., 2016*). A sentence is added to clarify this point on page 6, after line 25.

These two points can be demonstrated by comparing the propagation of damage in a simulation in which noise is initially introduced in the field of cohesion (see figure 6) and a simulation started with a uniform field of C (see below). Highly damaged features emerge in both cases in similar locations. In both cases also, ice bridges develop in the same locations, which is therefore not attributable to a pattern in the field of cohesion but to the flow conditions and domain geometry. A notable difference between the simulation is the width of the first damaged features simulated by the model, that is, the features formed in initially undamaged ice (field b, t = 6 hrs). In the uniform cohesion case, these features are wider, due to the fact that all model elements can become over-critical and trivially fail, at the same time. This is also visible in the field of ice concentration (c) and translates into higher value of the damage rate (a) compared to the noisy cohesion case (see figure 6a). However, as discussed in *Dansereau et al., 2016* (see section 6.1), as soon as there are some damage present in the ice cover, the heterogeneities introduced in the stress field by these damaged features contribute and, over time, prevail over the noise in C in setting the location and timing of subsequent events. This explains why damage in an non-intact ice cover becomes highly localized even in the uniform cohesion case (t = 24 hrs, 48 hrs). In the present simulation, a highly homogeneous wind forcing is used and simulations are started from uniform ice conditions. If simulations were started from realistic, heterogeneous ice conditions, with non-uniform thickness and concentration, and used realistic, time and space-dependant wind forcing, the first damage events would probably be highly localized, independently of the degree of disorder introduced through the cohesion field (eg., *Bouillon and Rampal*, 2015).

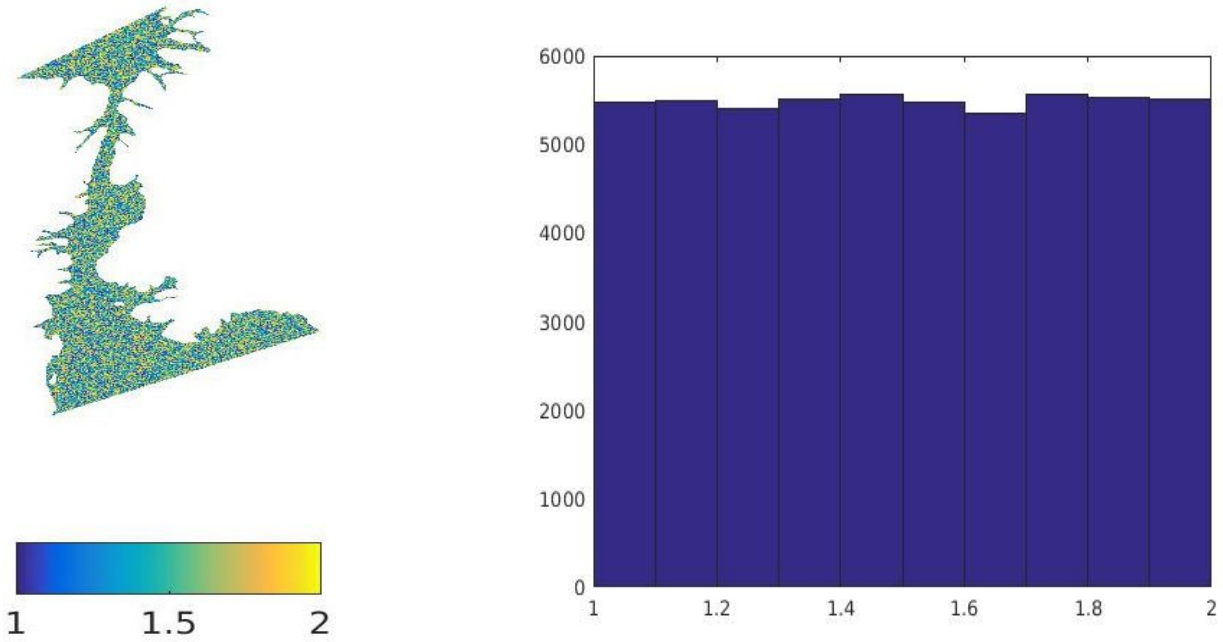

Left panel: noise on the field of cohesion. This field is multiplied by C_{min}, such that $C \subset [C_{min}, 2 \times C_{min}]$. Right panel: distribution of the noise on the field of cohesion shown in the right panel.

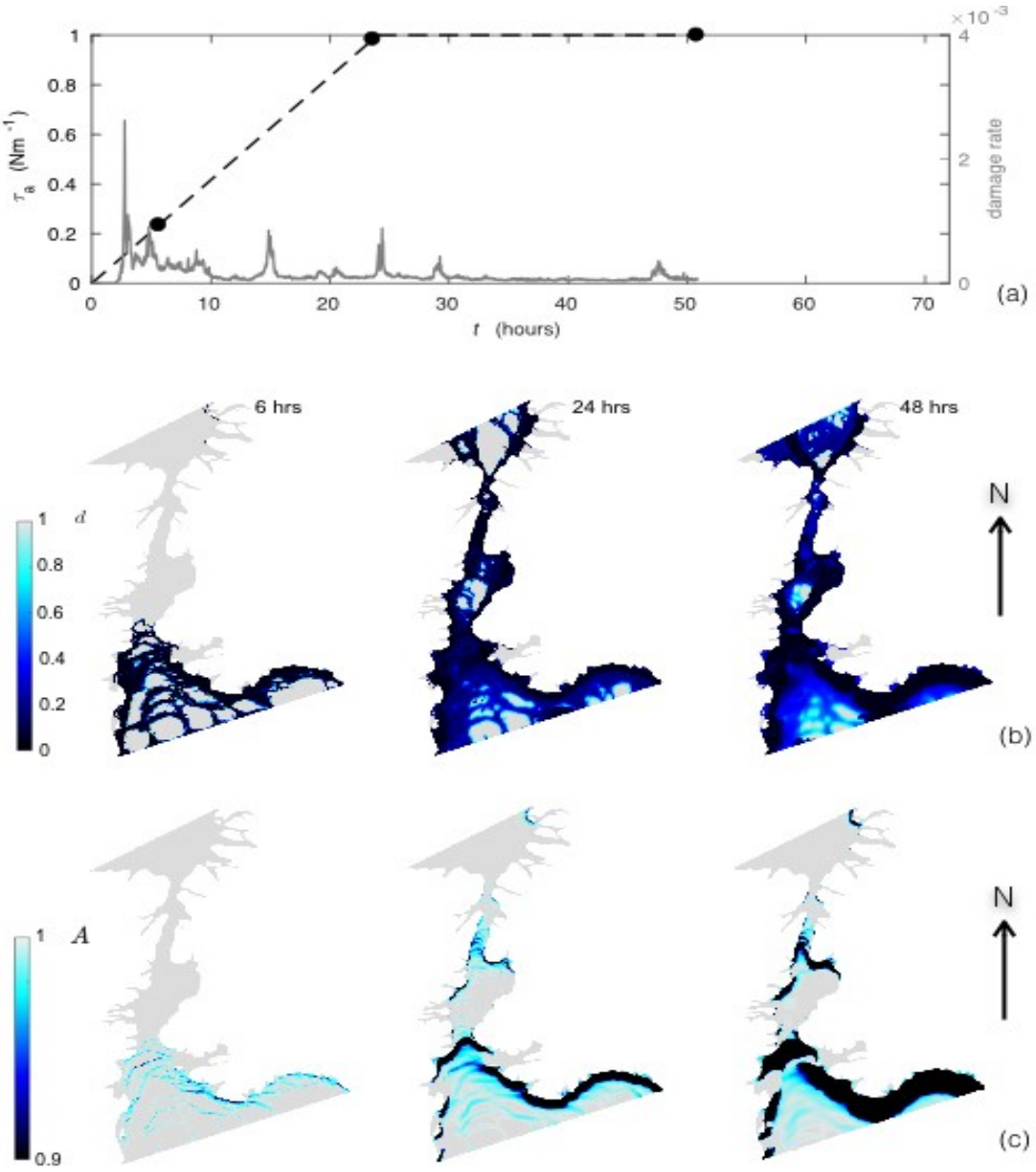

(a) Time series of the wind forcing (dashed curve) and of the damage rate (solid grey curve) over the realistic Nares Strait in a simulation using a uniform field of cohesion, C. Instantaneous fields of the simulated (b) level of damage and (c) ice concentration at t = 6, 24 and 48 hours. This simulations was run for about 50 hours instead of 72 hours as in figure 6 of the paper.

As the setting of the noise in the field of cohesion in both the idealized and realistic cases is described in the text (page 11, line 10-17), so that the reader can reproduce the results, and as a figure does not provide more information, we do not believe that including a figure of the field of *C* in the paper is necessary. An example of the random noise on the cohesion field and distribution of this noise is shown above for the realistic case.

page 12, l.16 (and elsewhere): "(see (Dansereau et al., 2016))" -> (see Dansereau et al., 2016).

page 12, l.18: For the claims made in the introduction and background sections, VP simulations at this resolution are absolutely required (have not been done to my knowledge). Please tone done the statements in the appropriate places.

The EVP simulations of *Dumont et Gratton, 2009* have a resolution of approximately 3 by 4 km, which is comparable to the resolution used here in our realistic experiments (we note that there is an error on the horizontal resolution, i.e., an inversion between the latitude and longitude, reported in their table 1, otherwise their model resolution is something like 17 km by 1 km). The authors state that there

are 14 grid cells across the narrowest point (46 km) of their channel in the idealized experiment which corresponds to the narrowest point between Kane Basin and Smith Sound. In the present realistic and idealized experiments, there are about 19-22 grid cells at the narrowest point between Kane Basin and Smith Sound (56 km on our grid) where the main ice bridge form, which is again comparable. The other EVP simulation of ice bridges in Nares Strait mentioned here (*Rasmussen et al.*, 2010) indeed use a coarser resolution (between 4 km in the Lincoln sea, 83 N, and 10 km in Baffin Bay, < 74 N, and about 7 km between Kane Basin and Smith Sound). However, as mentioned in section 5.2 about the ice thickness distribution in the idealized case, lower resolution (4 km, which gives 13-14 grid cells across the constriction point of the idealized channel, as in *Dumont et al., 2009*, and 8 km, which gives 6-7 grid cells across the constriction point, as in *Losch and Danilov, 2012*) idealized simulations produced similar results. It is also the case for other variables (level of damage, ice concentration, velocity profiles, etc., see figures below) and for the realistic experiments at lower resolution (not shown) which demonstrate that the results obtained here do not depend on the model resolution.

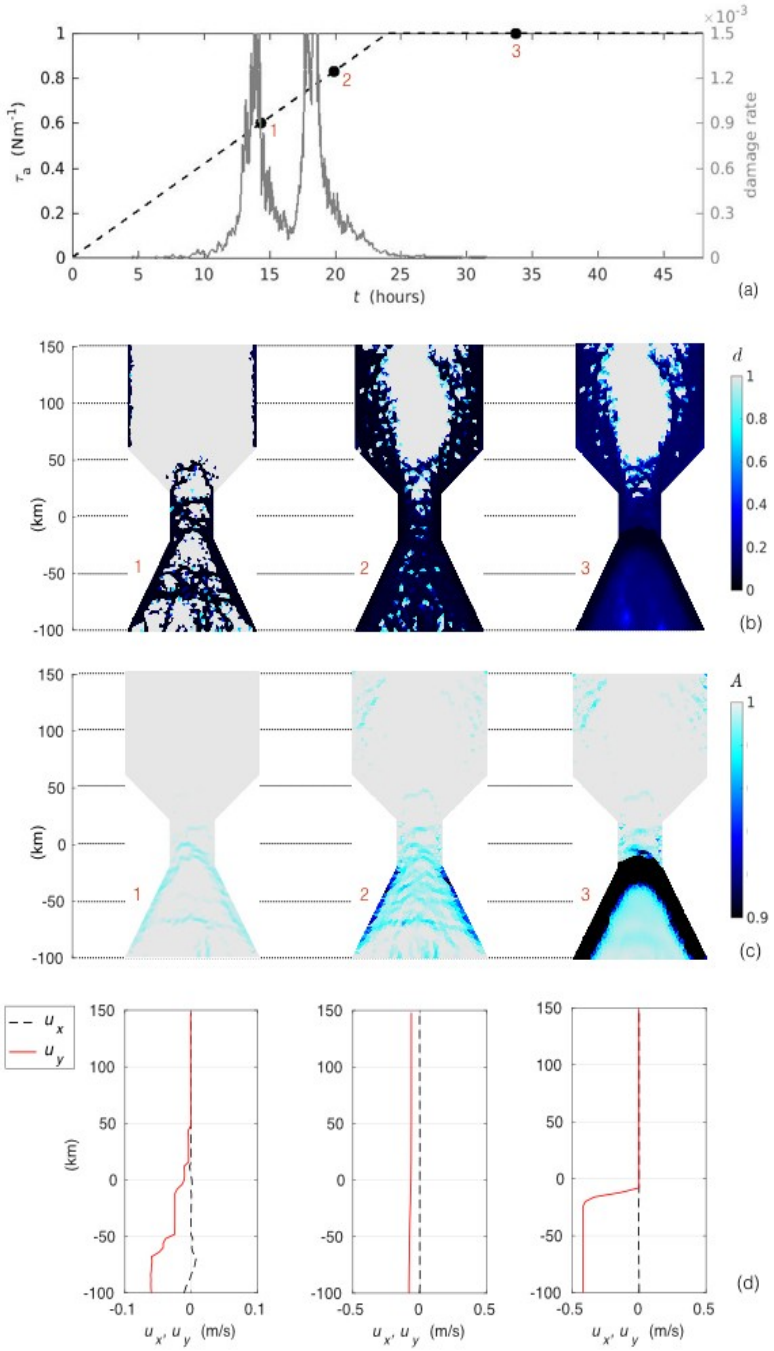

(a) Time series of the wind forcing (dashed curve) and of the damage rate (solid grey curve) in an idealized channel simulation using C_{min} = 20 kPa. Instantaneous spatial distribution of (b) the level of damage and (c) ice concentration at the times indicated by the numbers 1, 2 and 3 on the time series of panel (a). Instantaneous profiles of the vertical and horizontal velocities at the times indicated by the numbers 1, 2 and 3 on panel (a). The horizontal resolution is of 4 km.

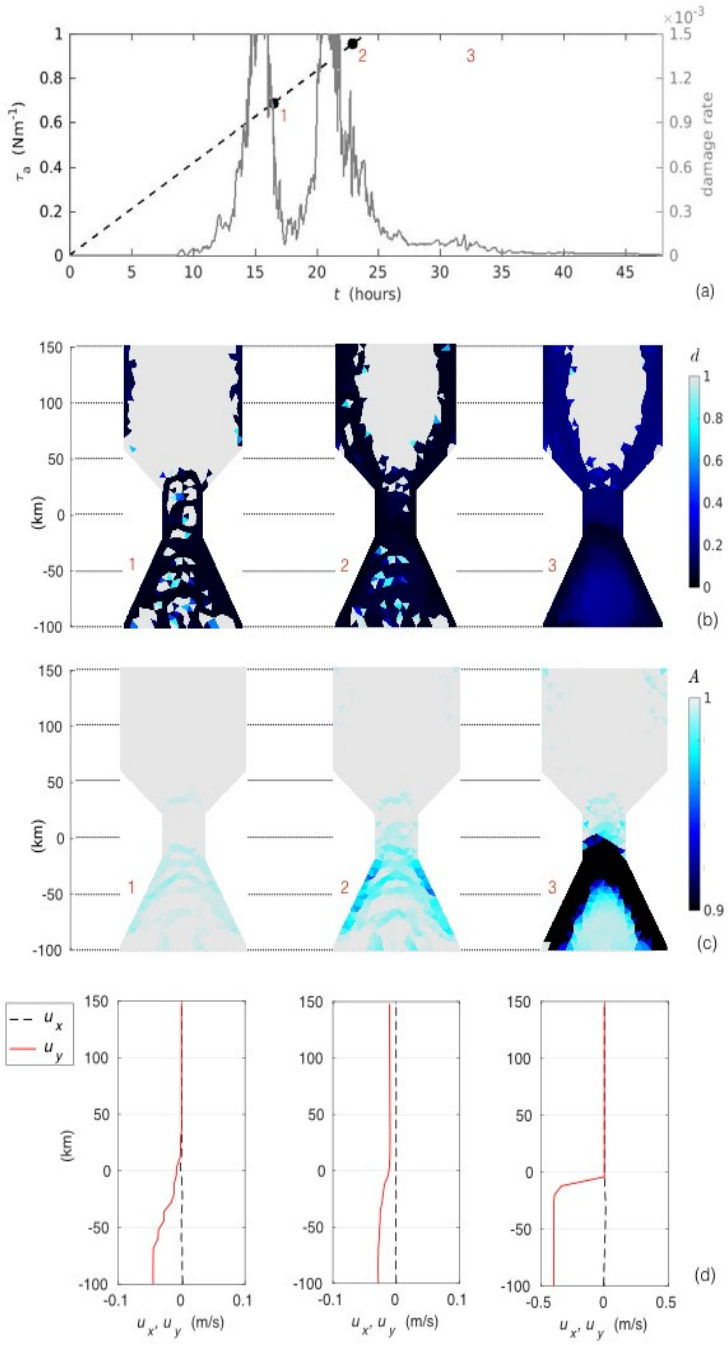

(a) Time series of the wind forcing (dashed curve) and of the damage rate (solid grey curve) in an idealized channel simulation using C_{min} = 20 kPa. Instantaneous spatial distribution of (b) the level of damage and (c) ice concentration at the times indicated by the numbers 1, 2 and 3 on the time series of panel (a). Instantaneous profiles of the vertical and horizontal velocities at the times indicated by the numbers 1, 2 and 3 on panel (a). The horizontal resolution is of 8 km.

Modifications have been made in the text regarding the comparison between the Maxwell-EB and the VP/EVP rheology (see our responses to your earlier comments). We stress the point that this paper was never about making a comparison between the two types of models, *but to demonstrate the capabilities of the Maxwell-EB model.* Moreover, we believe that the capability of a model to represent a given physical phenomenon should *not* depend on model resolution, as long as the resolution is sufficient to resolve the relevant processes.

page 13, l.1-2: please state the range of x

page 13, l.16-17: "(see Dansereau et al. (2016))" -> (see Dansereau et al., 2016)

page 13, l.19-20: I think this statement requires, that you have tried a fully implicit scheme and compared the results. Have you? If not, this statement is no really supported by anything and should be changed.

Yes, we have tried a fully implicit scheme, in which all variables were updated as part of the fixed point iteration. This did not have significant impact on the simulation results both in highly idealized and realistic cases, as mentioned in the text.

page 14, l.8-9: Please say, how much the "drift velocity on the order of that associated with strictly elastic deformations within an undamaged ice cover." really is (in m/s or cm/s or whatever) so that others can compare.

This reference has been added ($\boldsymbol{u}$ is on the order of 10^{-5} ms^{-1} maximum for strictly elastic deformations).

page 14, l.11: "relatively undamaged" -> rephrase to "stagnant ice with low damage" or similar

Ok.

page 14, l. 20-21: "the width of the distribution of C impacts the rate of propagation of the damage, with the propagation being more progressive for a larger distribution." Since the cohesion appears to be an important parameter, it would be useful to add more information about the choice of C, i.e. the actual distribution of C that is generated (page 11, ll.10) in case the reader would like to reproduce the results.

Because this comment is not relevant to understand the results presented here, it is now removed. The main point of using different values of cohesion in mentioned in the previous sentence, which is that the minimum value of cohesion over the domain controls the timing of the onset of damaging in the simulations.

Idealized simulations exploring the specific role of disorder (i.e., the width of the distribution of *C* here) in elasto-brittle models are now being performed, and show that this statement, "the propagation being more progressive for a larger distribution" is not exactly correct. We therefore believe that removing this sentence will avoid any confusion on this point. Besides, channel flow simulations with a uniform cohesion have produced results similar to that reported here (see our response to your earlier comment), demonstrating that the width of the distribution of cohesion is not an important factor in these simulations.

The distributions of *C* that are generated for these simulation are explained on page 11, line 10-17 (see our response to your earlier comment).

page 15, l.2: "differs" -> differ

page 15, l.23: "(see Fig. 4b and 4c, panel 3)" Should be Fig. 5b and 5c. . .

page 15, l.23-26: "This is an important point, as standard viscous-plastic sea ice models do not account for pure uniaxial or biaxial tensile strength and hence would not be able to reproduce the formation of a stable ice arch with self-obstruction to flow under the conditions simulated here." I don't agree: (1) From the figure, the location of the arch is not visible if you mean it is defined by the location of black elements. (2) the de- tails of the yield curve (Figure 2) should not matter, one can tune the elliptic yield curve to resemble the Mohr-Coulomb and tensile failure criteria (see Figure 1 in Lemieux et al, 2016). (3) even without isotropic/biaxial tensile strength, Dumont could simulate arches with VP rheology, so do Losch and Danilov (2012) in similar idealized simulations, even with "a standard VP model" for order 1000 days. (4) why do VP models not account for pure uniaxial tensile strength? I think that this statement needs to change.

(1) The location of the ice bridge is not defined by the location of black elements. In the text, the location of the ice bridge is associated to *the collocation of a minimum/maximum in the second and first principal stresses*. The location of the ice arch is clearly visible from the profile of ice velocity and (now included) the field of ice concentration. This last point is now mentioned in the text. Also, in the following sentence, there was a mistake : "downstream" should be "upstream".

(2) First, it is important to stress the point that the yield/damage criterion and the rheology (i.e., the constitutive law) are separate components of a mechanical model. The details of the yield curve do matter because to sustain ice bridges, the ice needs to have some cohesive strength (see *Dumont et al., 2009* and *Lemieux et al., 2016*). *Lemieux et al., 2016* refers to the standard elliptical yield curve as accounting uniaxial tensile strength (2nd page, 3rd paragraph). This wording is false. The standard elliptical yield curve accounts for some biaxial tensile-compressive strength (see our response to your earlier comment), uniaxial

compressive strength but no uniaxial tensile strength. In this paper, the authors have modified the standard elliptical yield curve to account for uniaxial and biaxial tensile strength for a better representation of landfast ice in VP models, hence implying that the details of the yield curve do matter.

(3) As mentioned in our response to your earlier comment, the elliptical yield curve used by *Dumont et al., 2009* and *Losch and Danilov, 2012*, does not include biaxial (or uniaxial) tensile strength, but biaxial compressive-tensile strength and uniaxial compressive strength. Therefore ice in these models can not sustain biaxial tensile stresses. Here, as shown by the profile of the principal stress components, the state of stress just upstream of the ice bridge is *biaxial* tensile, which demonstrates that the bridge sustains biaxial tensile stresses. In the paper, we thus make the point that models that do not account for biaxial tensile strength would not be able to reproduce a stable ice bridge in the conditions simulated here, i.e., in which the states of stress are biaxial tensile.

(4) We do not understand this question fully because of your earlier comment, which states that there is uniaxial tensile strength in the standard elliptical yield curve. There is indeed no uniaxial nor biaxial tensile strength in the standard, Hibler elliptical yield curve. This yield curve was chosen based on the early AIDJEX assumptions that sea ice did not exhibit pure tensile strength (see *Coon et al., 2007*).

We made some adjustment to this paragraph (and figures) to indicate the location of the ice bridge as well as the states of stresses upstream of this bridge more clearly. We also made modifications to section 2.1 and figure 2 to better explain what is cohesion and the difference between uniaxial/biaxial tensile, biaxial tensile-compressive and uniaxial compressive strength. We also modified the statement concerned by this comment as "This is an important point, *as models based on the standard elliptical yield curve* do not account for uniaxial or biaxial tensile strength and hence would not be able to reproduce the formation of a stable ice arch with self-obstruction to flow under the *stress* conditions simulated here" and believe that otherwise it does not need to change.

page 16, l.24: In this comparison (Figure 8), one might ask why the specific failure curves where chosen differently for the model, when there are estimates for the parameters available (c = 250, and μ = 0.9). Should be discussed somewhere.

This value of q (i.e., μ) and σ_c was taken by *Weiss et al., 2007* and *Weiss and Schulson, 2009* to draw the Mohr-Coulomb envelope on this figure because it was the one available value, reported by *Schulson et al. 2006a* for the failure envelope of first-year arctic sea ice obtained from biaxial tests in the laboratory at −10 °C. This is now mentioned in a footnote. In the Maxwell-EB model, we use $\mu = 0.7$, equivalent to an internal friction angle of 35 degrees, a value commonly used for geomaterials and ice (*Byerlee, 1978* and *Jaeger and Cook, 1979*). A lower value of q could also be deduced from figure 8a. Conversely, using $\mu = 0.9$ (internal friction coefficient of 42 degrees, not shown) does not impact the behaviour of the Maxwell-EB model.

page 17, l.3: "later" -> more recent ?

We changed it for the 1990's, which is the correct period reported by *Barber et al., 2001*.

page 17, l.16: "According with"-> In line with

We changed it for "in accordance with", as suggested by reviewer 1.

page 17, l.21: "'differentiated" does not sound right, rephrase if necessary

We now use "distinguished".

page 17, l.29-31: "However, in all of the weaker ice cover scenarios (2002-2008 period and/or summer), none of the ice arches formed near the exit of Kane Basin nor secondary arches formed elsewhere sustain the applied wind forcing and all ice bridges eventually collapse." Is there a similar behaviour in observations in this period? Please add a comment.

Yes, a similar behaviour was observed over the same time period, as discussed at the beginning of section 5.1.3 (first paragraph). For instance, no ice bridge formed between Kane Basin and Smith Sound in the winters of 2007/2008 to 2009/2010, except for a 2 months period (*Munchow et al., 2016*). We have modified this paragraph to include this and a more recent reference (*Ryan et al., 2017*).

Since we perform simulations with an initially uniform ice thickness and simplified wind forcing, i.e., not representative of specific conditions over the period 1979-2001 or 2002 and 2008, we do not think making a direct comparison to ice conditions in the Strait during that period is relevant at this point in the text.

page 18, l.7: "widely different dynamical behaviours" -> a wide range of dynamical behaviour

page 18, l.7-9: The big question remains: how do you determine the appropriate cohesion? It appears to be vital parameter, similar to P* in Hibler's VP model.

Cohesion is indeed an important parameter in the model as it controls the shear strength of the ice and as for $C = 0$, the model would not allow any form of tensile strength. However, we do not believe a direct comparison to P^* is relevant. Indeed, in-situ stress measurements do indicate the importance of the cohesion parameter, by the fact that these measurements fit well a Mohr-Coulomb criterion with non-zero cohesion (see figure 8a). On the contrary, these measurements do not support the role of P^*, the biaxial compressive strength, as being a relevant parameter to describe the shape of the damage criterion (or yield criterion in the case of the VP model). The measurements do not give an indication of an appropriate value for this parameter either.

As mentioned on page 11, line 17, some studies (e.g., S*chulson, 2004; Weiss et al., 2007*) assume a scale effect on shear strength, set by the size of the defects (thermal cracks, brine pockets, ...) present in the ice cover. According to this scaling, lower values of C are consistent with larger defect sizes and a lower shear strength. It is difficult to infer a proper spatial scale for the in-situ stress measurements reported here (from Weiss et al., 2007), but it should be smaller than the spatial resolution of the present experiments, hence a lower cohesion should be used in the model.

As mentioned in section 4, the *highest* values of C employed here (i.e., the upper bound of the distri*b*ution of C in the case of C_{min} = 30 kPa, which is 60 kPa) are consistent with the in-situ stress measurements reported by *Weiss et al., 2007* (see figure 8b). We obtained the formation of stable ice bridges in the model for lower values of C.

However, the fact that we obtained the formation of a stable ice bridge in the present idealized and realistic simulations using C_{min} = 20 kPa does not mean this is the appropriate value of cohesion for sea ice or for the Maxwell-EB model, nor that it is the only value for with the Maxwell-EB model can reproduce the formation of a stable ice bridge between Kane Basin and Smith Sound. As mentioned in lines 7 to 9, this result depends on

- the prescribed initial thickness. Bridges form at lower cohesion for thicker ice. Here we used h_0 = 1 m but a higher h_0 might be more representative of ice conditions for some years.

- on the specific value used for the Young's modulus. A higher value allows the formation of stable ice bridges for lower values of cohesion. As mentioned in the response to your earlier comment, the value used for E_0 is at the lowest bound of the range of reported values.

- the magnitude of the applied wind forcing. In the model simulations, we increase the wind forcing up to 1 Nm^{-2} and hold it constant, which corresponds to a wind speed of 82 km h^{-1} or 22 ms^{-1}. While daily-averaged model wind stress values of 0.7–1.0 N m^{-2} have been reported in Nares Strait, see *Samelson et al., 2006*, a uniform, sustained wind stress of 1 Nm^{-2} for *several days* is most probably an overestimation of the reality. Were we made this choice of wind forcing to simplify the analysis.

Therefore, If we were to increase h_0, increase E_0 and decrease the applied wind forcing, stable ice bridge would be obtained for lower values of C, and conversely for a lower h_0 and E_0 and higher wind forcing. In the passage you are reporting, we therefore made it clear that the goal of these experiments was not to determine an appropriate range of value for the cohesion.

page 19, l.5-6: "A Lagrangian model would perhaps be more suitable to simulate the edge of the detached ice"; or a better advection scheme with less numerical diffusion (i.e. higher order basis functions in your finite element method)

The diffusivity of the numerical scheme and order of the polynomial approximations used are described in the sentences above, from p. 18, line 31, to p. 19, line 3. The sentence you are referring to does not refer to diffusion, but to the fact that Lagrangian approaches, i.e., which follow ice particles, are better suited to track the ice edge. The use of higher polynomial approximation does not *change* the numerical scheme.

Also, we have replaced "more suitable" by "a more natural approach".

page 19, l.13-14: "Nevertheless, at all times the simulated probability density function is strongly asymmetric, consistent with thickness distributions estimated for sea ice with little history of melting (e.g., Haas, 2009)." Please discuss in how far this special experimental geometry with many coastlines and the low Cmin is suitable to compare to observations made for open ocean Arctic sea ice as described in Haas (2009).

Here, we referred to measurements from the open Arctic ocean with little history of melting specifically because the model does not represent thermodynamic effects and hence the simulated ice thickness distribution and hence a comparison with measurements from a region where the melting signal is important should not be made. Asymmetric thickness distribution have not been obtained from open Arctic ocean measurements only. For instance, *Hass et al., 2006* report an asymmetric thickness distribution with an exponential tail from AEM measurements at the entrance of Nares Strait. We now include this reference in the text.

Concerning the value of cohesion, a higher value (e.g., C_{min} = 20 kPa) also give a strongly asymmetric thickness distribution, however, it does not allow the thickness to increase to values as high as in the C_{min} = 10 kPa case in the same simulation time, only because ice bridges form and stop the flow of ice through the channel, hence reducing the amount of ice entering the channel that can be

incorporated into ice ridges. This point is now clarified in this section. Moreover, as discussed in the response to your earlier comment, there is no observational nor physical evidences at this point to characterize C_{min} = 10 kPa as a "low" or "too low" cohesion for the ice cover.

page 19, l.18: This term (7) is not correct and should not be used. See e.g. Schulkes (1995), JGR, for correct equations and a nice explanation of ridging in general.

This is a typo in the text on the development of the term $\nabla\cdot(h\,u)$ (see response to reviewer 3 and to your earlier comment). This was not an error in the code.

page 19, l. 23: "Fig. 11b" -> Fig. 10b 10b

page 20, l. 2-3: "In coupled thermodynamic and dynamic models, a high density of leads is expected to impact the simulated heat fluxes between the atmosphere, the ice and the ocean (Smith et al., 1990)." This is not really a conclusion, but part of a discussion.

We agree and move this comment to the discussion part of this section (page 20, end of second paragraph).

page 20, l. 11-13: "the presence of land fast ice along. . ." This has hardly been discussed and comes as a surprise. Needs more attention in Section 5 if you want to keep this conclusion

We do not agree with this comment, as the presence of landfast ice is discussed in section 5.1.2 and 5.1.2, along with other features reproduced by the model. This remains in the list of conclusions. We have added additional references on the observed presence of landfast ice in Nares Strait.

page 20, l. 24: "a process that is known to be underestimated in VP models using a two-level scheme" This is new to me. At correspondingly high resolution I would expect a VP model to behave in a similar manner, see also Losch and Danilov (2012), Fig6. which shows very similar ice thickness distribution in a similar channel experiment.

The statement made here compares the thickening of the ice cover between a VP model with a two-level versus a multi-categogies thickness redistribution scheme. It is our understanding that in *Losch and Danilov, 2012*, a two-level categories scheme was used as was not compared to a multi-categories scheme. An ice thickness distribution was not computed in this study. The results reported represent a steady state after 10 years of integration and hence would not be directly comparable with the present Maxwell-EB simulations.

This sentence was moved to the discussion of the two-level and multi-categories scheme, section 2.2.

page 20, l.26-28: See above, I don't think, that you can say this, because you'd have to show that the same model configuration with a VP model would not have your thickness distribution. I am pretty sure that you would get a similar result.

The sentences you are referring to is:

"In the Maxwell-EB model, this capability of accounting for a sufficient thickening of the ice as well as the spatial localization of extreme thickness values arises from the appropriate description of extreme strain localization. On a mechanical point of view, this may therefore question the relevance of using multi-categories redistribution schemes."

The sentences therefore discusses the capability of the Maxwell-EB model, not the VP model, to represent the localization of increased ice thickness, in relation with the localization of ice deformation. The next sentence questions the use of a multi-categories thickness model versus a simpler thickness redistribution model to obtain this localization of high thickness values. As mentioned an earlier comment, the thickness redistribution scheme is independent of the rheology used and here, the VP model is not mentioned. Therefore this does not prevents us from writing this sentence.

page 21, l. 14: "later" -> recent

page 21, l. 33: "Haas, C.: Dynamics Versus Thermodynamics: The Sea Ice Thickness Distribution, p. 638, Wiley-Blackwell, 2009." Please correct citation as book chapter in Sea Ice (eds D. N. Thomas and G. S. Dieckmann)

page 22, l.10: "III, W. D. H.: Modeling a Variable Thickness Sea Ice Cover,. . ." -> wrong name

page 25, l.27: "Weiss, J. and Dansereau, V.: Linking scales in sea ice mechanics, Philosophical Transactions A, pp. –, doi:10.1098/XXXX, 2016." Is this a submitted manuscript? If so it is not properly cited.

page 26, Figure 5: What is Cmin in this simulations? Did you consider to show a sea ice concentration plot for the idealized experiments as well? That would help to see the arches directly.

C_{min} = 20 kPa (it is the same simulation as in Figure 4, as mentioned in the caption). This is now also stated at the beginning of section 5.1.1. The corresponding fields of ice concentration are now added to this figure.

page 29, Figure 8: An indication of the probability of single stress states using a colormap or transparency would be helpful, to get an impression how frequently biaxial tensile states (and all other stress states) occur.

To indicate the proportion of each types of stress through time, a time series of stress state types (tensile, biaxial tensile-compressive, biaxial compressive) during the corresponding simulation is now included in Figure 8. Figure 8b (now 8c) corresponds to a snapshot at t = 72 hours, when the probability of each stress states and repartition in the principal stresses plane has stabilized. This point is now clarified in the text.

page 31, Figure 10: Why are the PDFs for x = 4km and 8km given at t=5days, whereas the other results are shown for t=3days?

Thank you for catching this. This is a typo from an earlier simulation. The PDFs for x = 4 km and 8 km are indeed given for t = 3 days. This has been corrected in the figure caption.

RESPONSE TO REVIEWER 3

General comments

1) **It would be helpful to explain more about the advantage of the Maxwell-EB rheology compared with the traditional elliptic curve rheology. The authors pointed out the capability to represent the extreme localization of damage and deformation (P4L13). However, there is a possibility that it comes just from the horizontal resolution of the grid cell in the model. I mean that the traditional plastic rheology might be able to reproduce the phenomena if finer grid cells are used. Thus I want to know why they consider the continuum elasto-brittle rheology should be more appropriate than the continuum viscous plastic rheology for this phenomena, and whether this rheology can be applicable to the general sea ice conditions.**

The difference between the VP and Maxwell-EB rheology is two-folds: it lies in the rheology itself (i.e., the viscous-elastic-brittle versus the viscous-plastic constitutive relationship) and in the prescribed damage (or yield) criterion. Of course, both aspects impact the simulated mechanical behaviour.

First, the goal in developing the Maxwell-EB framework was to suggest an alternative to the traditional Viscous-Plastic (VP) rheology that is more physically sound, as in recent years, the viscous hypothesis and other underlying physical assumptions of the VP model have been revisited and found to be inconsistent with the observed mechanical behaviour of sea ice in many aspects, e.g., with respect to the order of magnitude of the observed strain rates (*Weiss et al., 2007*; *Rampal et al., 2008*), the anisotropic distribution of ridges and leads and associated discontinuities in the velocity field on scales both small and large (> 100 km) (*Hibler, 2001; Schulson, 2004; Coon et al., 2007*), the relation between stresses and strain-rates (*Weiss et al., 2007*), the strength of pack ice in tension (*Weiss et al., 2007; Coon et al., 2007*) and the normal flow rule (*Weiss et al., 2007*) . The aim in building this new continuum model was to represent accurately the *deformation and drift* of sea ice. In particular, we wished to developing a modelling framework that allows representing both the small deformations associated with brittle failure and the large deformations occurring within a fractured ice cover. In the paper, these points are introduced in the last paragraph of the introduction and in the first paragraph of section 3 (which presents the model). As they are discussed in the first paper that presents the motivations for and the details of the Maxwell-EB rheology (*Dansereau et al., 2016*) and references to this paper are included both in the introduction and in section 3, we do not think repetition is needed in the present paper, which we wish to be relatively short and to focus on the implementation of the model on geophysical scales.

One particularity of the Maxwell-EB model is that the localization of deformation indeed *does not* depend on the spatial resolution, *in the sense that the tendency to localize damage and deformation at the smallest available scale, i.e., the scale of the model grid cell, is intrinsic to the rheological framework*. In other words, no matter the spatial resolution, the Maxwell-EB model reproduces a localized deformation. This point is also discussed in more details in the paper that first presents this new rheology (see *Dansereau et al., 2016*, section 6.1) hence, an in-depth discussion was not included here. The fact that the representation of ice bridges and leads does not depend on the choice of spatial resolution (over the range of spatial resolutions that allow resolving the flow of ice through the channel) is mentioned in the description of the simulation setup (p. 12, line 18 and page 13, lines 1 and 2) and discussed in terms of the representation of the thickness redistribution (figure 10b).

We also discussed the issue of spatial resolution in our response to reviewer 2. As mentioned in section 4 and discussed in section 5.2, we analyzed lower resolution simulations. These simulations show that the model reproduces a stable ice bridge, a clearly defined ice front, arch-like and linear leads upstream of the ice bridge, and a distribution of ice thickness with a tail that follows an exponential function as in the higher resolution cases. Since we did not perform VP model simulations, in the paper we did not speculate on the fact that VP models at very high resolution can or cannot reproduce ice bridges in narrow passages. However, we believe that if a model can reproduce ice bridges and other important processes *only* at high to very high resolution it is not good news, as the physics represented by a model should not be resolution-dependant.

Second, the main advantage of using a Mohr-Coulomb (MC) failure criterion instead of the elliptical yield curve for the damage criterion in the Maxwell-EB model is that the MC criterion appears in agreement with in-situ stress measurements (see figure 8 a). Also in agreement with observations, the current damage criterion allows accounting directly for some resistance of the ice in pure ($\sigma_1<0$ and $\sigma_2<0$) tension. As demonstrated in the present as well as in previous papers (ex., *Dumont et al., 2009*), resistance of the ice in tension is especially important for simulating stable ice bridges. This point is discussed in section 2.1. Another advantage of the MC damage criterion is that the cohesive strength of the ice (i.e., σ_t and σ_c) can be set and adjusted directly by varying the cohesion parameter, *C*, rather than indirectly, by changing the ratio of the ellipse.

To answer your last comment, the simulations performed here are indeed on a regional scale, and concern very specific flow conditions. However, the results gives us no reasons to think that the model could not be applied to more general conditions. On the contrary, the model proves to behave well in this "extreme" case, i.e., a case chosen especially to test the ability of the model to represent (1) the complex mechanical behaviour associated with the formation of an ice bridge and (2) the

discontinuities in ice velocity, concentration, thickness, etc., associated with the presence of this bridge.

2) **Intuitively my feeling is that the floe size distribution of sea ice should also play an important role in the brittle ice rheology. Therefore, in the question at P17L7-8 it would be natural that the change in floe size distribution may also contribute to the phenomena. What do you think?**
This is a good point. The paper discussed in this section (*Gimbert et al., 2012b*) identified a mechanical weakening of the ice cover that is independent of an ice thinning and suggested that this weakening is related to the degree of fragmentation of the ice cover. A more fragmented ice pack is indeed in agreement with an evolution towards smaller ice floes. We now add a mention to this effect in section 5.1.3, paragraph 2. It is also consistent with a change in the shape (circularity) of the floes, a less cohesive state ice cover, an enhanced deformation and an increased ice drift (*Rampal et al., 2009*).
Of course, continuum models by definition, whether using a VP, EVP, EB or Maxwell-EB rheology, do not resolve ice floes per se nor the mechanical interactions between individual floes. Hence it would be interesting to explore this question further using a discrete element model (ex., *Rabatel et al., 2015*; *Hopkins, 2004*; *Herman, 2011*; *Wilchinsky et al., 2011*), that is, to try relating the floe size distribution to the cohesive strength of the ice cove in a quantitative manner.

2) **On the whole, I am somewhat concerned about why the authors did not pay so much attention to the horizontal scale. For example, the scales of ice bridges seem to be different depending on the straits. Accordingly the mechanism might be different depending on the regions. Could you explain how the Maxwell-EB rheology influence the results depending on the scales.**
We are sorry we might not understand this comment fully.
The horizontal scale of ice bridges is the width of the constriction point across which it forms. In general, the limiting span that can support a stable arch between vertical walls or in a vertical tube depends on several properties of the material (its density, cohesion, internal friction) and the friction between the material and the walls (*Richmond and Gardner, 1962*). In the case of sea ice, the presence of a stable ice bridge should depend on the cohesion of the ice cover, its thickness, concentration, etc., the friction between the ice and the coast (here we prescribe a no-slip boundary condition), but also on the wind and ocean forcings. *Rallabandi et al., 2017* for instance developed a one-dimensional theory for the wind-driven formation of ice bridges in narrow straits in a VP model and investigated the formation of a stable ice bridge at a given wind stress, maximum and minimum channel width, ice thickness and compactness in this model. A study of the limiting span of ice bridges observed to form in the Arctic with a comparison to Maxwell-EB model simulations would indeed be interesting but is beyond the scope of the present paper.
However, as mentioned on page 10, lines 6 to 8, simulations with different idealized domains (narrower, longer channels, smaller basins) were performed to verify that the dynamics described in the paper is not specific to the shape and dimension of the idealized channel. Moreover, the use of a realistic domain allows investigating the formation of ice arches at different locations, hence with different spans, in the Maxwell-EB model.

Although the description on the scale dependence (P19L17-25) is interesting, in general it seems that the localization of deformation depends on the grid cell size. Could you explain why this property is independent of resolution?
As mentioned in our response to your major comment (above), the tendency to localize the damage and deformation at the smallest available scale is intrinsic to the Maxwell-EB rheology. Hence there is no characteristic scale for the localization of damage and deformation in the model beyond the scale of the model element (see *Dansereau et al., 2016*, sections 6.1 and 6.2). Therefore, at all spatial resolutions, the simulated deformation is highly localized. In the present simulations, this translates into a localization of the mechanically redistributed, i.e., the "ridged" ice and an exponential tail of the ice thickness PDF at the spatial resolutions explored (2 km, 4 km and 8 km in the idealized channel case). This point is now made clearer in section 5.2.

Specific points:
***(P1L2)"on geophysical scales" I wonder if we can assume ice bridges and ridges to be on a geophysical scale. It would be preferable to describe the specific phenomena like "ice bridges on a few tens of kilometers".**
The model is used here to simulate the drift of sea ice through a channel that is 500 kilometres long and a few tens to hundreds of kilometres wide. Ice bridges and ridges are smaller-scale features resulting from the associated deformation of the ice cover. We believe it would have indeed been wrong to claim that the model was used on *global* scales, but the setup used here does qualifies this application as to apply on "geophysical" scales.

***(Figure 1) The red dotted line in Fig.1b is hard to see. Please make it more prominent. In Fig.1c there are two red dotted lines. I guess the northern one should be deleted.**
Yes, thank you for catching this.

***(P5L17) Please insert "Hibler"**

***(P8L9, Eq.3) I think "A" is not needed.**
The air and water drag terms in the momentum equation are indeed both multiplied by the ice concentration. This approach was suggested by *Gray and Morland, 1994* and *Connolley et al., 2004*, to account for the contribution of the ice-free and ice-covered fraction of a grid cell to the wind and water stress. *Connolley et al., 2004*, explains the necessity of introducing this weighting to maintain physical consistency in the free-drift limit. Without it, the free-drift solution of the momentum equation (when including the Coriolis term)

depends on ice concentration, i.e., ice floes with the same thickness would not be drifting at the same velocity based on their concentration, even in the limit of negligible mechanical interactions. Here, this "correction" is included for the sake of physical consistency, even if not strictly necessary since the Coriolis term is neglected in the present implementation of the model. We now add a reference to the work of Connolley et al., 2004 when introducing the form of the momentum equation solved here (Eq. A1).

This weighting approach is quite standard and was used for instance in the sea ice models of *Tremblay and Mysak, 1997*, *Lieataer et al., 2009*, *Danilov et al., 2015* (FESIM), and others. Interestingly, in the present model, it has effectively little effect on the simulation results, a point also noted by *Connolley el al., 2004* and *Tremblay and Mysak, 1997*.

***(P17L4) Please replace "than" by "that".**
Yes, thank you.

***(P19L10) I agree, but there are some discrepancies in the slope of the thickness pdf around 1 m. Is that a negligible problem?**
This discrepancy is explained by the fact that a uniform thickness of h = 1.0 m is prescribed as the initial condition in all simulations presented here. Hence we naturally expect a mode to stand out at h = 1.0 m. The tail of the PDF, which represents the ridged ice, is therefore the part of the distribution with h > 1.0 m. Here, the PDF was effectively fitted with an exponential function for all values of h > 1.0 m. The presence of the mode indeed results in a systematic misfit near h = 1.0 and fitting the distribution for larger values of h only gives a somewhat better fit. Nevertheless, the values of the coefficient for the goodness of the fit obtained here vary between 90% and 98% in the idealized and are > 95% in the realistic case.

***(P19L18) In the equation, h cdot nabla u should be h nabla cdot u.**
Yes, thank you for catching this.

***(P21L11-12) "prescribing a cut-off for biaxial compressive strength. . . appears unnecessary" I could not understand this. Can you add some additional explanation?**
As suggested both by in-situ stress measurements (see figure 8a) and the realistic numerical simulations performed here (see figure 8b), large biaxial compressive stresses seldom occur in the sea ice cover. This is an interesting result, since the flow conditions here are convergent over a large part of the domain. The stress states measured and reproduced by the model indicates that the ice fails frequently under pure tensile and biaxial tensile-compressive (i.e., shear) stresses (which is also illustrated in figure 5c). This point is further discussed in the response to reviewer 2.
Because large biaxial compressive stresses and pure biaxial compressive stresses, i.e., compressive states of stress involving little shear ($\sigma_1 \sim \sigma_2$), are marginal, imposing a biaxial compression damage criterion, would not significantly affect the number of damage events and propagation of damage in the Maxwell-EB model. The addition of such a cutoff is not supported (and not well constrained) by the observations. Instead, in-situ stress measurements suggest that the uniaxial (unconfined) compressive strength, σ_c and maximum tensile strength (or σ_t) are more relevant parameters to describe the failure strength of the ice cover.

To make this point clearer, we modify this paragraph as follow:
"Besides numerical efficiency, other advantages of using a simple redistribution scheme such as the one employed here is that no thickness redistribution function needs to be assumed and the redistribution is not directly tied to the prescribed failure strength of the ice. In the Maxwell-EB model, the prescribed strength is instead based on in-situ stress measurements, which point to a Mohr-Coulomb failure criterion and directly provide information on the order of magnitude of the shear strength and tensile strength. In particular, both the observations and numerical simulations here suggest that prescribing a cut-off for biaxial compressive strength (equivalent to the pressure, P, in VP models) is unnecessary. Instead, the uniaxial (unconfined) compressive strength, or sigma_c and maximum tensile strength, sigma_t appear to be more relevant to represent adequately the strength of the ice cover. The Maxwell-EB model presents the advantage that both these quantities are set through a single parameter, the cohesion C."

***(P23L10) "Hibler" is missing.**

Ice bridges and ridges in the Maxwell-EB sea ice rheology

Véronique Dansereau[1], Jérôme Weiss[1], Pierre Saramito[2], Philippe Lattes[3], and Edmond Coche[4]

[1]Institut des Sciences de la Terre, CNRS UMR 5275, Université de Grenoble, Grenoble, France
[2]Laboratoire Jean Kuntzmann, CNRS UMR 5224, Université de Grenoble, Grenoble, France
[3]TOTAL S.A. - DGEP/DEV/TEC/GEO, Paris, France
[4]TOTAL S.A. - DGEP/AF/CG-TEPCG/DBD/DDP/DMHB, Pointe Noire-Poincare, Congo

Correspondence to: Véronique Dansereau (veronique.dansereau@univ-grenoble-alpes.fr)

Abstract.

This paper presents a first implementation of ~~the Maxwell-EB model~~ a new rheological model for sea ice on geophysical scales. This continuum model, called Maxwell-Elasto Brittle (Maxwell-EB), is based on an Maxwell constitutive law, a progressive damage mechanism that is coupled to both the elastic modulus and apparent viscosity of the ice cover and a Mohr-Coulomb damage criterion that allows for pure (uniaxial and biaxial) tensile strength. The model is tested on the basis of its capability to reproduce the complex mechanical and dynamical behaviour of sea ice drifting through a narrow passage. Idealized as well as realistic simulations of the flow of ice through Nares Strait are presented. These demonstrate that the model reproduces the formation of stable ice bridges as well as the stoppage of the flow, a phenomenon occurring within numerous channels of the Arctic. In agreement with observations, the model captures the propagation of damage along narrow arch-like kinematic features, the discontinuities in the velocity field across these features dividing the ice cover ~~in~~ into floes, the strong spatial localization of the thickest, ridged ice~~and~~, the presence of landfast ice in bays and fjords and the opening of polynyas downstream of the Strait~~are all represented~~. The model represents ~~different~~ various dynamical behaviours linked to an overall weakening of the ice cover and to the shorter lifespan of ice bridges, with implications in terms of increased ice export through narrow outflow pathways of the Arctic.

1 Introduction

The formation of ice bridges is a common phenomenon in the Amundsen Gulf, Bering Strait as well as in many narrow passages of the Canadian Arctic Archipelago (Sodhi, 1977). Commonly referred to as ice *arches* because of their curved and concave shape, these structures can remain stable for several weeks or months and stop the flow of ice through outflow channels (Kwok, 2005; Kwok et al., 2010; Münchow, 2016). Downstream of ice bridges, ~~expenses~~ expanses of ice-free water and polynyas open, which strongly impacts the local atmosphere-ocean heat exchanges and promotes the generation of new ice (Smith et al., 1990). Upon breakup of a bridge, the outflow of ice, stored in the basin upstream, drastically increases. Therefore, the capability of representing adequately the complex dynamical behaviour of ice drifting through narrow passages might constitute a key asset when using numerical models to asses the seasonal and interannual variability in the circulation and export of fresh water and sea ice in the Arctic.

Figure 1b shows an example of such an ice arch present ~~in May 2005~~ on July 2nd, 2010, at the Lincoln Sea entrance to Nares Strait, in the Canadian Arctic Archipelago (see Fig. 1a), one of the most extensively studied outflow pathways for seasonal and multi-year Arctic sea ice ~~(Barber et al., 2001; Kwok, 2005; Kwok et al., 2010; Münchow, 2016)~~(Barber et al., 2001; Kwok, 2005; Kwok et
5 The annual mean ice volume flux through this channel, only a few tens of kilometers wide ($30-40$ km) in some places, is thought to be equivalent to about 7% of the annual mean flux through Fram Strait ($\sim 130-140$ km^3, Kwok, 2005; Kwok et al., 2010). Poleward of the Strait, ice converges towards the coast of Ellesmere Island and Greenland, where multiyear ice coverage is known to be high ($> 80\%$, Kwok, 2006). Convergence leads to the formation of pressure ridges and the thickness of the ice cover there reaches values among the highest encountered in the Arctic Ocean (Wadhams, 1994; Haas et al., 2006).
10 Analyses of RADARSAT imagery have shown that the ice flux out of Nares Strait stops seasonally after the formation of stable ice bridges in mid- to late-winter, allowing the wide North Water polynya to open downstream of the Strait (Barber et al., 2001; Ingram et al., 2002), and resumes upon breakup of the bridges in ~~the~~ summer (Kwok, 2005; Kwok et al., 2010).

In this paper, these unique flow and ice coverage conditions are used as a benchmark for testing a new rheological framework developed as an alternative to the traditional Viscous-Plastic (VP) rheology to represent accurately the deformation and drift of
15 sea ice in continuum models at regional (~ 100 km) to global (~ 1000 km) scales (Dansereau et al., 2016). This framework, called Maxwell-Elasto-Brittle~~(Dansereau et al., 2016)~~, combines the concepts of elastic memory, viscous-like relaxation of the internal stress and progressive damage mechanics. Highly idealized simulations have ~~allowed demonstrating~~ demonstrated that the Maxwell-EB model reproduces the important characteristics of sea ice deformation revealed by the analysis of available ice buoy and satellite data : anisotropy, high localization in both space and time and the associated scaling laws (Dansereau
20 et al., 2016; Weiss and Dansereau, 2017). Here, this rheological framework is implemented on geophysical scales and in a realistic context. This work focusses on two main aspects. We aim to establish the capability of the model to represent (1) the localization of the ice deformation along arch-like features in the vicinity and within a channel as well as the formation of stable ice bridges and (2) the strong localization of the thickest ice along narrow oriented features representing pressure ridges. Based on our simulation results, we also discuss how the ~~observed~~ mechanical weakening of the ice cover ~~(Gimbert et al., 2012a) is~~
25 estimated over the period 2002-2008 relative to the period 1979-2001 (Gimbert et al., 2012a) can be linked to a shorter lifespan of ice arches and consequently, to an increased ice export through Nares Strait.

2 Background

2.1 Ice bridges

Granular materials have been known for a long time to form concave stress-free surfaces and exhibit self-obstruction to flow
30 under certain conditions (e.g., Richmond and Gardner, 1962; Walker, 1966). By assimilating sea ice as a 2-dimensional continuum material obeying Coulomb's failure criterion, Sodhi (1977) applied the concepts of granular models developed to describe the formation of stress-free arches in hoppers and chutes to the formation of stable ice bridges in the Bering Strait and Amundsen Gulf and obtained good agreement with ice deformation patterns as observed via satellite (Landsat) imagery.

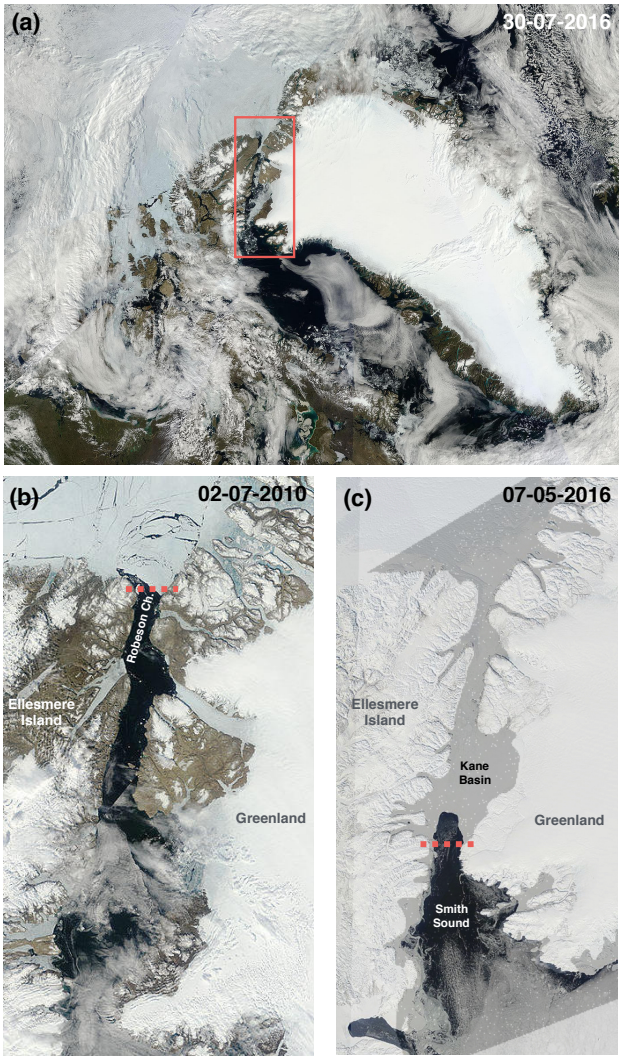

Figure 1. (a) Moderate Resolution Imaging Spectroradiometer ~~reflectance~~ (MODIS) reflectance image indicating (a) the location of Nares Strait (red rectangle), (b) the presence of an ice bridge prior to a partial breakup event, on July ~~8~~2, 2010, with multiple arch-like leads upstream of Robeson Channel (red dotted line) (c) a stable ice bridge at the constriction between Kane Basin and Smith Sound, indicated by the red dotted line, with the North Water polynya open on May 7, 2016. The superimposed grey shading indicates the coverage of the domain used in ~~our~~ the realistic Nares Strait simulations. *NASA/GSFC MODIS Rapid Response at http://rapidfire.sci.gsfc.nasa.gov/imagery/* .

Stable ice bridges have also been successfully reproduced by plastic-type sea ice models, providing the prescribed plastic yield criterion allowed for some ~~tensile strengthor *cohesion*, i.e, that the ice could sustain shear stresses under zero confining pressure (Ip, 1993; Hibler et al., 2006)~~cohesive strength, that is, the capability to sustain uniaxial (tensile and/or compressive) stresses (e.g., Ip, 1993; Hibler et al., 2006). Recently, Dumont et al. (2009) were able to simulate the formation of ice arches in

both idealized and realistic representations of Nares Strait using ~~the Viscous-Plastic model of Hibler (1979) with the standard~~ a dynamic Elastic-Viscous-Plastic (EVP) model (Hunke, 1997), the ice mechanics component of which is based on the VP rheology and elliptical yield curve of Hibler (1979). This rheological framework typically does not account for ~~(~~uniaxial or biaxial (i.e., pure) tensile strength ~~.~~(see Fig. 2, stress states 0 and 1). In the case of Dumont et al. (2009), stable ice bridges and flow stoppage were obtained by decreasing the ellipticity of the yield curve below its original value (2, Hibler, 1979), to increase the ~~area of the yield envelope in the second (or fourth) quadrant in the space of the principal stresses σ_1 and σ_2 (~~shear and *uniaxial compressive strength* of the ice (see Fig. 2~~), corresponding to a cohesive state . This effectively increases the uniaxial unconfined compressive strengthσ_c (the maximum value of σ_1 that the material can sustain when $\sigma_2 = 0$, see Fig. 2, stress state 3). Rasmussen et al. (2010) also~~ , stress state 2), which increases its cohesive strength. Rasmussen et al. (2010) performed numerical simulations of the sea ice dynamics in Nares Strait and the North Water Polynya ~~,~~using the dynamic-thermodynamic CICE sea ice model, ~~the ice mechanics component of which is also based on a viscous-plastic rheologyand elliptical yield curve (Hunke, 1997)~~based on the EVP rheology. The authors noted a lack of stability and shorter lifespan of the simulated ice bridges, leading to a slower opening and lower extent of the North Water polynya and to an earlier draining of Nares Strait compared to estimates from satellite imagery. They attributed this deficiency to a too low ice strength in their model, either caused by a too thin ice cover or to the inability of their rheology to reproduce the correct internal strength of sea ice.

Channel flow simulations have not yet been performed using elastic-brittle models. Hence such experiments constitute an interesting test case of their mechanical behaviour. Moreover, while other rheological models have been shown to simulate both the occurrence of ice bridges and flow stoppage, it is not at all clear if these models, even with a fine spatial resolution (e.g., ~~0.32° degrees or~~ 4 km ~~to 10 km between~~ in the Lincoln Sea~~and~~ , about 7 km at the constriction between Kane Basin and Smith Sound and 10 km in Baffin Bay in the model of Rasmussen et al. (2010) and ~~0.15° × 0.04° degrees~~ about 3 km by 4 km in the realistic simulations of Nares Strait of Dumont et al. (2009)), are also able to account for the presence of *multiple* arch-like leads within and upstream of the channel, as observed from satellite imagery ~~(e.g., see Fig. 1b and Sodhi, 1977).~~(e.g., see Fig. 1b). In coupled thermodynamic and dynamic models, a high density of leads is expected to impact the simulated heat fluxes between the atmosphere, the ice and the ocean (Smith et al., 1990). With its capability to represent the extreme localization of damage and deformation (Dansereau et al., 2016), the Maxwell-EB model might be ~~better~~ suited to simulate these fine features.

Ice drift and coverage conditions within a channel moreover represent a severe test of the numerical scheme in terms of handling discontinuities within the simulated fields, as once a stable ice bridge forms, the ice downstream detaches from the bridge and is driven out of the channel without mechanical resistance. At this point, extremely sharp gradients in ice velocity, thickness and concentration are expected to arise (see Fig. 1b and 3a).

2.2 Ice ridges

Sea ice models are most often compared to each other and to observations in terms of the spatial distribution of the simulated ice thickness (e.g., Johnson et al., 2012). An equally important, and perhaps more appropriate, metric to investigate the mechanical behaviour of the sea ice cover is the probability density function (PDF) of the ice thickness, of which some valuable information

have been available for some time from drill-hole, ~~sub-marine mounted~~ submarine-mounted sonar and airborne electromagnetic sounding measurements (Lindsay, 2003). In particular, the tail of PDFs represents the ice that has thickened, not only due to thermodynamic but also to mechanical redistribution processes~~, i. e, the ice~~ . This ice is incorporated in pressure ~~ridges~~*ridges*, which are long, linear rubble piles of ice ~~,~~ meters or tens of meters wide ~~,~~ formed under convergent and shearing motions. A recurrent statistical property of the tail of ~~these PDFs~~ the PDF of ice thickness is that it appears to fit a negative exponential function (Wadhams, 1994; Haas, 2009). To this day, it is not clear why it takes this particular form. The important point however is that it ~~indicates the~~ is the signature of the tendency of mechanical redistribution to ~~create extremes (Thorndike et al., 1975), or, in~~ "create extremes" (Thorndike et al., 1975). In other words, it characterizes the strong localization of the thickest ice in space.

Over the years, there have been different attempts to represent the formation of pressure ridges in numerical ~~simulation~~ simulations of the sea ice cover (e.g., Parmerter and Coon, 1972; Kovacs and Sodhi, 1980; Hopkins, 1994), but no model is yet capable of describing the entire process. Continuum sea ice models typically have a spatial resolution of a few kilometers to tens of kilometers and hence do not resolve ridges per se. In such models, two main approaches are taken to handle the redistribution of ice thickness associated with ridge building.

The so-called multi-thickness categories scheme based on the ~~pioneer~~ pioneering work of Thorndike et al. (1975) and Rothrock (1975) is widely used in current sophisticated sea ice and coupled models. This scheme introduces an areal thickness distribution function which evolves in time due to both thermodynamics and dynamics processes. Ridging is treated "explicitly" by allowing a prescribed thin ice portion of the thickness distribution to be redistributed into thicker ice categories in response to the simulated deformation. The main advantage of this scheme is that it allows accounting for variations in the ice thickness at the sub-grid scale. The relation between the redistribution process and the strength of the ice (often characterized by a pressure, P) in this modelling framework is ~~however dubiously~~ based on energy conservation principles ~~(~~: the deformational work is equated to the work done in building ridges, which is partitioned between potential energy changes (Thorndike et al., 1975), the frictional dissipation in ridging (Rothrock, 1975) and dissipation in shearing deformation (Pritchard, 1981), all of which ~~being~~ are very hard to estimate~~).~~ . This theory does not take into account other mechanisms such as crushing, buckling, flexural breakage, inelastic contacts and frictional sliding contacts between rubble ice blocks (Hopkins, 1998). As the simulated strain rate tensor does not provide directly the information on the relative amount of opening and ridging (and also sliding) within the ice cover, expressions for the modes of redistribution need to be assumed, the correct form of which remain uncertain to this day (Hunke et al., 2010). These redistribution functions can be set in an ad-hoc manner (Thorndike et al., 1975), estimated empirically from strain rates observations (Stern et al., 1995) or, in the case of plastic models such as the VP and EVP models, determined based on the prescribed form of the yield criteria and flow rule (Rothrock, 1975; Hibler, 1980; Flato and Hibler, 1995). The multi-categories ~~schemes also introduce~~ scheme introduces several additional parameters (e.g., a frictional dissipation coefficient, a prescribed percentage of the thickness distribution participating in the ridging, ...), which are all ~~badly~~ poorly constrained and to which the simulated thickness distribution and patterns can be highly ~~sensible (Flato and Hibler, 1995; Bitz et al., 2001). Moreover, it~~ sensitive (Flato and Hibler, 1995; Bitz et al., 2001). This framework necessitates solving an additional evolution equation for the thickness distribution function as well as thermodynamics and

transport equations for multiple ice thicknesses, which increases the cost of numerical schemes as the number of ice categories is increased.

The second approach is the simpler two-level model suggested by Hibler (1979) in which the simulated ice cover falls into two thickness categories: the effective thickness, representing the average ice thickness ~~over~~ of the ice-covered portion of a model grid cell, and zero thickness, or open water. As opposed to the multi-category scheme, ridge building is treated implicitly ~~(~~based on a volume conservation principle~~, see section 3)~~. Known shortcomings of this model when coupled to a VP (or EVP) rheological framework are the underestimation of ice thickening in regions of convergent and shearing ice motion~~compared to the multi-categories scheme, due to the unresolved~~ , which has been attributed to the unresolving of thin ice that participates in ridge building. This process has been more adequately simulated at the cost of increasing the number of ice thickness categories in a multi-categories redistribution scheme (e.g., Bitz et al., 2001). ~~Nevertheless, it is still unclear to this day if, when incorporated in viscous-plastic type models, either of~~

Here, we use a very simple redistribution scheme to test the capability of the ~~two-level scheme or the multi-categories scheme, even when tuned, is able to reproduce the form of tail of the PDFs calculated from Arctic sea ice thickness measurements (e.g., Flato and Hibler, 1995)~~Maxwell-EB rheological framework to reproduce the observed strong localization of thick ice in space.

3 The Maxwell-EB sea ice model

The Maxwell-EB model builds on the continuum Elasto-Brittle (EB) rheology, which has been used to model the fracturing of rocks (e.g., Amitrano et al., 1999) and was implemented for sea ice modelling by Girard et al. (2010) and Bouillon and Rampal (2015); Rampal et al. (2015). As the EB model is based on a linear-elastic constitutive law, it does not ~~solves~~ solve simultaneously for both the elastic (reversible) deformations associated with the fracturing of the ice pack and the permanent (irreversible) deformations occurring once the ice pack is fractured and ice floes move relative to each other. Therefore, it does not allow estimating ice drift velocities unambiguously. The Maxwell-EB model was developed to deal with these intrinsic shortcomings of the EB framework. This mechanical model has been described in full ~~details~~ detail by Dansereau et al. (2016). Here we only ~~recall~~ review its essential features and present the full system of equations and its numerical treatment in Appendix A.

In this augmented rheology, a ~~passage~~ transition between the small/elastic and large/permanent deformations is made possible by the addition of a viscous-like relaxation term in the linear-elastic constitutive law for a compressible, continuous solid ~~(see Dansereau et al. (2016), Eq. (4)).~~ (Dansereau et al., 2016). Associated with the linear elastic term in this constitutive equation (Eq. (A2)) is the true elastic modulus (E) of the material, i.e., of sea ice, at the scale of the model grid cell. The viscosity, η, associated with the viscous term, is *not* the true bulk viscosity of sea ice, but an apparent viscosity that represents the flow resistance of the fractured/fragmented ice cover averaged over the grid cell. The ratio of the two mechanical properties, $\lambda = \frac{\eta}{E}$, has the dimension of a time, and sets the rate of dissipation of the stress through permanent viscous-like deformations. Alternatively, it quantifies the capability of the ice pack to retain the memory of elastic deformations. In the Maxwell-EB model,

these three mechanical parameters vary with the local level of damage of the material, quantified by a scalar variable d that evolves between 1 for an undamaged and 0 for a "completely damaged" ice cover.

Damage occurs when the state of stress becomes overcritical with respect to a Mohr-Coulomb failure criterion or a tensile cut-off. The combined criteria are represented in Fig. 2 (thick ~~solid~~ black lines) in the principal stresses space ~~,~~ (σ_1, σ_2), with the convention that compressive stresses are positive. With such criterion, ~~the~~ uniaxial (unconfined) compressive strength, σ_c, ~~and maximum~~ uniaxial tensile strength, σ_t, ~~are~~ (and biaxial tensile) strength are accounted for and are directly related to a cohesion parameter C ~~as~~ as

$$\sigma_c = \frac{2C}{(\mu^2+1)^{1/2}-\mu}, \tag{1}$$

$$\sigma_t = -2C(\mu^2+1)^{1/2}+\mu. - \frac{\sigma_c}{q}, \tag{2}$$

[1] where μ is the internal friction coefficient and $q = \left[(\mu^2+1)^{1/2}+\mu\right]^2$ is the slope of the Mohr-Coulomb failure envelope in the internal stress space. In the model, the damage criterion varies spatially, as some disorder in C is introduced at the local scale to represent the natural heterogeneity of the ice cover associated with the presence of various defects (e.g., brine pockets, thermal cracks) as well as of different ice types (first year versus multi-year ice), floe sizes and arrangments at the sub-grid scale~~(Dansereau et al., 2016; Weiss and Dansereau, 2017).~~ . This heterogeneity ensures the progressive failure of an initially undamaged ice cover even under fully homogeneous forcing conditions (Dansereau et al., 2016).

A healing mechanism counterbalances the effects of damaging over much larger time scales and represents the refreezing of leads. This mechanism is distinct ~~and independent~~ from pure thermodynamic growth as it allows the level of damage variable to re-increase and recover *at most* the undamaged value of $d = 1$ (see Dansereau et al. (2016), section 3.3.2). Both processes, damaging and healing, are combined in a single equation for the evolution of ~~damage (see Dansereau et al. (2016), eq. 17~~d (Eq. (A3)).

The coupling of E, η and λ with d (Eq. 18 to 20, Dansereau et al., 2016) is such that the mechanical strength, as well as the capability of the material to retain the memory of elastic deformations, decreases with increasing damage $(d \to 0)$ and increases with healing~~(see Dansereau et al. (2016), Eq. (18) to (20)).~~ . It is this coupling of the mechanical properties ~~and~~ with the level of damage of the ice cover that allows the model to dissipate internal stresses in large, permanent deformations along ~~faults, or leads ,~~ leads once the ice pack is highly damaged ~~,~~ while reproducing the small deformations associated with the fracturing process and retaining the memory of elastic deformations over relatively low damage areas.

Analyses of the deformation and damage fields simulated using idealized geometries, simple forcing conditions and mechanical parameters values consistent with sea ice on geophysical scales (Dansereau et al., 2016) have demonstrated that the Maxwell-EB rheological framework successfully reproduces the anisotropy of sea ice deformation as well as the strong strain localization in both space and time and associated spatial scaling laws (Stern et al., 1995; Kwok, 2001; Marsan et al., 2004; Rampal et al., 2008, 2009; Weiss, 2008). The observed spatial and temporal coupling between these scalings is also repre-

[1] Note that there is an error in the expression for σ_t, Eq. 10, in Dansereau et al. (2016): $\sigma_t = -\frac{\sigma_c}{q}$, but $\sigma_t \neq -2C\left[(\mu^2+1)^{1/2}+\mu\right]$.

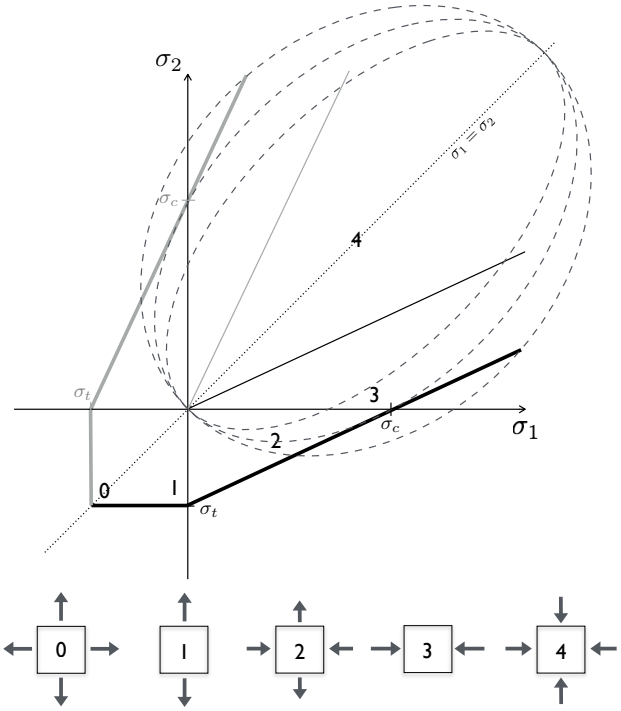

Figure 2. Damage criterion in the Maxwell-EB model represented symmetrically in the principal stresses plane (thick solid ~~line~~lines)~~, which are defined here as $\sigma_1 = \frac{(\sigma_{11}+\sigma_{22})}{2} + \sqrt{\left[\frac{\sigma_{11}-\sigma_{22}}{2}\right]^2 + \sigma_{12}^2}$ and $\sigma_2 = \frac{(\sigma_{11}+\sigma_{22})}{2} - \sqrt{\left[\frac{\sigma_{11}-\sigma_{22}}{2}\right]^2 + \sigma_{12}^2}$~~. The thin solid lines radiating from the origin represent the damage criterion in the case of no cohesion ($C = 0$). The ellipses represents the yield criterion in the standard VP model of Hibler (1979) for different aspect ratios (< 2, outer; 2, center; > 2, inner ellipse). The numbers ~~1~~ 0 to 4 indicate the states of (0) biaxial tension, (1) uniaxial tension, (2) biaxial tension and compression, (3) uniaxial compression and (4) biaxial compression.

sented (Weiss and Dansereau, 2017). Sensitivity analyses on the damage parameter α~~(see Weiss and Dansereau (2017))~~, which sets the rate of viscous dissipation of the internal stress as a function of the increasing level of damage of the ice cover, have shown that the model, with few independent variables, can represent a large range of mechanical behaviours: from a regular, predictable stick-slip with a single damaging frequency related to the prescribed rate of healing, to a marginally stable, unpredictable deformation with temporal correlations in the damaging activity at all time scales below the material's healing time (Weiss and Dansereau, 2017). Over a range of values of this parameter, the model reproduces both the persistence of creeping leads in the ice cover and the activation of new leads with different shapes and orientations (Dansereau et al., 2016; Weiss and Dansereau, 2017).

In the channel flow simulations presented here, this new rheological model is implemented in a continuum modelling framework typical of regional and global sea ice models. In such framework, the ice cover is ~~assimilated to~~ simulated as a 2-dimensional plate. Hence plane-stresses are assumed. The motion of the ice is described by the following Navier-Stokes type

equation:

$$\rho h \left[\frac{\partial \mathbf{u}}{\partial t} + (\mathbf{u} \cdot \nabla)\mathbf{u} \right] = A(\tau_a - \tau_w) - \rho h f \mathbf{k} \times \mathbf{u} - \rho h g \nabla H + \nabla \cdot (h\sigma), \tag{3}$$

with $\mathbf{u}$, the ice velocity, σ, the stress tensor, ρ, the ice density, τ_a and τ_w, the air and water drags, $-\rho h f \mathbf{k} \times \mathbf{u}$, the Coriolis pseudo-force with f, the Coriolis parameter and $\mathbf{k}$, the upward unit vector normal to the ice surface and $-\rho h g \nabla H$, the force due to gradients in the sea surface dynamic height, H, with g, the gravitational acceleration, and which can be expressed ~~alternatively~~ in terms of the geostrophic ocean current velocity, $\mathbf{u}_w$ (e.g. Thomson et al., 1988).

In this 2-dimensional momentum equation, the variables h and A represent respectively the mean ice thickness and ice concentration over a model grid cell. The mean thickness~~is assumed to be~~ , h, is the weighted sum of ~~two ice categories: thick ice , with thickness $h_{thick} = \frac{h}{A}$, and open water, with thickness$h_{thin} = 0$ m (Hibler, 1979). Mass~~ the average ice thickness over the ice-covered portion of the grid cell, h_{thick}, often referred to as the thickness of thick ice (e.g., Hibler, 1979), and the remaining open water (zero thickness). Hence $h = h_{thick} A$.

In the present uncoupled implementation of the Maxwell-EB model, thermodynamic processes are not accounted for. The ice density is considered constant and for $0 \leq A \leq 1$, mass conservation is ensured by the following evolution ~~equation for h:~~

$$\frac{\partial h}{\partial t} + \nabla \cdot (h\mathbf{u}) = S_h,\ h \geq 0,$$

~~where the term S_h represents the ice thickening/thinning through thermodynamic processes and~~ equations for the ice concentration and mean thickness of the ice-covered portion of the grid cell:

$$\frac{\partial A}{\partial t} + \nabla \cdot (A\mathbf{u}) = 0, \tag{4}$$

$$\frac{\partial h_{thick}}{\partial t} + \mathbf{u} \cdot \nabla h_{thick} = 0. \tag{5}$$

Ice thickening through mechanical redistribution, i.e., ~~through~~ pressure ridge formation~~.~~

~~In the present implementation of the Maxwell-EB model, the mechanical redistribution~~ , is accounted for in a very simple manner. This is done on purpose, to test the input of the new rheology in the representation of the thickness distribution. ~~Following the parametrizations of Hibler (1979), Thomson et al. (1988) and Lietaer et al. (2008), an evolution equation for the ice concentration is first solved~~

$$\frac{\partial A}{\partial t} + \nabla \cdot (A\mathbf{u}) = S_A,\ 0 \leq A \leq 1.$$

~~where S_A accounts for both the thermodynamics and mechanical sources and sinks of ice concentration.~~ If as a result of convergent ice motion, the ice coverage A over a given model element exceeds unity, the excess concentration, ~~$\max[0, (1 - A)]$~~$\max[0, (A - 1)]$, is used to increment the ~~thickness of thick ice~~ ice thickness over that element, and the ice concentration is reset to 1 (see Appendix A, section A2.1). The mechanical ~~contribution (sink) to S_A~~ sink of A in this case reads:

$$A^- = -\max[0, (A - 1)] \tag{6}$$

and the associated mechanical ~~contribution (source) to S_h in eq. 5 is~~ source of h_{thick}, equivalent to h for $A = 1$, is

$$h_{thick}{}^{+} = \max[0,(1-A)]\max[0,(A-1)]h_{thick}. \quad (7)$$

This redistribution scheme implies that ridging does not occur for $A < 1$. In the absence of quantitative observational support for the dependance of the amount of ridging on sea ice concentration, we chose the simplest possible approach.

Finally, the mechanical parameters E and η are coupled to the ice concentration A, as follows :

$$E = f_1(E^0, d)\exp\left[-c^*(1-A)\right], \quad (8)$$

$$\eta = f_2(\eta^0, d)\exp\left[-c^*(1-A)\right], \quad (9)$$

with E^0 and η^0, the elastic modulus and apparent viscosity of an undammaged ice cover, f_1 and f_2, the functional dependence of E and η on ~~the level of damage of the ice cover~~ d, given respectively by Eq. (18) and (19) in Dansereau et al. (2016), and c^* a non-dimensional, constant parameter. The ~~functional~~ dependence on the ice concentration follows the one suggested by Hibler (1979) and widely employed in VP models for the pressure term (P)~~setting~~ , which sets the ice strength in compression. The exponential function of A simply allows the value of both E and η to be maximal when the ice concentration is ~~of~~ 100% ($A = 1$) and to decrease rapidly when leads open and A drops ($\sim 10\%$ at $A = 90\%$, representing essentially a free drift state). It is employed to characterize the dependence of the elastic modulus (or effective elastic stiffness) on A in the elasto-brittle models of Girard et al. (2010) and of Bouillon and Rampal (2015). In the case of η, this parametrization is compatible with the rapid decay of the apparent viscosity of granular media when decreasing their packing fraction from the close-packed limit (Aranson and Tsimring, 2006). In the present implementation of the Maxwell-EB model, this simple parametrization as well as the value of the non-dimensional parameter c^* is the same for both mechanical parameters, but this could ~~eventually~~ be refined in future developments of the rheology.

4 Channel flow simulations

The drift of sea ice within Nares Strait is thought ~~of being~~ to be primarily driven by the prevalence of ~~sturdy~~ northerly winds associated with the strong pressure gradient between the Lincoln ~~sea~~ Sea to the north and Baffin Bay to the south, and which are orographically channelled by the steep coastal topography of Ellesmere Island and Greenland (Ingram et al., 2002; Gudmandsen, 2004; Samelson and Barbour, 2008; Münchow, 2016). The most recurrent location for an ice bridge is in the southern Kane Basin (see Fig. 1c) (Kwok et al., 2010)~~)~~, where a stable arch is observed to form almost every year between November and March (Barber et al., 2001) as a result of the convergence of a mixture of first and multi-year ice into Kane Basin ~~(Kwok et al., 2010; Gudmandsen, 2004)~~(Gudmandsen, 2004; Kwok et al., 2010). Disintegration of the ice cover downstream of this arch leads to the opening of the North Water polynya (see Fig. 1c) in Smith Sound (Barber et al., 2001; Ingram et al., 2002).

In both the idealized and realistic simulations presented here, we aim to reproduce the formation of such an ice bridge. In the idealized case, the domain consists in a 120 km wide rectangular basin that converges into a 40 km wide, 40 km long

channel (see Fig. 3b). The geometry, similar to that used in the idealized simulations of Dumont et al. (2009), is conceived to be roughly consistent with the shape of the constriction between Kane Basin and Smith Sound (dashed box, Fig. 3a). This simple configuration, symmetric with respect to the $y-$axis, facilitates the analysis of the dynamical behaviour of the model and, in particular, of the simulated states of stress. The dynamics described in the next section is however not specific to this geometry : simulations were also performed over different domains (narrower, longer channels, smaller basins) and produced similar results. The realistic domain covers the entire Strait down to ~~northern~~ Smith Sound (see Fig. 1c, grey shading). This configuration allows investigating the formation of secondary arches in various locations as well as other phenomena related to the presence of topographic features such as islands and fjords. In this case the mesh was built using the Gmsh mesh generator (Geuzaine and Remacle, 2009) and the GSHHG high resolution shoreline data (http://www.soest.hawaii.edu/pwessel/gshhg/) between 73 and 85° N and 280 and 320° W. This data is available in geodetic longitude/latitude on the WGS-84 ellipsoid. Here it is converted ~~in~~ to Cartesian coordinates using a stereographic projection. The projection is centered on the North Pole, with the Greenwich meridian aligned on the positive x-axis and the Strait ~~is~~ roughly oriented along the y-axis (see Fig. 3a).

The prescribed wind forcing is made as simple as possible to facilitate the analysis. Consistent with observations of orographic channelling, ~~a uniform~~ an along-channel, i.e., ~~northerly~~southward, wind stress, τ_a, is applied. The stress is spatially uniform and increased steadily between 0 and 1 Nm^{-2} over a period of 24 hours, and then held constant, to simulate the passage of a storm (Kwok, 2006; Samelson et al., 2006; Samelson and Barbour, 2008). Considering a simplified quadratic wind drag based on the absolute, instead of the relative, wind speed of the form

$$\tau_{\mathbf{a}} = \rho_a C_{da} |\mathbf{u}_a| \mathbf{u}_a, \tag{10}$$

with $\mathbf{u}_a$, the wind velocity, $\rho_a = 1.3\ \mathrm{kg\ m}^{-3}$, the surface air density and C_{da}, the air drag coefficient, commonly set to $1.2{\cdot}10^{-3}$ in sea ice models following Hibler (1979), this corresponds to a maximum wind speed of $\sim 22\ \mathrm{ms}^{-1}$ ($\sim 82\ \mathrm{km\ h}^{-1}$). The ocean is at rest ($\mathbf{u}_w = 0$), hence the oceanic drag is given by the following quadratic formula

$$\tau_{\mathbf{w}} = \rho_w C_{dw} |\mathbf{u}| \mathbf{u}, \tag{11}$$

where $\rho_w = 1027\ \mathrm{kg\ m}^{-3}$ is the density of sea water and C_{dw} is the drag coefficient, set to $5.5 \cdot 10^{-3}$ (McPhee, 1980). ~~Following Gray and Morland (1994), both drag terms are weighted by the local ice concentration (see Eqn. 3) to account for the fraction of open water within a grid cell.~~

~~Together with the constitutive equation (eqn. 4, Dansereau et al. (2016), 3 components), the damage equation (eqn.17, Dansereau et al. (2016)) and an equation for the transport of the cohesion, C, that sets the local value of the damage criterion, Eq. (two horizontal components), and above form a system of nine equations that are solved for the nine variables σ (3 components), $\mathbf{u}$ (2 components), d, C, h, A.~~ In both the idealized and realistic simulations, ~~a reduced form of the~~ the Coriolis term in the the momentum equation (3) is ~~solved in which the acceleration and advection terms are neglected. To~~ discarded to retain symmetry in forcing conditions~~, the Coriolis term is also set to zero. As the~~ . The ocean is at rest, hence the force associated with gradients in the sea surface dynamic height is also zero. ~~All other quantities (σ, d, C, h, A) are advected~~

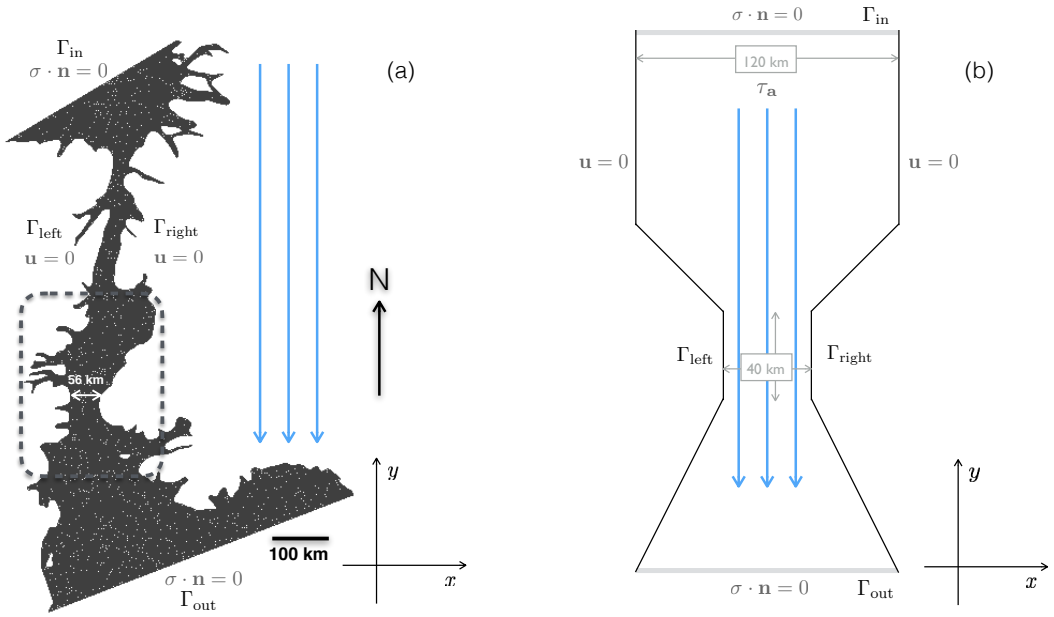

Figure 3. ~~(a)~~ Domain and boundary conditions for (a) the realistic simulations of Nares Strait and (b) the idealized simulations of the constriction point between Kane Basin and Smith Sound (dashed box, panel a).

~~with the ice flow. Thermodynamics~~ As the goal of these numerical experiments is to investigate the dynamical behavior of the Maxwell-EB model, thermodynamic processes are not accounted for~~, hence S_h and S_A in Eqn. 5 and 6 represent only the mechanical redistribution of ice thickness and concentration~~. Simulations are therefore analyzed over a short period of time (3 days).

Mechanical parameter values are based on measurements within sea ice. An undamaged elastic ~~modulus~~ (Young's~~modulus) of $E^0 = 5.0 \cdot 10^8$ Pa)~~ modulus of $E^0 = 5.85 \cdot 10^8$ Pa, on the order of that used by Girard et al. (2010) and consistent with an elastic shear wave speed of 500 ms^{-1} in an heterogeneous ice pack (Marsan et al., 2011) is considered. Poisson's ratio is set to $\nu = 0.3$ (Timco and Weeks, 2010). The undamaged relaxation time, λ^0, is set to 10^7 s (~ 115 days), a value that allows the numerical scheme to converge, while also ensuring that non-physical viscous dissipation over low damage areas of the ice cover is insignificant (Dansereau et al., 2016). The characteristic time for the healing process, t_h, which corresponds to the time required for the local level of damage d to re-increase from 0 to 1, is set to $5 \cdot 10^5$ s (~ 5.7 days) based on estimates of ice growth within open leads: Petrich et al. (2007) reported a time for the growth of 1 m of ice within an opening of 10 cm under air temperatures of $-15°$C between 10^5 and 10^6 seconds. ~~As~~ A constant healing rate is used (see Eq. (A3)). As thermodynamic processes are not accounted for and as healing is meant to represent only the local recovery of the ice mechanical strength within refreezing leads, not the thermodynamic growth of ice within polynyas, healing ~~in the simulation~~ is turned off as soon as the ice concentration locally drops below 75% in the simulations, which occurs when and where the ice detaches from a stable ice bridge ~~.~~ or from the coast. This avoids unphysical situations where healing would cause d to reincrease towards the

undamaged value of 1 over low ice concentration or even open water areas. As the dependancy of the mechanical parameters on the ice concentration (Eq. (8) and Eq. (9)) ensures that the rheology term drop to less than 1% of its undamaged value for $A = 75\%$, including this threshold has no significant impact on the results presented here. Table 1 summarizes all model parameter values employed in the simulations presented here.

As a determining factor for the formation of stress-free ~~surface~~ surfaces is the cohesive ~~nature~~ strength of the material, simulations with a different range of values of cohesion were compared. The field of C was set as ~~in quenched disorder as~~ follows. First, its spatial distribution for all simulations using the idealized or realistic domain was obtained by randomly ~~by~~ drawing a value in the non-dimensional interval $[1, 2]$ over each model element. This noise was then multiplied by a minimum value of cohesion, C_{min}, such that $C \in [C_{min}, 2 \times C_{min}]$. This minimum cohesion was varied between $2, 5, 10, 20, 30$ kPa. Hence, the same *spatial distribution* of C was used in all simulations, but the magnitude of C was varied between simulations. In all simulations, the disorder introduced in the field of cohesion is quenched (Herrmann and Roux, 1990): it is set once, at the beginning of each simulation, and is passively advected with the ice flow. It is important to note that this disorder, because it is set randomly, does not introduces spatial correlations in the model. Therefore, it does not prescribe the location of the simulated ice leads and bridges. The largest values of C employed are consistent with in-situ stress measurements in the Beaufort Sea reported by Weiss et al. (2007) and Weiss and Schulson (2009) (see Fig. 8a). According to the presumed scale effect on shear strength, set by the size of the defects~~(thermal cracks, brine pockets, ...)~~ /heterogeneities present in the ice cover (Schulson, 2004; Weiss et al., 2007), lower values of C are consistent with larger ~~defect~~ defects/heterogeneties sizes and a lower shear strength.

~~In all simulations , the ice is initially undamaged ($d = 1$) and has a uniform~~ All simulations are initialized with a uniform ice thickness of 1 m. ~~Although a higher value of h would perhaps be more representative of the mean thickness of the mixture of first year and multi-year ice reported in the Strait (0.9 to 1.6 meters, Haas et al., 2006)~~This value is consistent with the median ice draft in Nares Strait over the 2003-2012 period reported by Ryan and Münchow (2017). Moreover, we find that the evolution of the simulated fields described in the following sections does not depend on ~~this prescribed initial~~ the specific value of the initial ice thickness, as long as the coverage is initially uniform. The domain is initially completely covered with undamaged ice ($A = 1$, $d = 1$), so that the location of ice bridges is not prescribed. Simulations are started from rest. A no-slip condition ($\mathbf{u} = 0$) is applied at the lateral boundaries Γ_{left}, Γ_{right}, representing the coasts (see Fig. 3a and b). The channel is open at its top (Γ_{in}) and bottom (Γ_{out}) boundaries with the Neumann condition $\sigma \cdot \mathbf{n} = 0$. The value of all transported quantities is prescribed on ~~the upstream part of~~ Γ_{in} and Γ_{out} and represent undamaged ice entering the channel~~through Γ_{in}~~ (, i.e., with $d = 1$, $A = 1$, $h = 1$ m, $\sigma = 0$~~) and open water through Γ_{out} ($d = 0.1$, $A = 0$, $h = 0$ m, $\sigma = 0$)~~ and with C randomly drawn from the same uniform distribution prescribed as initial conditions.

The model is entirely developed within the C++ environment RHEOLEF (Saramito, 2013a). The numerics is based on finite elements and variational methods. The equations of motion are cast in the Eulerian frame and discontinuous Galerkin methods are used to handle advective processes (Saramito, 2013b), as well as the non-linear terms arising in the objective derivative of

Parameters		Values
Internal friction coefficient	μ	0.7
Ice density	ρ	$900\ \mathrm{kg\ m^{-3}}$
Undamaged elastic modulus	E^0	$E^0 = 5.0 \cdot 10^8$ Pa
Undamaged apparent viscosity	η^0	$10^7 \times E^0$ Pa s
Undamaged relaxation time	λ^0	10^7 s
Minimum cohesion	C_{min}	$2, 5, 10, 20, 30$ kPa
Damage parameter	α	4
Characteristic time for damage	t_d	4 s (idealized sim.), 6 s (realistic sim.)
Characteristic time for healing	t_h	$5 \cdot 10^5$ s
Mean model resolution	Δx	2 km (idealized sim.), 3 km (realistic sim.)
Model time step	Δt	4 s (idealized sim.), 6 s (realistic sim.)
	c^*	20
Air drag coefficient	C_{da}	$1.5 \cdot 10^{-3}$
Air density	ρ_a	$1.3\ \mathrm{kg\ m^{-3}}$
Water drag coefficient	C_{dw}	$5.5 \cdot 10^{-3}$
Water density	ρ_w	$1027\ \mathrm{kg\ m^{-3}}$

Table 1. Model parameters for the idealized and realistic channel flow simulations.

the stress tensor (see ~~(Dansereau et al., 2016)~~Appendix A). Polynomial approximations of degree 1 are used for the velocity field and all advected fields (σ, A, h, d, C) are piecewise constant. Appendix A presents the details of the numerical scheme.

Unstructured meshes with triangular elements are used. The average spatial resolution, Δx, is constant. It is of 2 km in the idealized simulations and of 3 km in the realistic simulations. The ~~results presented here are not sensitive to the choice of Δx over the range of Δx that allows resolving the flow of ice through the constriction (i.e., the narrowest) point of the channel.~~

~~The numerical scheme is divided into linear sub-problems. A semi-implicit scheme is used to linearize the momentum and constitutive equations. The internal stress term in the momentum equation is discretized using an implicit scheme while the water drag term is linearized as $\tau_{\mathbf{w}} = \rho_w C_{dw} |\mathbf{u}^n| \mathbf{u}^{n+1}$ and the ice thickness and concentration are taken at the n^{th} time step . In the constitutive equation, the advection, rotation and deformation terms of the internal stress tensor (see Dansereau et al. (2016), Eqn.~~ time step is of 4 ~~and 5) as well as the ice concentration are taken at the n^{th} time step. The momentum, constitutive and damage equation are solved simultaneously in time as follow. First the momentum and constitutive equations are solved for σ^{n+1}, using the level of damage at the previous (n^{th}) time step. Then σ^{n+1} is used in the damage equation, linearized using an explicit scheme, to estimate d^{n+1} and the level of damage is updated in the constitutive equation. A fixed point iterates this operation until the residual on σ drops below a chosen tolerance. Then the resulting field of $\mathbf{u}^{n+1}$ is used to solve the cohesion, ice thickness and concentration equations, all linearized using an explicit scheme. Redistribution of the ice thickness and the associated adjustment of the ice concentration is finally applied where $A > 1$. While the advection, rotation and deformation~~

terms in the constitutive equation could be updated in the fixed point iteration, we find that this does not significantly affect the solution since the time step employed in the simulations is taken very small (6 s for $\Delta x = 3$ km and 4 s for $\Delta x = 2$ km) in order to simulate the propagation of damage over the ice cover with the highest possible resolution(see Dansereau et al. (2016)). Similarly, the ice thickness and concentration could also be solved for using an implicit scheme and be updated as part of s in the fixed point iteration. However, variations in the mechanical parameters associated with changes in h and A are small and slow compared to the changes due to damaging. Hence we find that solving for these equations explicitly does not impact the solution. idealized and of 6 s in the realistic simulations. The results obtained here are not conditional to the choice of spatial resolution, as long as it allows resolving the flow of ice through the narrowest point of the channel with the no-slip boundary condition.

5 Results

5.1 Dynamical behaviour

Here we investigate the formation of arches and stable ice bridges in the Maxwell-EB model and analyze the evolution of the simulated level of damage, ice velocity and internal stresses.

Idealized and realistic simulations with a different range of values of C (see section 4) were compared.

The evolution of the applied wind forcing (dashed line) and of the damage rate (solid grey line), defined as the number of damaged elements per model time step times their respective distance to the Mohr-Coulomb or tensile damage criterion (see Dansereau et al. (2016)), is represented in the case of one idealized for one idealized and one realistic simulation using $C_{min} = 20$ kPa in Fig. 4a . The spatial distribution and Fig. 6a respectively. The spatial distributions of the level of damage is and ice concentration are shown at three different stages of the forcing (numbered 1, 2, 3) for this idealized simulation in these two simulations on Fig. 4band at the corresponding stages in a realistic simulation using $C_{min} = 20$ kPa in , c and Fig. 6ab, c. We first discuss the idealized simulations results and then comment on the realistic case.

5.1.1 Idealized simulations

In all simulations using different values of C_{min}, high deformation rates first concentrate along narrow, concave damaged features that form in the interior and downstream of the channel (Fig. 4b, panel 1). The profile of the y-component of the ice velocity, u_y (red curve), for the simulation with $C_{min} = 20$ kPa shown in Fig. 4 is plotted along the central meridional axis (see of the idealized domain (red curve, Fig. 5a, stage 1)). It shows that after the onset of damaging (indicated by the first peak in damage rate on Fig. 4a), the ice over this portion of the domain is set in motion while the undamaged ice upstream remains motionless . (Fig. 5a, stage 1). The sharp no-flow transition coincides with the constriction point that defines the entrance to the channel, across which an ice arch has clearly formed . formed (see Fig. 4c). It is important to note that here, "no-flow" or, as later mentioned, "flow stoppage" is not defined as a zero drift speed, but rather as a drift velocity on the order of that associated

with strictly elastic deformations within an undamaged ice cover ~~.~~(here, $|\mathbf{u}|$ is on the order of 10^{-5} ms^{-1} before the onset of damage).

As the wind forcing is further increased, damage propagates upstream of the channel, which corresponds to the second peak in the damage rate seen on Fig. 4a. Linear converging features form along both sides of the channel, leaving some ~~relatively undamaged, stagnant ice~~ stagnant ice with low damage near the coasts in the converging part of the basin (see Fig. 4b, panel 2). This creates an inner flow channel, inside of which the ice is set in motion everywhere and the drift is almost uniform (see Fig. 5, panel 2). Similar results were also obtained by Dumont et al. (2009) and are consistent with the observed jamming of grains and sand along the walls of a silo (Munch-Andersen, 1986; Munch-Andersen et al., 1992) as well as with previous discrete elements (Morrissey et al., 2013) and continuum (Wang and Ooi, 2015) model simulations of the discharge of a granular solid in a silo.

Up to that point, the overall spatial and temporal evolution of damage is similar between the simulations using different ranges of cohesion. However, as the local value of C sets the local damage criterion in the Maxwell-EB model, i.e., the local value of σ_c and σ_t, the minimum value of cohesion over the domain controls the timing of the onset of damaging in the simulations, with damaging occurring sooner as C_{min} is lower. ~~Furthermore, the width of the distribution of C impacts the rate of propagation of the damage, with the propagation being more progressive for a larger distribution.~~

Beyond this point, drift velocities in the middle of the domain progressively decrease as ice converges into the inner ice channel (not shown). The simulated dynamics then ~~differs~~ differ between the simulations using different values of C. For the smaller values of cohesion used ($C_{min} = 2, 5, 10$ kPa) ~~the ice arch~~ ice arches that form at the opening of the channel eventually collapses as the wind forcing is further increased. In the simulations with higher values of cohesion ($C_{min} \geq 20$ kPa), ~~the ice arch forms~~ a stable bridge forms and the flow of ice within and upstream of the channel effectively stops (see Fig. 5a, panel 3).

We further investigate the mechanism behind the formation of the ice arches by analyzing the simulated states of stress for the idealized simulation with $C_{min} = 20$ kPa. Similar results were obtained for $C_{min} = 30$ kPa. The symmetry of the idealized domain facilitates the analysis, but the same general conclusions also apply to the realistic simulations. Figure 5b represents the instantaneous profiles along the central meridional axis of the principal stresses σ_1 and σ_2 at the times indicated by the numbers 1, 2 and 3 on Fig. 4a.

Internal stresses within the initially undamaged ice cover are compressive ($\sigma_1, \sigma_2 > 0$) over the basin, change sign at the middle of the channel (at $y = 0$) and are tensile ($\sigma_1, \sigma_2 < 0$) downstream of the channel (not shown). At the onset of damage, σ_2 becomes negative (i.e., tensile, see Fig. 2) over the converging part of the basin ($y < 50$ km) and in the interior of the channel. Within and downstream of the channel, *multiple* minima in σ_2 are observed. These minima are collocated with either a maximum (positive) value of σ_1 (shearing state of stress) or a minimum (negative) value of $\sigma_1 < 0$ (tensile state of stress) and correspond to the location of arch-like features (see Fig. 4b, panel1). Figure 5c, panel 1 shows the elements that have exceeded either the local Mohr-Coulomb (in blue)~~or~~ , the tensile (in red) criterion or both criteria (in black) from the beginning up to this point in the simulation and confirms that these features were formed by a shear, tensile or a combination of both failure mechanisms.

Later in the simulation, the ice cover fails preferentially in shear upstream of the channel, while tensile failure progressively becomes predominant within and near the exit of the channel (see Fig. 5~~b and~~ c, panels 2 and 3). Once the stable ice bridge is formed, its location is clearly ~~indicated by collocated extrema of the value of the principal stresses ($\sigma_1 > 0$, $\sigma_2 < 0$, on~~ seen on the field of ice concentration (Fig. 4c, panel 3) and on the profile of vertical ice velocity (Fig. 5~~b~~a, panel 3). ~~Both the profiles~~ The profile of the principal stress components ~~and the spatial distribution of the over-critical elements downstream of the bridge give~~ just upstream of the bridge gives evidence that this structure sustains ~~biaxial tensile stresses (see Fig. 4band 4c~~*biaxial tensile* stresses (Fig. 5b, panel 3). This is an important point, as ~~standard viscous-plastic sea ice models~~ models based on the standard elliptical yield curve do not account for ~~pure~~ uniaxial or biaxial tensile strength and hence would not be able to reproduce the formation of a stable ice arch with self-obstruction to flow under the stress conditions simulated here. Consistent with the formation of a stable stress-free surface and with the detachment of the ice from the ~~stable~~ bridge, both principal stress components decrease to zero ~~near the exit and outside of the channel (see Fig. 4~~downstream of the bridge (Fig. 5b, panel 3). Velocity profiles (Fig. 5a, panel 3) are ~~effectively~~ uniform downstream of the no-flow transition with $u_x \approx 0$ and ~~$u_y \approx 0.44$ ms^{-1}~~ $u_y \approx 0.43$ ms^{-1} corresponding to the free drift velocity

$$u_y = \sqrt{\frac{\tau_a}{\rho_w C_{dw}}}, \tag{12}$$

for $\tau_a = 1$ Nm^{-2}. Simulations with a spatial resolutions of 2, 4 and 8 km were compared and produced similar results (not shown), demonstrating that the mechanical and dynamical behaviour of the Maxwell-EB model described here does not depend on its spatial resolution.

5.1.2 Realistic simulations

The temporal evolution of damage, velocity and internal stress in the realistic simulations is similar to the idealized case. The ice first fails near the exit of Kane Basin and rapidly weakens in Smith Sound (see Fig. 6~~a~~b, $t = 6$ hours). Damage then progressively propagates within and upstream of Kane Basin along closed arches up to the entrance of Robeson Chanel and eventually along open arches and more linear features upstream of the Strait (Fig. 6~~a, $t = 20$~~ b, $t = 24$ and 72 hours). The opening of multiple arch-like leads under the effect of the wind forcing appears clearly on the corresponding fields of ice concentration (Fig. 6~~b~~c). Comparison of these fields and corresponding snapshots of the ice drift velocity over the domain indicates that these leads divide the ice into relatively undamaged plates, or floes. Drift speeds are piecewise constant over the floes and discontinuous across the floes (~~see~~ Fig. 7, $t = 6$ hours and left inset), a feature that is also reproduced in the idealized simulations, as shown by the "stair-case" like profiles of u_y (see Fig. 5a). This behaviour is consistent with the motion of the Arctic ice cover as revealed by Synthetic Aperture Radar imagery analysis and RGPS motion products (Kwok, 2001; Moritz and Stern, 2001).

Also evident from the fields of ice concentration and corresponding fields of ice drift speed are regions where the ice remains landfast even under strong wind forcing, either enclosed in bays~~and narrow~~, inlets and fjords or between islands and the nearby shore~~(see Fig. 7, $t = 72$ hours), consistent with the observation of landfast ice along the coast of~~. This is consistent with

observations of landfast first year ice in the Strait in protected areas along the coasts of Ellesmere and Greenland and within Kane Basin and Smith Sound in winter and spring ~~(Mundy and Barber, 2001).~~ (Mundy and Barber, 2001; Yackel et al., 2001). Fig. 6c shows that the ice progressively detaches from the coast or landfast ice covered areas. The sharp gradients in ice velocity between these motionless regions and the fast flowing ice downstream are well simulated ~~.~~ (see Fig. 7, $t = 72$ hours, right inset).

For $C_{min} \geq 20$ kPa, stable ice arches form in the realistic simulations. Consistent with observations, the main bridge is located at the constriction point between Kane Basin and Smith Sound (see Fig. 6~~b and 7, $t = 72$ hours~~c and 7). Downstream of this bridge, the ice concentration rapidly drops, as the ice detaches and is driven out the channel at the free drift speed, leading to the opening of the North Water polynya (see Fig. 6~~b~~c, $t = 72$ hours). The model also simulates the detachment of the ice from the leeward side of islands (see Fig. 7, $t = 72$ hours) and, as the wind forcing is further increased, from a secondary bridge at the entrance of Kane Basin (see Fig. 6~~b~~c, $t = 72$ hours), which is also observed on satellite imagery (Kwok et al., 2010).

Internal stresses in the realistic simulations also evolve similarly to the idealized case. ~~After the onset of damage, the simulated~~ Figure 8a shows the evolution of the proportion of the simulated (uniaxial and biaxial) tensile, biaxial tensile-compressive and biaxial compressive stresses over the domain in the realistic simulation shown in Fig. 6 and 7. The instantaneous states of stress ~~,~~ are represented in the principal ~~stress plane , appear in good agreement with~~ stresses plane in Fig. 8c ($t = 72$ hours) after the formation of a stable ice bridge, i.e., after the proportion of the three stress types and the repartition of stresses in the principal stresses plane has stabilized. The states of stresses are compared to in situ stress measurements from the Beaufort Sea reported by ~~Weiss et al. (2007) (see~~ Weiss and Schulson (2009) (Fig. 8b[2]). Consistent with these observations, biaxial tensile stresses occur in a large number both prior and after the formation of ~~stable ice bridges~~ a stable ice bridge in the Strait. This again supports the relevance of accounting for some resistance ~~of the ice~~ in pure tension in sea ice models. Biaxial tensile-compressive, i.e., shear, stresses are the dominant type of stresses at all times during the simulation. Also consistent with in-situ measurements, ~~large~~ *large* biaxial compressive stresses do not appear so frequent compared to pure tensile and biaxial tensile-compressive states (Weiss et al., 2007; Weiss and Schulson, 2009), although convergent ice motion occurs over a significant portion of the domain. It is important to note that isotropic stresses ($\sigma_1 = \sigma_2$) are frequent in the observations and absent in the model. Theses are associated with thermal processes, i.e., thermal expansion/contraction (Richter-Menge et al., 2002), which are not represented in the present Maxwell-EB framework.

5.1.3 Consequences in terms of sea ice export

While studies have highlighted the strong interannual variability of the flux of ice through Nares Strait (Kwok et al., 2010), observations have also shown a tendency for ice bridges to form later and break earlier in ~~later years~~ the 1990s than in the 1980s (Barber et al., 2001), suggesting ~~than~~ that an increased ice outflow through the Strait ~~is~~ should be expected in a future climate.

[2] The value of q used on this figure by Weiss and Schulson (2009) is based on a value of the internal friction coefficient μ of 0.9 estimated by Schulson (2006a) from laboratory tests on first-year Arctic sea ice and is slightly higher than the value used in the model (0.7).

Except for a 2 months period, no ice bridge formed between Kane Basin and Smith Sound in the winters of 2007/2008 to 2009/2010. During that time, the (southward) ice and ocean velocities in the Strait were observed to increase and surface waters became fresher (Münchow, 2016). The year 2007 ~~for instance~~ in particular was characterized by the absence of ~~flow stoppage (Münchow, 2016)~~any ice bridge and flow stoppage in the Strait, which resulted into a record ~~areal and volume outflow~~ice area and volume export, equivalent to twice their estimated average value over the 1997 to 2009 period (Kwok et al., 2010) and into a maximum observed median draft of the drifting ice over the 2003 to 2012 period (Ryan and Münchow, 2017). The following question arises: ~~is this~~ would a tendency towards shorter lifespan of ice bridges and ~~associate~~ associated increased ice export through straits be the consequence of a thinning and/or of a mechanical weakening of the ice cover~~in recent years~~?

In a recent study, Gimbert et al. (2012b) analyzed in the frequency domain the drift of Arctic sea ice over the period 1979-2008 as estimated from the International Arctic Buoy Data Programme dataset and identified an increase of the inertial motion of the ice cover. With the use of a simple ice-ocean boundary layer, dynamically coupled model, Gimbert et al. (2012a) were able to relate this evolution to a *genuine* mechanical weakening of the ice pack in the Arctic and peripheral zone over the period 2002-2008 relative to the previous 22 years, that is, a weakening that is independent of a concomitant sea ice thinning and could be due to an evolution towards a more fractured ice cover and smaller ice floes. In this section we analyze a supplemental set of simulations which allows investigating the model's behaviour when changing few of its mechanical parameters to represent this mechanical weakening scenario.

~~According~~ In accordance with Gimbert et al. (2012a), who estimated a decrease in mechanical strength by a factor of about 1.5 to 1.75 between the periods 1979-2001 and 2002-2008 in both summer and winter, we compare realistic simulations of Nares Strait in which both the minimum uniaxial compressive strength and minimum tensile strength, set in the model by the cohesion, C, are reduced by a factor of 2 compared to the simulation with $C_{min} = 20$ kPa (in which a stable ice arch does form under the specific forcing conditions applied here, see section 5.1.2). The initial prescribed ice thickness ($h = 1$ m) is unchanged. Summer conditions are ~~differentiated~~ distinguished from winter conditions by increasing the prescribed healing time to $t_h = 365$ days, so that the recovering of mechanical strength associated with the refreezing of leads is negligible over the short duration of the simulations. Figure 9a shows the time series of the meridional component of the simulated ice drift velocity, averaged zonally across the Strait ($\overline{u_y}$) near the exit of Kane Basin, i.e., just upstream of the Kane Basin ice bridge. Four scenarios are compared: a stronger ($C_{min} = 20$ kPa) and a weaker ($C_{min} = 10$ kPa) ice cover, corresponding respectively to 1979-2001 and 2002-2008 conditions, in both winter and summer. Figure 9b shows instantaneous fields of the ice drift speed, $|\mathbf{u}|$, over the domain at $t = 48$ hours in these four cases.

In all cases, arch-like leads are still clearly defined and occur in similar locations as in the stronger ice (1979-2001) winter case discussed in section 5.1.2 (not shown). ~~However, in~~ In this winter case, the stable ice arch that forms at the exit of Kane Basin causes the meridional ice flow to stop completely within 48 hours (see figure 9a). In all of the weaker ice cover scenarios (2002-2008 period and/or summer), none of the ice arches formed near the exit of Kane Basin nor secondary arches formed elsewhere sustain the applied wind forcing and all ice bridges eventually collapse. While the flow of ice can be significantly slower over narrower than over larger portions of the Strait (see Fig. 9b), complete flow stoppage does not occur in any of these weaker ice cover scenarios over the time period analyzed here (see Fig. 9a), which allows a much larger portion of ice to be

flushed out of the Strait. Comparison of the fields of $|\mathbf{u}|$ in the summer and winter cases moreover suggests that ~~refreezing of leads may~~ the healing of the fractured ice cover might play a significant role ~~not only~~ in supporting stable ice bridges~~, but also in maintaining the ice landfast along portions of the coast~~. The reduction of the extent of landfast ice between the summer and winter cases implies that healing also helps maintaining the stagnant ice within bays and fjords.

It is important to note that these numerical experiments are by no means an attempt to determine the physically appropriate value of the cohesion of the ice cover in either of these scenarios, as the presence or not of a stable ice bridge also depends on ~~the~~ other mechanical parameter values (in particular, the elastic modulus), on the magnitude and form of the applied wind forcing as well as on the prescribed initial ice thickness. Instead, this exercise serves to show that by varying few mechanical strength parameters in a range of values which, based on observations, seems physically appropriate, the Maxwell-EB model is able to reproduce ~~widely different~~ a wide range of dynamical behaviours. Conversely, the simulations suggest that mechanical weakening, independent of thinning of the ice cover, can play a role in increased ice exports through narrow outflow pathways of the Arctic. This has implications in terms of ice export because the ice cover is expected to continue weakening, i.e., being more fragmented in the future.

5.2 Ice thickness distribution

We now investigate the ice thickness distribution simulated by the Maxwell-EB model and, in particular, the distribution of ridged ice, i.e. the ice that has thickened through mechanical redistribution. In the simulations analyzed for this purpose we set $C_{min} = 10$ kPa. In these conditions, a stable ice bridge does *not* form over the 3 days period analyzed here: the flow of ice upstream the channel ~~therefore~~ slows but does not stop, ~~such that the ice is more readily~~ which allows the ice to be more rapidly redistributed under the applied wind forcing.

Figure 10 shows the instantaneous fields of the mean ice thickness over a grid cell, h, after 3 days of simulation in an idealized case using $C_{min} = 10$ kPa and the probability density functions, $P(h)$, corresponding to instantaneous fields of h at different times after the onset of damaging in this simulation. As the spatial resolution is approximately constant over the domain, $P(h)$ here is estimated by the frequency histogram of h and normalized by the total number of model grid cells (i.e., h values are not weighted by the areal fraction of the corresponding grid cell). This PDF is dominated by a strong mode at 1 m that corresponds to the initial prescribed value of h. The ice thickness increases over time within the channel in the converging part of the basin, defining oriented regions of ridged ice that correspond to the areas of shear failure identified on Fig. 4c. This part of the basin is essentially represented by the tail of the distribution ($h > 1$ m), which at all times is well described by a negative exponential (the coefficient of determination for the goodness of the fit varies between ~~96%~~ 90% and 98%). This function is of the form

$$P(h) \sim \exp^{-\frac{h}{h^*}}, \tag{13}$$

with h^* increasing in time until the convergence and thickening of ice at the entrance of the channel ~~starts slowing significantly the ice flow~~ reduces the flow of ice (see Fig. 10). The flattening of the PDF is a signature of the thickening of the ice along these highly localized features.

The part of the distribution with $h < 1$ is characterized by a second mode near $h = 0$ associated with the presence of open water (e.g., Wadhams, 1981, 1994; Haas et al., 2006; Haas, 2009), which becomes more important as ice is driven out of the domain. At $t = 3$ days (orange curve), the ice downstream of the channel has nearly left the domain and a large patch of ice is almost completely detached from the interior of the channel. The fact that $P(h)$ is not zero for values of $h \in]0, 1[$ at this point is mostly attributable to numerical diffusion. For polynomial approximations of degree 0 of advected quantities (see section 4), the Galerkin discontinuous method coincides with a finite volume scheme with upwinding, which is known to be diffusive. As expected, numerical diffusion is most important at the edge of the detached ice, where mechanical stresses vanish, gradients between the ice and opening water are the strongest and drift velocities the highest. It is important to note however that the present continuum model is not meant to represent the dynamical behaviour of sea ice in regions of low ice concentration dominated by free drift conditions such as the marginal ice zone, but rather that of the ice pack. A Lagrangian ~~model~~ scheme would perhaps be ~~more suitable~~ a more natural approach to simulate the edge of the detached ice, although some diffusion would be unavoidable in free drift mode as some remeshing would be required. Where ice concentration is high ($A > 90\%$), mechanical stresses are significant and constantly redistributed under damaging. In the Maxwell-EB model, the associated deformation is highly localized in both space and time, which acts to mitigate numerical diffusion and re-increase gradients in all fields.

The realistic simulations show a similar evolution of the ice thickness in the channel. In the funnel-like entrance to Nares Strait, the converging part of Kane Basin and upstream of coasts and islands, the ice builds-up along narrow and oriented features (see Fig. 11a). The effect of numerical diffusion in smoothing these features and reducing the localization of the thickest ice increases with ice drift velocities downstream of the domain. Nevertheless, at all times the simulated probability density function is strongly asymmetric, consistent with thickness distributions estimated for sea ice with little history of melting ~~(e.g., Haas, 2009)~~in the open Arctic ocean (e.g., Haas, 2009) and at the entrance of Nares Strait (Haas et al., 2006). As in the idealized case, the strong localization of the ridged ice translates into an exponential tail for $P(h)$ of the form of (13) with h^* increasing in time (see Fig. 11b).

According to Eqn. (5) and to the simple redistribution scheme employed here, the evolution of h is a function of the ~~flux $\nabla \cdot (h\mathbf{u}) = \mathbf{u} \cdot \nabla h + h \cdot \nabla \mathbf{u}$ and of the~~ mechanical redistribution term given by Eqn. (7), which itself is a function of the flux of ice concentration ~~$\nabla \cdot (A\mathbf{u})$~~$\nabla \cdot (A\mathbf{u}) = \mathbf{u} \cdot \nabla A + A \nabla \cdot \mathbf{u}$. The spatial distribution of h in the present Maxwell-EB model therefore depends essentially on the simulated velocity field. Furthermore, both simulations, idealized and realistic, show a similar exponential decrease for the tail of $P(h)$. This suggests that the localization of the thickest ice does not arise from the complexity of the domain geometry. The shape of the tail of $P(h)$ is also conserved when using a lower spatial resolution, for instance, with $\Delta x = 4$ and 8 km in idealized simulations (orange, dotted and dotted-dashed curves on Fig. ~~11~~10b), suggesting that this property of $P(h)$ is not resolution-dependant either. ~~The~~ This is consistent with the fact that there is no characteristic scale for the localization of damage and deformation in the model beyond the scale of the model element (see Dansereau et al., 2016, sections 6.1 and 6.2), i.e., that at all spatial resolutions, the simulated deformation is highly localized. Additional simulations with different ranges of cohesion (not shown) indicate that the value of C not impact the shape of the ice thickness

distribution either, but only the rate at which the exponential tail flattens, i.e., the rate at which the ice cover thickens. In brief, the strong localization of ridged ice in the model therefore appears to be only the consequence of its capability to reproduce the extreme localization of ice deformation and associated sharp gradients in the ice velocity field.

6 ~~Summary and conclusion~~Conclusions

In this paper we have presented the results of a first implementation of the Maxwell-EB rheology for modelling sea ice on geophysical scales. Idealized and realistic simulations of the flow of ice through Nares Strait have shown that the Maxwell-EB sea ice model is able to reproduce

- the formation of multiple arch-like leads within the ice cover downstream, in the interior and upstream of the channel, in agreement with observations of ice conditions in narrow straits of the Arctic (Sodhi, 1977; Kwok et al., 2010). As these features appear in high numbers in both highly idealized and realistic simulations, they are not attributable to the complexity of the domain geometry or boundary conditions but to the mechanical behaviour of the Maxwell-EB model itself. ~~In coupled thermodynamic and dynamic models, a high density of leads is expected to impact the simulated heat fluxes between the atmosphere, the ice and the ocean (Smith et al., 1990).~~

- the formation of a stable, concave ice bridge, the associated stoppage of the ice flow upstream and the opening of a polynya downstream of the bridge. In the realistic simulations of Nares Strait, the location of the main bridge is consistent with the stable arch observed to form seasonally downstream of Kane Basin.

- regions of relatively undamaged ice with uniform, plate-like motion, and extreme gradients in ice velocity across the leads that delimit these regions, consistent with RGPS observations (see Kwok (2001); Moritz and Stern (2001)). In particular, the model reproduces the very sharp gradients in ice velocity, concentration and thickness associated with the edge of the ice bridge while remaining numerically stable.

- the presence of landfast ice along portions of the coast of Nares Strait, in agreement with observations ~~(Mundy and Barber, 2001)~~(Mu In the model, this landfast ice resists the strong applied wind forcing. The associated sharp gradients in ice velocity ~~, thickness and concentration~~ between this stagnant and the nearby fast flowing ice are well represented.

- states of stress that are overall in good agreement with in-situ measurements in Arctic sea ice. In particular, the simulations have shown that ~~pure (i.e., uniaxialor biaxial) tensile states of stress~~ uniaxial/biaxial tensile stresses are rather frequent, hence pointing out the importance of accounting for some resistance ~~of the ice in~~ in pure tension in sea ice models.

- the strong localization of ridged ice and an associated thickness distribution with an exponential tail, in agreement with probability density functions calculated from sea ice thickness measurements.

This last point is an important outcome of this first implementation of the Maxwell-EB rheology in a realistic context, as the treatment of the mechanical redistribution of the ice thickness, in particular of the ridging process, has been the subject of numerous studies since the 1970's and continues to challenge the sea ice modelling community to this day. Although the ~~excessively~~ very simple redistribution scheme used here does not include multiple ice categories nor allows prescribing the thickness of the ice involved in the ridging, the Maxwell-EB model seems to allow ice to thicken in regions of strong convergence and shear~~, a process that is known to be underestimated in VP models using a two-level scheme and which has been more adequately simulated at the cost of increasing the number of ice thickness categories in VP (or EVP) models using a multi-categories redistribution scheme (e.g., Bitz et al., 2001)~~. In the Maxwell-EB model, this capability of accounting for a sufficient thickening of the ice as well as the spatial localization of extreme thickness values arises from the appropriate description of extreme strain localization. On a mechanical point of view, this may therefore question the relevance of using multi-categories redistribution schemes.

In terms of the simulated thermodynamic fluxes and ice energy balance however, a number of studies have highlighted the sensitivity of simulation results to the number of ice thickness categories used (e.g., Castro-Morales et al., 2014), and have pointed to an overall underestimation of ice thickness due the under-representation of the thermodynamic growth of thin ice using a two-level versus a multi-categories model (e.g., Walsh et al., 1985). As opposed to mechanical redistribution processes, thermodynamic processes are expected to "seek the mean" (Thorndike et al., 1975) and smooth the distribution by allowing ice to grow over open water, thinner ice to thicken faster than thick ice and thicker ice to melt comparatively faster (Haas, 2009). A thorough comparison of simulated ice thickness distributions model against observations therefore calls for larger scale, longer term simulations including thermodynamic processes. The coupling of the Maxwell-EB rheology with a thermodynamic component is under-way and will allow evaluating the impact of the representation of multiple, fine ice leads in the Maxwell-EB model on the simulated heat fluxes between the atmosphere, ice and ocean.

Besides numerical efficiency, other advantages of using a simple redistribution scheme such as the one employed here is that no thickness redistribution function needs to be assumed and the redistribution is not directly tied to the prescribed failure strength of the ice. In the Maxwell-EB model, the ~~assumed~~ prescribed strength is instead based on in-situ stress measurements, which point to a Mohr-Coulomb failure criterion and directly provide information on the ~~order of magnitude of the shear~~ relative amount of shear and tensile strength. In particular, both the observations and numerical simulations here suggest that prescribing a cut-off for biaxial compressive strength (equivalent to the pressure, P, in VP models) ~~appears unnecessary . In the model,~~ is unnecessary (see figure 8) Instead, the uniaxial compressive strength, σ_c and maximum uniaxial tensile strength, σ_t appear to be more relevant to represent adequately the strength of the ice ~~is~~ cover. The Maxwell-EB model presents the advantage that both these quantities are set through a single parameter, the cohesion, C. The channel flow simulations performed here moreover showed that varying this single parameter in the limit of physically acceptable values and in agreement with the suggested evolution of the failure strength of the ice pack in ~~later~~ recent years (Gimbert et al., 2012a), while keeping the initial thickness unchanged, is sufficient to reproduce different dynamical behaviours of the ice cover (the presence of stable or unstable bridges, the opening of different size polynyas and the associated ice fluxes). This therefore suggests that the

Maxwell-EB model could be an efficient tool for modelling the deformation and drift of sea ice in complex flow regimes and under different climate scenarios.

Appendix A: Equations and numerical scheme

A1 System of equations

With the Coriolis term neglected, the ocean at rest and the mean ice thickness over the grid cell given by $h = h_{thick}A$, the momentum equation, reads

$$\rho h_{thick} A \left[\frac{\partial \mathbf{u}}{\partial t} + (\mathbf{u}\cdot\nabla)\mathbf{u}\right] = A(\tau_{\mathbf{a}} - \rho_w C_{dw}|\mathbf{u}|\mathbf{u}) + \nabla\cdot(h_{thick}A\sigma). \tag{A1}$$

Following Connolley et al. (2004), both the air and water drag terms are weighted by the local ice concentration to account for the fraction of open water within a grid cell.

The Maxwell-EB constitutive law writes

$$\frac{1}{E}\left[\frac{\partial \sigma}{\partial t} + (\mathbf{u}\cdot\nabla)\sigma + \beta_a(\nabla\mathbf{u},\sigma)\right] + \frac{1}{\eta}\sigma = \mathbf{K}\colon\dot{\varepsilon}.$$

where $\dot{\varepsilon}$ is the strain rate tensor, here equivalent to the rate of strain tensor, and the term β_a in the objective Gordon-Schowalter derivative of σ accounts for the effect of rotation and deformation of the stress tensor. This term reads

$$\beta_a(\nabla\mathbf{u},\sigma) = \sigma W(\mathbf{u}) - W(\mathbf{u})\sigma - (\sigma D(\mathbf{u}) + D(\mathbf{u})\sigma)$$

in the upper convected form, with $D(\mathbf{u}) = \frac{\nabla\mathbf{u}+\nabla\mathbf{u}^T}{2}$ and $W(\mathbf{u}) = \frac{\nabla\mathbf{u}-\nabla\mathbf{u}^T}{2}$, the symmetric and anti-symmetric parts of the velocity gradient. In plane stress conditions, the dimensionless stiffness tensor, $\mathbf{K}$, is defined in terms of ν, Poisson's ratio, such that for all symmetric tensors $\epsilon = \epsilon_{ij}\ \forall\ i,j;\ 1\le i,j\le 2$, $(\mathbf{K}\colon\epsilon)_{ij} = \frac{\nu}{1-\nu^2}\mathrm{tr}(\epsilon)\delta_{ij} + 2\frac{1}{2(1+\nu)}\epsilon_{ij}$. With the following coupling of the mechanical parameters with respect to the level of damage and ice concentration,

$$E = E^0 d\exp[-c^*(1-A)],$$
$$\eta = \eta^0 d^\alpha \exp[-c^*(1-A)],$$
$$\lambda = \frac{\eta^0}{E^0}d^{\alpha-1} = \lambda^0 d^{\alpha-1},$$

(Eq. 18-20, 24 and 25 Dansereau et al., 2016), where α is a constant greater than one such that the relaxation time for the stress, λ, decreases with increasing level of damage and increases with healing (see Dansereau et al. (2016), section 4.1.5), the constitutive equation can be alternatively written in the following form

$$\lambda^0 d^{\alpha-1}\left[\frac{\partial\sigma}{\partial t} + (\mathbf{u}\cdot\nabla)\sigma + \beta_a(\nabla\mathbf{u},\sigma)\right] + \sigma = \eta^0 d^\alpha\exp[-c^*(1-A)]\mathbf{K}\colon D(\mathbf{u}). \tag{A2}$$

The damage evolution equation reads

$$\frac{\partial d}{\partial t} + (\mathbf{u}\cdot\nabla)d = \left(\min\left[1, \frac{\sigma_t}{\sigma_2}, \frac{\sigma_c}{\sigma_1 - q\sigma_2}\right] - 1\right)\frac{1}{t_d}d + \frac{1}{t_h},\ \ 0 < d \le 1, \tag{A3}$$

with t_d, the characteristic time for damaging, set by the ratio $\frac{\Delta x}{c}$ with Δ_x, the spatial resolution and c, the speed of propagation of elastic waves in the ice cover which carry the damage information (see Dansereau et al. (2016), sections 3.3.1 and 4.4.1), t_h, the characteristic time for healing (see Dansereau et al. (2016), sections 3.3.2 and 4.4.2), σ_c and σ_t defined in terms of C as in Eq. (1) and Eq. (2) respectively and σ_1 and σ_2 the principal stresses, defined as

$$\sigma_1 = -\frac{(\sigma_{11}+\sigma_{22})}{2} + \sqrt{\left[\frac{\sigma_{11}-\sigma_{22}}{2}\right]^2 + \sigma_{12}^2}, \quad \sigma_2 = -\frac{(\sigma_{11}+\sigma_{22})}{2} - \sqrt{\left[\frac{\sigma_{11}-\sigma_{22}}{2}\right]^2 + \sigma_{12}^2}.$$

As the internal stress is assumed to be homogeneously distributed over the thickness of the ice cover, the momentum, constituttive and damage equations are written in terms of the *internal stress* rather than the *vertically integrated internal stress*. This allows a direct comparison between the local state of stress and the damage criterion.

As thermodynamic processes are not accounted for in the present implementation of the model, the conservation equations for the thickness of the ice-covered portion of the grid cell, $h_{thick} = \frac{h}{A}$, and ice concentration read

$$\frac{\partial h_{thick}}{\partial t} + (\mathbf{u}\cdot\nabla)h_{thick} = 0, \tag{A4}$$

$$\frac{\partial A}{\partial t} + (\mathbf{u}\cdot\nabla)A = -A(\nabla\cdot\mathbf{u}). \tag{A5}$$

for $0 \leq A \leq 1$. Adjustements to the concentration and thickness are applied when and where $A > 1$ and calculated as (6) and (7).

An additional equation handles the transport of the passive field of cohesion, which sets the local value of the damage criterion, with the ice flow:

$$\frac{\partial C}{\partial t} + (\mathbf{u}\cdot\nabla)C = 0. \tag{A6}$$

Together, Eq. (A1) (2 horizontal components), (A2) (3 components), (A3), (A4), (A5), (A6) form a system of nine equations that are solved for the nine variables σ (3 components), $\mathbf{u}$ (2 components), d, A, h_{thick} and C.

A2 Numerical scheme

The system of Eq. (A1) to (A6) is closed by suitable initial and boundary conditions and solved over a domain Ω and a time $t \in [0, +\infty[$. Initial conditions are given by

$$\mathbf{u}(t=0) = 0 \text{ ms}^{-1} \text{ in } \Omega,$$
$$\sigma(t=0) = 0 \text{ Pa in } \Omega,$$
$$d(t=0) = 1 \text{ in } \Omega,$$
$$A(t=0) = 1 \text{ in } \Omega,$$
$$h_{thick}(t=0) = 1 \text{ m in } \Omega,$$
$$C(t=0) = C_0 \text{ Pa in } \Omega,$$

where C_0 is the initial field of cohesion, set as described in section 4. The domain boundary $\partial\Omega$ is partitioned as $\partial\Omega = \Gamma_{\text{in}} \cup \Gamma_{\text{left}} \cup \Gamma_{\text{out}} \cup \Gamma_{\text{right}}$. A no-slip condition is applied at the lateral boundaries (Γ_{left}, Γ_{right}). The channel is open at its top (Γ_{in}) and bottom (Γ_{out}) boundaries with the Neumann condition $\sigma \cdot \mathbf{n} = 0$. The value of the transported quantities $\mathbf{u}$, σ, d, A, h_{thick} and C are prescribed on the *upstream* part of the top and bottom boundaries, Γ_-, defined as

$$\Gamma_- = \{x \in \Omega; \mathbf{u}(x) \cdot \mathbf{n}(x) < 0\}.$$

These are chosen to represent inflowing undamaged ice, with $d = 1$, $A = 1$, $h_{thick} = 1$ m, $\sigma = 0$ and C randomly drawn from the same uniform distribution prescribed as initial condition. The velocity of the inflowing ice is taken as the ice velocity at the nearest upstream boundary node, $\mathbf{u}_-$. The complete set of boundary conditions writes:

$$\begin{aligned}
\mathbf{u}(t) &= 0 \text{ ms}^{-1} \text{ on } \Gamma_{\text{left}} \times]0, +\infty[\text{ and } \Gamma_{\text{right}} \times]0, +\infty[, \\
\sigma(t) \cdot \mathbf{n} &= 0 \text{ Pa on } \Gamma_{\text{in}} \times]0, +\infty[\text{ and } \Gamma_{\text{out}} \times]0, +\infty[, \\
\mathbf{u}(t) &= \mathbf{u}_-(t) \text{ Pa on } \Gamma_- \times]0, +\infty[, \\
\sigma(t) &= 0 \text{ Pa on } \Gamma_- \times]0, +\infty[, \\
d(t) &= 1 \text{ on } \Gamma_- \times]0, +\infty[, \\
A(t) &= 1 \text{ on } \Gamma_- \times]0, +\infty[, \\
h_{thick}(t) &= 1 \text{ m on } \Gamma_- \times]0, +\infty[, \\
C(t) &= C_0 \text{ Pa on } \Gamma_- \times]0, +\infty[.
\end{aligned}$$

A2.1 Time discretization

Let $\Delta t > 0$ be the model time step and $t_n = n\Delta t$, $n \geq 0$. The system of equations is discretized in time as follow.

- A semi-implicit scheme is used for the momentum equation: the internal stress term is discretized using an implicit scheme, the water drag term is linearized as $\tau_{\mathbf{w}} = \rho_w C_{dw} |\mathbf{u}^n| \mathbf{u}^{n+1}$ and ice thickness and concentration are both taken at the n^{th} time step. The total derivative of the ice velocity $\frac{D\mathbf{u}}{Dt} = \frac{\partial \mathbf{u}}{\partial t} + (\mathbf{u} \cdot \nabla)\mathbf{u}$ is approximated using a Lagrange-Galerkin method as

$$\frac{D\mathbf{u}}{Dt}(t_{n+1}, x) = \frac{\mathbf{u}(t_{n+1}, x) - \mathbf{u}(t_n, X_n(x))}{\Delta t} + O(\Delta t) \tag{A7}$$

  where $O(\Delta t)$ denotes the neglected higher order terms and $X_n(x)$ is the position of a particle at time t_n that is at the position x at time t_{n+1} and is transported by the velocity field $\mathbf{u}^n$. The first-order Euler approximation for this position is

$$X_n(x) \approx x - \Delta t \, \mathbf{u}^n(x).$$

  The second term on the right hand side of (A7) is denoted $\mathbf{u}^n \circ X^n$ (Saramito, 2013a).

– A semi-implicit scheme is used for the constitutive equation in which the advection, rotation and deformation terms are estimated using the fields of velocity and internal stress at the n^{th} model time step. The ice concentration is taken at the n^{th} time step.

– The damage evolution equation is discretized using an explicit scheme in which the damage term is evaluated using the states of stress at the $n+1^{th}$ time step and the damage criterion (σ_c and σ_t) at the n^{th} time step.

– The cohesion, ice thickness and concentration equations use an explicit scheme and the value of the ice velocity at the $(n+1)^{\text{th}}$ time step.

Hence a semi-implicit, first order discretization of the problem reads:

(P) *For all* $n \geq 0$*, with* $\mathbf{u}^n$*,* σ^n*,* d^n*,* A^n*,* h^n_{thick}*,* C^n *known, find* $\mathbf{u}^{n+1}$*,* σ^{n+1}*,* d^{n+1}*,* A^{n+1}*,* h^{n+1}_{thick} *and* C^{n+1} *such that*

$$\rho h^n_{thick} A^n \frac{\mathbf{u}^{n+1} - \mathbf{u}^n \circ X^n}{\Delta t} = A^n \left(\tau_{\mathbf{a}} - \rho_w C_{dw} |\mathbf{u}^n| \mathbf{u}^{n+1}\right) + \nabla \cdot (h^n_{thick} A^n \sigma^{n+1})$$

$$\lambda^0 (d^{n+1})^{\alpha-1} \left[\frac{\sigma^{n+1} - \sigma^n}{\Delta t} + (\mathbf{u}^n \cdot \nabla)\sigma^n + \beta_a(\nabla \mathbf{u}^n, \sigma^n)\right] + \sigma^{n+1}$$

$$= \eta^0 (d^{n+1})^{\alpha} \exp[-c^*(1 - A^n)] \mathbf{K} \colon D(\mathbf{u}^{n+1})$$

$$\frac{d^{n+1} - d^n}{\Delta t} + (\mathbf{u}^n \cdot \nabla) d^n = \left(\min\left[1, \frac{\sigma^n_t}{\sigma^{n+1}_2}, \frac{\sigma^n_c}{\sigma^{n+1}_1 - q\sigma^{n+1}_2}\right] - 1\right) \frac{1}{t_d} d^n + \frac{1}{t_h},\ 0 < d^{n+1} \leq 1$$

$$\frac{h^{n+1}_{thick} - h^n_{thick}}{\Delta t} + (\mathbf{u}^{n+1} \cdot \nabla) h^n_{thick} = 0$$

$$\frac{A^{n+1} - A^n}{\Delta t} + (\mathbf{u}^{n+1} \cdot \nabla) A^n = -A^n (\nabla \cdot \mathbf{u}^{n+1})$$

$$\frac{C^{n+1} - C^n}{\Delta t} + (\mathbf{u}^{n+1} \cdot \nabla) C^n = 0$$

with

$$\mathbf{u}^{n+1} = 0 \text{ on } \Gamma_{\text{left}} \cup \Gamma_{\text{right}}$$

$$\sigma^{n+1} \cdot \mathbf{n} = 0 \text{ on } \Gamma_{\text{in}} \cup \Gamma_{\text{out}}$$

$$\mathbf{u}^{n+1} = \mathbf{u}^{n+1}_- \text{ on } \Gamma_-$$

$$\sigma^{n+1} = 0 \text{ on } \Gamma_-$$

$$d^{n+1} = 1 \text{ on } \Gamma_-$$

$$A^{n+1} = 1 \text{ on } \Gamma_-$$

$$h^{n+1} = 1 \text{ on } \Gamma_-$$

$$C^{n+1} = C_0 \text{ on } \Gamma_-.$$

These equations are coupled and hence, the problem is nonlinear. To solve it we use a decoupled semi-implicit scheme that divides it into a set of smaller subproblems at each time step as follow. (1) A fixed point algorithm is used in which the

momentum and constitutive equations are first solved simultaneously, and the damage equation solved exactly. (2) The value of d, is then updated in the constitutive equation and the two computations are iterated until the residual of the constitutive equation drops below a prescribed tolerance or a prescribed maximum number of iterations. (4) The conservation equations for the ice thickness and concentration are solved using $\mathbf{u}^{n+1}$ and both fields are adjusted for mechanical redistribution. (5) The cohesion transport equation is then solved using $\mathbf{u}^{n+1}$ and the local damage criterion is updated.

Using the superscript $k \geq 0$ for the fixed point sub-iterations, the fixed point algorithm for decoupling the momentum, constitutive and damage equations reads:

When $k = 0$*, let* $\left(\sigma^{n+1,0}, \mathbf{u}^{n+1,0}, d^{n+1,0}\right) = (\sigma^n, \mathbf{u}^n, d^n)$,
For all $k \geq 0$*, by recurrence, assume that* $(\sigma^{n+1,k}, \mathbf{u}^{n+1,k}, d^{n+1,k})$ *are known.*

- *(P1) Find* $\sigma^{n+1,k+1}$ *and* $\mathbf{u}^{n+1,k+1}$ *such that*

$$\rho h_{thick}^n A^n \left[\frac{\mathbf{u}^{n+1,k+1} - \mathbf{u}^n \circ X^n}{\Delta t}\right] = A^n \left(\tau_{\mathbf{a}} - \rho_w C_{dw} |\mathbf{u^n}| \mathbf{u^{n+1,k+1}}\right) + \nabla \cdot (h_{thick}^n A^n \sigma^{n+1,k+1}) \tag{A8a}$$

$$\lambda^0 (d^{n+1,k})^{\alpha-1} \left[\frac{\sigma^{n+1,k+1} - \sigma^n}{\Delta t} + (\mathbf{u}^n \cdot \nabla)\sigma^n + \beta_a(\nabla \mathbf{u}^n, \sigma^n)\right] + \sigma^{n+1,k+1}$$

$$= \eta^0 (d^{n+1,k})^{\alpha} \exp[-c^*(1-A^n)] \mathbf{K} \colon D(\mathbf{u}^{n+1,k+1}) \tag{A8b}$$

$$\mathbf{u}^{n+1,k+1} = 0 \text{ on } \Gamma_{\text{left}} \cup \Gamma_{\text{right}} \tag{A8c}$$

$$\sigma^{n+1,k+1} \cdot \mathbf{n} = 0 \text{ on } \Gamma_{\text{in}} \cup \Gamma_{\text{out}} \tag{A8d}$$

$$\mathbf{u}^{n+1,k+1} = \mathbf{u}_-^{n+1,k+1} \text{ on } \Gamma_- \tag{A8e}$$

$$\sigma^{n+1,k+1} = 0 \text{ on } \Gamma_-. \tag{A8f}$$

- *(P2) Find* $d^{n+1,k+1}$*, such that* $0 < d^{n+1,k+1} \leq 1$ *and*

$$\frac{d^{n+1,k+1} - d^n}{\Delta t} = \left(\min\left[1, \frac{\sigma_t^n}{\sigma_2{}^{n+1,k+1}}, \frac{\sigma_c^n}{\sigma_1^{n+1,k+1} - q\sigma_2^{n+1,k+1}}\right] - 1\right) \frac{1}{t_d} d^n, \tag{A9a}$$

$$d^{n+1,k+1} = 1 \text{ on } \Gamma_-. \tag{A9b}$$

- *Stopping criterion : compute*

$$\text{res}_\sigma = \Big| \lambda^0 (d^{n+1,k+1})^{\alpha-1} \left[\frac{\sigma^{n+1,k+1} - \sigma^n}{\Delta t} + (\mathbf{u}^n \cdot \nabla)\sigma^n + \beta_a(\nabla \mathbf{u}^n, \sigma^n)\right] + \sigma^{n+1,k+1}$$
$$- \eta^0 (d^{n+1,k+1})^{\alpha} \exp[-c^*(1-A^n)] \mathbf{K} \colon D(\mathbf{u}^{n+1,k+1}) \Big|$$

If $\text{res}_\sigma < \text{tol}$ then
set $\left(\mathbf{u}^{n+1}, \sigma^{n+1}, d^{n+1}\right) = \left(\mathbf{u}^{n+1,k+1}, \sigma^{n+1,k+1}, d^{n+1,k+1}\right)$.
stop iteration in index k.

Subproblem (P1) is solved in two steps. From (A8b), the following explicit expression for $\sigma^{n+1,k+1}$ in obtained in terms of the unknown $\mathbf{u}^{n+1,k+1}$ and other known variables:

$$\sigma^{n+1,k+1} = K\left[\lambda^0\left(d^{n+1,k}\right)^{\alpha-1}\left(\frac{\sigma^n}{\Delta t} - (\mathbf{u}^n\cdot\nabla)\sigma^n - \beta_a(\nabla\mathbf{u}^n,\sigma^n)\right) + \eta^0\left(d^{n+1,k}\right)^{\alpha}\exp[-c^*(1-A^n)]\mathbf{K}\colon D(\mathbf{u}^{n+1,k+1})\right], \tag{A10}$$

where $K = \left[\lambda^0\left(d^{n+1,k}\right)^{\alpha-1}\frac{1}{\Delta t}+1\right]^{-1}$. Substituting for this expression in (A8a) leads to an expression of (A8b) with $\mathbf{u}^{n+1,k+1}$ as the only unknown. This linear equation is solved, after discretization with respect to space, by a direct method. Then, $\sigma^{n+1,k+1}$ is computed explicitly from (A10). Subproblem (P2) leads to an explicit computation of $d^{n+1,k+1}$.

The machine used for these simulations allows reaching a value of the residual of the constitutive equation, res_σ, on the order of 10^{-12}. In the simulations presented here, the tolerance, tol, was set to 10^{-7}, which allowed res_σ to drop by 4 to 9 orders of magnitude relative to its initial value through the iterative fixed point algorithm. A maximum number of sub-iteration of 10 was imposed. In these simulations, the number of instances for which the residual res_σ did not drop below the fixed tolerance in the prescribed number of fixed point iteration represent 2% or less of the total number of model time steps. Imposing a larger maximum number of subiterations (20, 40, 50) reduces this percentage but has shown to have no effect on the results.

Using the superscript $'$ for the variables *before* mechanical redistribution, the ice thickness and concentration are obtained from

(P4) Find $A^{'}$ and $h^{'}_{thick}$ such that

$$\frac{h^{'}_{thick}-h^n_{thick}}{\Delta t} + (\mathbf{u}^{n+1}\cdot\nabla)h^n_{thick} = 0$$

$$\frac{A^{'}-A^n}{\Delta t} + (\mathbf{u}^{n+1}\cdot\nabla)A^n = -A^n(\nabla\cdot\mathbf{u}^{n+1})$$

$$h^{'}_{thick} = 1 \text{ on } \Gamma_-$$

$$A^{'} = 1 \text{ on } \Gamma_-.$$

and

$$h^{n+1}_{thick} = h^{'}_{thick} + \max[0,(A-1)]h^{'}_{thick},$$
$$A^{n+1} = A^{'} - \max[0,(A-1)].$$

The transport equation for the cohesion is solved as

(P5) Find C^{n+1} such that

$$\frac{C^{n+1}-C^n}{\Delta t} + (\mathbf{u}^{n+1}\cdot\nabla)C^n = 0,$$

$$C^{n+1} = C_0 \text{ on } \Gamma_-.$$

The damage criterion, i.e., σ_c^{n+1} and σ_t^{n+1}, is then obtained directly from Eq. (1) and (2) and the time step is complete.

While the advection, rotation and deformation terms in the momentum, constitutive and damage equations could all be updated in the fixed point iteration, we find that this has no impact on the results presented here since the time step employed in the simulations is taken very small (6 s for $\Delta x = 3$ km and 4 s for $\Delta x = 2$ km) in order to simulate the propagation of damage over the ice cover with the highest possible resolution (see Dansereau et al. (2016)). Similarly, the cohesion, ice thickness and concentration could also be solved for using an implicit scheme and could be updated as part of the fixed point iteration. However, because variations in the mechanical parameters associated with changes in C, h and A are slow compared to the changes due to damaging, we find that this does not significantly impact our model solution either.

A2.2 Space discretization

The velocity field is discretized in space by a continuous first order polynomial finite element method while all others variables are discretized by a piecewise constant discontinuous approximation. The transport operator $\mathbf{u}.\nabla$ (as well as the terms for the rotation and deformation of the stress tensor) are discretized by a discontinuous Galerkin method, that coincides, when using piecewise constant approximation, with the usual upwind finite volume scheme on unstructured meshes.

Author contributions. Véronique Dansereau wrote the paper, developed the Maxwell-EB model and performed the simulations. This work was supervised by former Ph.D. advisors Jérôme Weiss, Pierre Saramito, Philippe Lattes and Edmond Coche.

Acknowledgements. The financial support of TOTAL EP RECHERCHE DEVELOPPEMENT is gratefully acknowledged. We also thank Christian Haas and Kaj Riska for useful discussions on this work.

References

Amitrano, D., Grasso, J.-R., and Hantz, D.: From diffuse to localised damage through elastic interaction, Geophysical Research Letters, 26, 2109–2112, 1999.

Aranson, I. S. and Tsimring, L. S.: Patterns and collective behavior in granular media: Theoretical concepts, Rev. Mod. Phys., 78, 641–692, doi:10.1103/RevModPhys.78.641, http://link.aps.org/doi/10.1103/RevModPhys.78.641, 2006.

Barber, D., Hanesiak, J., Chan, W., and Piwowar, J.: Seaice and meteorological conditions in Northern Baffin Bay and the North Water polynya between 1979 and 1996, Atmosphere-Ocean, 39, 343–359, doi:10.1080/07055900.2001.9649685, 2001.

Bitz, C. M., Holland, M. M., Weaver, A. J., and Eby, M.: Simulating the ice-thickness distribution in a coupled climate model, Journal of Geophysical Research: Oceans, 106, 2441–2463, doi:10.1029/1999JC000113, http://dx.doi.org/10.1029/1999JC000113, 2001.

Bouillon, S. and Rampal, P.: Presentation of the dynamical core of neXtSIM a new sea ice model, Ocean Modelling, 91, 23–37, doi:http://dx.doi.org/10.1016/j.ocemod.2015.04.005, 2015.

Castro-Morales, K., Kauker, F., Losch, M., Hendricks, S., Riemann-Campe, K., and Gerdes, R.: Sensitivity of simulated Arctic sea ice to realistic ice thickness distributions and snow parameterizations, Journal of Geophysical Research: Oceans, 119, 559–571, doi:10.1002/2013JC009342, http://dx.doi.org/10.1002/2013JC009342, 2014.

Connolley, W. M., Gregory, J. M., Hunke, E., and McLaren, A. J.: On the Consistent Scaling of Terms in the Sea-Ice Dynamics Equation, Journal of Physical Oceanography, 34, 1776–1780, 2004.

Dansereau, V., Weiss, J., Saramito, P., and Lattes, P.: A Maxwell elasto-brittle rheology for sea ice modelling, The Cryosphere, 10, 1339–1359, doi:10.5194/tc-10-1339-2016, http://www.the-cryosphere.net/10/1339/2016/, 2016.

Dumont, D., Gratton, Y., and Arbetter, T. E.: Modeling the dynamics of the north water polynya ice bridge, Journal of Physical Oceanography, 39, 1448–1461, doi:http://dx.doi.org/10.1175/2008JPO3965.1, 2009.

Flato, G. M. and Hibler, W. D.: Ridging and strength in modeling the thickness distribution of Arctic sea ice, Journal of Geophysical Research: Oceans, 100, 18 611–18 626, doi:10.1029/95JC02091, http://dx.doi.org/10.1029/95JC02091, 1995.

Geuzaine, C. and Remacle, J.-F.: Gmsh: A 3-D finite element mesh generator with built-in pre- and post-processing facilities, International Journal for Numerical Methods in Engineering, 79, 1309–1331, doi:10.1002/nme.2579, 2009.

Gimbert, F., Jourdain, N. C., Marsan, D., Weiss, J., and Barnier, B.: Recent mechanical weakening of the Arctic sea ice cover as revealed from larger inertial oscillations, Journal of Geophysical Research: Oceans, 117, n/a–n/a, doi:10.1029/2011JC007633, http://dx.doi.org/10.1029/2011JC007633, c00J12, 2012a.

Gimbert, F., Marsan, D., Weiss, J., Jourdain, N. C., and Barnier, B.: Sea ice inertial oscillations in the Arctic Basin, The Cryosphere, 6, 1187–1201, doi:10.5194/tc-6-1187-2012, http://www.the-cryosphere.net/6/1187/2012/, 2012b.

Girard, L., Bouillon, S., Weiss, J., Amitrano, D., Fichefet, T., and Legat, V.: A new modeling framework for sea ice models based on elasto-brittle rheology, Annals of Glaciology, 52, 2010.

Gray, J. M. N. T. and Morland, L. W.: A Two-Dimensional Model for the Dynamics of Sea Ice, Philosophical Transactions of the Royal Society of London A: Mathematical, Physical and Engineering Sciences, 347, 219–290, doi:10.1098/rsta.1994.0045, 1994.

Gudmandsen, P.: Lincoln sea and Nares Strait, in: Proceedings of the 2004 Envisat ERS Symposium (ESA SP-572), edited by Lacoste, H. and Ouwehand, L., Published on CD-R, 2004.

Haas, C.: Dynamics Versus Thermodynamics: The Sea Ice Thickness Distribution, in: Sea ice, edited by Thomas, D. N. and Dieckmann, G. S., p. 638, Wiley-Blackwell, 2009.

Haas, C., Hendricks, S., and Doble, M.: Comparison of the sea-ice thickness distribution in the Lincoln Sea and adjacent Arctic Ocean in 2004 and 2005, Annals of Glaciology, 44, 247–252, doi:doi:10.3189/172756406781811781, 2006.

Herrmann, H. J. and Roux, S., eds.: Statistical Models for the fracture of disordered meria, North-Holland, Amsterdam, 1990.

Hibler, W., Hutchings, J., and Ip, C.: Sea-ice arching and multiple flow states of Arctic pack ice, Annals of Glaciology, 44, 339–344, doi:doi:10.3189/172756406781811448, 2006.

Hibler, W. D. I.: A dynamic thermodynamic sea ice model, Journal of Physical Oceanography, 9, 815–846, 1979.

Hibler, W. D. I.: Modeling a Variable Thickness Sea Ice Cover, Monthly Weather Review, 108, 1943–1973, doi:10.1175/1520-0493(1980)108<1943:MAVTSI>2.0.CO;2, http://dx.doi.org/10.1175/1520-0493(1980)108<1943:MAVTSI>2.0.CO;2, 1980.

Hopkins, M. A.: On the ridging of intact lead ice, Journal of Geophysical Research: Oceans, 99, 16 351–16 360, doi:10.1029/94JC00996, http://dx.doi.org/10.1029/94JC00996, 1994.

Hopkins, M. A.: Four stages of pressure ridging, Journal of Geophysical Research: Oceans, 103, 21 883–21 891, doi:10.1029/98JC01257, http://dx.doi.org/10.1029/98JC01257, 1998.

Hunke, E.: An elastic-viscous-plastic model for sea ice dynamics, Journal of Physical Oceanography, 27, 1849–1867, 1997.

Hunke, E. C., Lipscomb, W. H., and Turner, A. K.: Sea-ice models for climate study: retrospective and new directions, Journal of Glaciology, 56, 1162–1172, doi:doi:10.3189/002214311796406095, http://www.ingentaconnect.com/content/igsoc/jog/2010/00000056/00000200/art00021, 2010.

Ingram, R. G., Bacle, J., Barber, D. G., Gratton, Y., and Melling, H.: An overview of physical processes in the North Water, Deep-Sea Research, 2, 4893–4906, 2002.

Ip, C. F.: Numerical investigation of different rheologies on sea-ice dynamics, Ph.D. thesis, Dartmouth College, New Hampshire, USA, 1993.

Johnson, M., Proshutinsky, A., Aksenov, Y., Nguyen, A. T., Lindsay, R., Haas, C., Zhang, J., Diansky, N., Kwok, R., Maslowski, W., Häkkinen, S., Ashik, I., and de Cuevas, B.: Evaluation of Arctic sea ice thickness simulated by Arctic Ocean Model Intercomparison Project models, Journal of Geophysical Research: Oceans, 117, n/a–n/a, doi:10.1029/2011JC007257, http://dx.doi.org/10.1029/2011JC007257, c00D13, 2012.

Kovacs, A. and Sodhi, D. S.: Shore ice pile-up and ride-up: Field observations, models, theoretical analyses, Cold Regions Science and Technology, 2, 210 – 288, doi:http://dx.doi.org/10.1016/0165-232X(80)90076-2, http://www.sciencedirect.com/science/article/pii/0165232X80900762, 1980.

Kwok, R.: Deformation of the Arctic Ocean sea ice cover: November 1996 through April 1997, in: IUTAM Symposium on Scaling Laws in Ice Mechanics and Ice Dynamics, edited by Dempsey, J. and Shen, H. H., Solid Mechanics and Its Applications, pp. 315–323, Springer Netherlands, doi:10.1007/978-94-015-9735-7, 2001.

Kwok, R.: Variability of Nares Strait ice flux, Geophysical Research Letters, 32, n/a–n/a, doi:10.1029/2005GL024768, l24502, 2005.

Kwok, R.: Exchange of sea ice between the Arctic Ocean and the Canadian Arctic Archipelago, Geophysical Research Letters, 33, n/a–n/a, doi:10.1029/2006GL027094, l16501, 2006.

Kwok, R., Pedersen, L., Gudmandsen, P., and Pang, S.: Large sea ice outflow into the Nares Strait in 2007, Geophysical Research Letters, 37, L03 502, doi:10.1029/2009GL041872, 2010.

Lietaer, O., Fichefet, T., and Legat, V.: The effects of resolving the Canadian Arctic Archipelago in a finite element sea ice model, Ocean Modelling, 24, 140–152, doi:10.1016/j.ocemod.2008.06.002, 2008.

Lindsay, R. W.: Sea-ice deformation rates from satellite measurements and in a model, Atmosphere-Ocean, 41, 35–47, doi:10.3137/ao.410103, 2003.

Marsan, D., Stern, H., Lindsay, R., and Weiss, J.: Scale dependance and localization of the deformation of Arctic sea ice, Physical Review Letters, 93, doi:10.1103/PhysRevLett.93.178501, 2004.

Marsan, D., Weiss, J., Metaxian, J.-P., Grangeon, J., Roux, P.-F., and Haapala, J.: Low frequency bursts of horizontally-polarized waves in the Arctic sea-ice cover, Journal of Glaciology, 57, 231–237, 2011.

McPhee, M. G.: Sea Ice Processes and Model, chap. An Analysis of Pack Ice Drift in Summer, pp. 62–75, University of Washington Press, Seattle, 1980.

Moritz, R. E. and Stern, H. L.: Relationship between geostrophic winds, ice strain rates and the piecewise rigid motions of pack ice, in: IUTAM Symposium on Scaling Laws in Ice Mechanics and Ice Dynamics, edited by Dempsey, J. and Shen, H. H., Solid Mechanics and Its Applications, pp. 315–323, Springer Netherlands, doi:10.1007/978-94-015-9735-7, 2001.

Morrissey, J. P., Ooi, J. Y., and Chen, J. F.: A DEM study of silo discharge of a cohesive solid, in: Proceedings of the III International Conference on Particle-based Methods, Fundamentals and Applications, edited by Bischoff, M., Ramm, E., Oñate, E., Owen, R., and Wriggers, P., pp. 315–323, International Center for Numerical Methods in Engineering (CIMNE), 2013.

Munch-Andersen, J.: The boundary layer in rough silos, in: Second International Conference on Bulk Materials Storage, Handling and Transportation:Preprints of Papers, pp. 160–163, Barton, ACT: Institution of Engineers, 1986.

Munch-Andersen, J., Askegaard, V., and Brink, A.: Silo model tests with sand, in: Bulletin No. 91, pp. 1–39, Danish Building Research Institute, 1992.

Mundy, C. and Barber, D.: On the relationship between spatial patterns of seaice type and the mechanisms which create and maintain the North Water (NOW) polynya, Atmosphere-Ocean, 39, 327–341, doi:10.1080/07055900.2001.9649684, 2001.

Münchow, A.: Volume and Freshwater Flux Observations from Nares Strait to the West of Greenland at Daily Time Scales from 2003 to 2009, Journal of Physical Oceanography, 46, 141–157, doi:10.1175/JPO-D-15-0093.1, http://dx.doi.org/10.1175/JPO-D-15-0093.1, 2016.

Parmerter, R. R. and Coon, M. D.: Model of pressure ridge formation in sea ice, Journal of Geophysical Research, 77, 6565–6575, doi:10.1029/JC077i033p06565, http://dx.doi.org/10.1029/JC077i033p06565, 1972.

Petrich, C., Langhorne, P., and Haskell, T.: Formation and structure of refrozen cracks in land-fast first-year sea ice, Journal of Geophysical Research, 112, C04,006, doi:10.1029/2006JC003466, 2007.

Pritchard, R. S.: Mechanical behaviour of pack ice, pp. 371–405, Elsevier, 1981.

Rampal, P., Weiss, J., Marsan, D., Lindsay, R., and Stern, H.: Scaling properties of sea ice deformation from buoy dispersion analysis, Journal of Geophysical Research: Oceans, 113, n/a–n/a, doi:10.1029/2007JC004143, http://dx.doi.org/10.1029/2007JC004143, c03002, 2008.

Rampal, P., Weiss, J., Marsan, D., and Bourgoin, M.: Arctic sea ice velocity field: General circulation and turbulent-like fluctuations, Journal of Geophysical Research: Oceans, 114, n/a–n/a, doi:10.1029/2008JC005227, c10014, 2009.

Rampal, P., Bouillon, S., Olason, E., and Morlighem, M.: neXtSIM: a new Lagrangian sea ice model, The Cryosphere Discussions, 9, 5885–5941, doi:10.5194/tcd-9-5885-2015, 2015.

Rasmussen, T. A. S., Kliem, N., and Kaas, E.: Modelling the sea ice in the Nares Strait, Ocean Modelling, 35, 161–172, 2010.

Richmond, O. and Gardner, G.: Limiting spans for arching of bulk materials in vertical channels, Chemical Engineering Science, 17, 1071 – 1078, doi:http://dx.doi.org/10.1016/0009-2509(62)80085-2, 1962.

Richter-Menge, J. A., McNutt, S. L., Overland, J. E., and Kwok, R.: Relating arctic pack ice stress and deformation under winter conditions, Journal of Geophysical Research, 107, doi:10.1029/2000JC000477, 2002.

Rothrock, D. A.: The energetics of the plastic deformation of pack ice by ridging, Journal of Geophysical Research, 80, 4514–4519, 1975.

Ryan, P. A. and Münchow, A.: Sea ice draft observations in Nares Strait from 2003 to 2012, Journal of Geophysical Research: Oceans, pp. n/a–n/a, doi:10.1002/2016JC011966, http://dx.doi.org/10.1002/2016JC011966, 2017.

Samelson, R. M. and Barbour, P. L.: Low-Level Jets, Orographic Effects, and Extreme Events in Nares Strait: A Model-Based Mesoscale Climatology, Monthly Weather Review, 136, 4746–4759, doi:10.1175/2007MWR2326.1, http://dx.doi.org/10.1175/2007MWR2326.1, 2008.

Samelson, R. M., Agnew, T., Melling, H., and Munchow, A.: Evidence for atmospheric control of sea-ice motion through Nares Strait, Geophysical Research Letters, 33, doi:10.1029/2005GL025016, 2006.

Saramito, P.: Efficient C++ finite element computing with Rheolef, CNRS-CCSD ed., http://cel.archives-ouvertes.fr/cel-00573970, 2013a.

Saramito, P.: Efficient C++ finite element computing with Rheolef: vol. 2. discontinuous Galerkin methods, CNRS-CCSD ed., 2013, CNRS-CCSD ed., http://cel.archives-ouvertes.fr/cel-00863021, 2013b.

Schulson, E. M.: Compressive shear faults within arctic sea ice: Fractures on scales large and small, Journal of Geophysical Research, 109, doi:10.1029/2003JC002108, 2004.

Schulson, E. M.: Failure envelope of first-year Arctic sea ice: The role of friction in compressive fracture, Journal of Geophysical Research, 111, doi:10.1029/2005JC003235, 2006a.

Smith, S. D., Muench, R. D., and Pease, C. H.: Polynyas and leads: An overview of physical processes and environment, Journal of Geophysical Research: Oceans, 95, 9461–9479, doi:10.1029/JC095iC06p09461, http://dx.doi.org/10.1029/JC095iC06p09461, 1990.

Sodhi, D. S.: Ice arching and the drift of pack ice through restricted channels, Crrel report 77-18, COLD REGIONS RESEARCH AND ENGINEERING LABORATORY, HANOVER, NEW HAMPSHIRE, 1977.

Stern, H. L., Rothrock, D. A., and Kwok, R.: Open water production in arctic sea ice: Satellite measurements and model parameterizations, Journal of Geophysical Research, 100, 20 601–20 612, 1995.

Thomson, N. R., Sykes, J. F., and McKenna, R. F.: Short-term ice motion modeling with application to the Beaufort Sea, Journal of Geophysical Research: Oceans, 93, 6819–6836, doi:10.1029/JC093iC06p06819, 1988.

Thorndike, A. S., Rothrock, D. A., Maykut, G. A., and Colony, R.: The thickness distribution of sea ice, Journal of Geophysical Research, 80, 4501–4513, doi:10.1029/JC080i033p04501, http://dx.doi.org/10.1029/JC080i033p04501, 1975.

Timco, G. and Weeks, W.: A review of the engineering properties of sea ice, Cold Regions Science and Technology, 60, 107 – 129, doi:http://dx.doi.org/10.1016/j.coldregions.2009.10.003, 2010.

Wadhams, P.: Sea-Ice Topography of the Arctic Ocean in the Region 70 degrees W to 25 degrees E, Philosophical Transactions of the Royal Society of London A: Mathematical, Physical and Engineering Sciences, 302, 45–85, doi:10.1098/rsta.1981.0157, 1981.

Wadhams, P.: Sea Ice Thickness Changes and their Relation to Climate, pp. 337–361, American Geophysical Union, doi:10.1029/GM085p0337, http://dx.doi.org/10.1029/GM085p0337, 1994.

Walker, D.: An approximate theory for pressures and arching in hoppers, Chemical Engineering Science, 21, 975 – 997, doi:http://dx.doi.org/10.1016/0009-2509(66)85095-9, 1966.

Walsh, J. E., Hibler, W. D., and Ross, B.: Numerical simulation of northern hemisphere sea ice variability, 1951–1980, Journal of Geophysical Research: Oceans, 90, 4847–4865, doi:10.1029/JC090iC03p04847, http://dx.doi.org/10.1029/JC090iC03p04847, 1985.

Wang, Y. and Ooi, J. Y.: A Study of Granular Flow in a Conical Hopper Discharge Using Discrete and Continuum Approach, Procedia Engineering, 102, 765 – 772, doi:http://dx.doi.org/10.1016/j.proeng.2015.01.183, http://www.sciencedirect.com/science/article/pii/S1877705815001848, 2015.

Weiss, J.: Intermittency of principal stress directions within Arctic sea ice, Physical Review E, 77, 056 106, doi:10.1103/PhysRevE.77.056106, 2008.

Weiss, J. and Dansereau, V.: Linking scales in sea ice mechanics, Philosophical Transactions A, 375, doi:10.1098/rsta.2015.0352, 20150352, 2017.

Weiss, J. and Schulson, E. M.: Coulombic faulting from the grain scale to the geophysical scale: lessons from ice, Journal of Physics D: Applied Physics, 42, 214 017, 2009.

Weiss, J., Schulson, E. M., and Stern, H. L.: Sea ice rheology from in-situ, satellite and laboratory observations: Fracture and friction, Earth and Planetary Science Letters, 255, 1–8, 2007.

Yackel, J. J., Barber, D. G., and Papakyriakou, T. N.: On the estimation of spring melt in the North Water polynya using RADARSAT-1, Atmosphere-Ocean, 39, 195–208, doi:10.1080/07055900.2001.9649676, 2001.

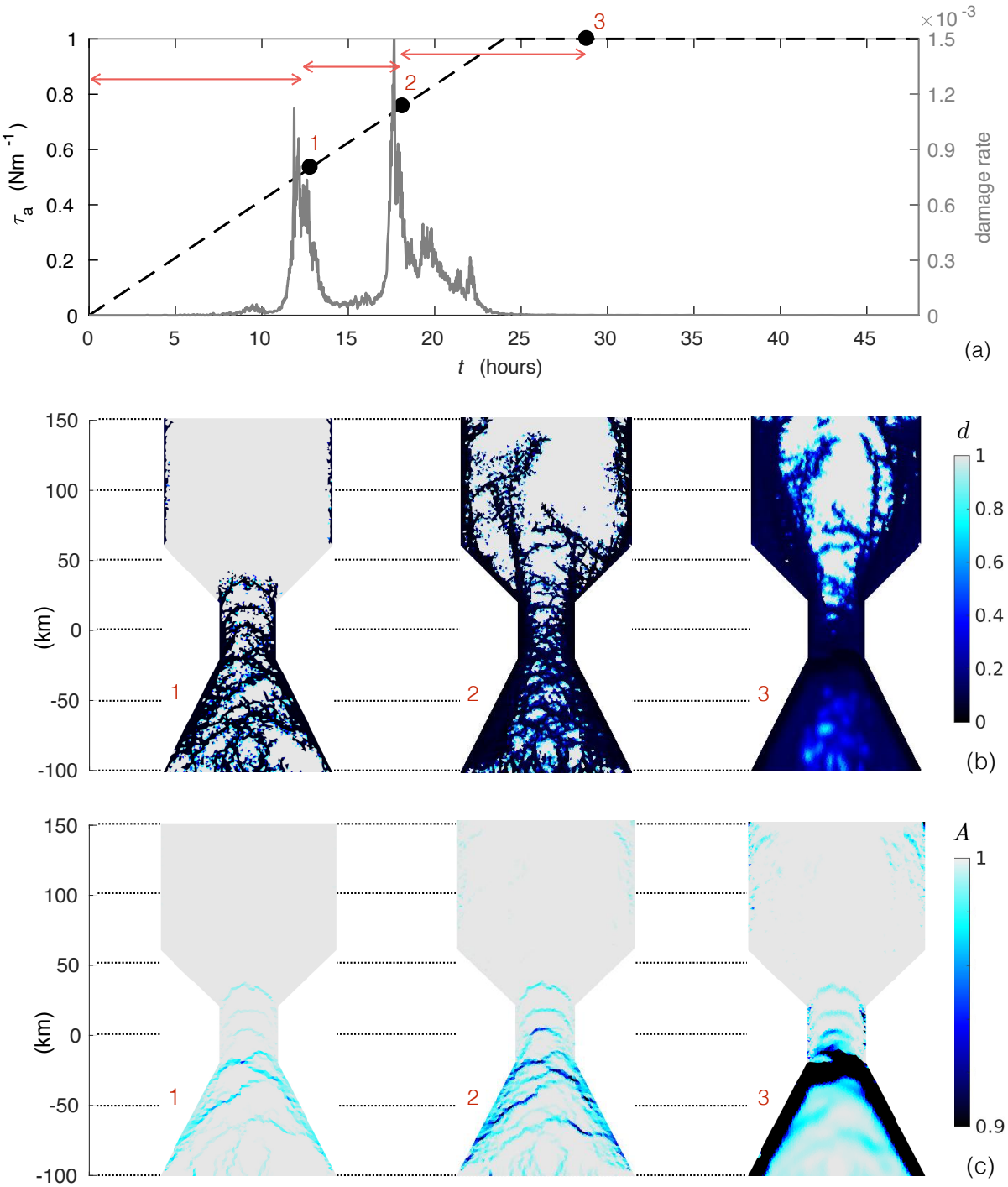

Figure 4. (a) Time series of the wind forcing (dashed curve) and of the damage rate (solid grey curve) in an idealized channel simulation using ~~$C_{min} = 20000$ Pa~~$C_{min} = 20$ kPa. ~~(b)~~ Instantaneous spatial distribution of (b) the level of damage and (c) ice concentration at the times indicated by the numbers 1, 2 and 3 on the time series of panel (a).

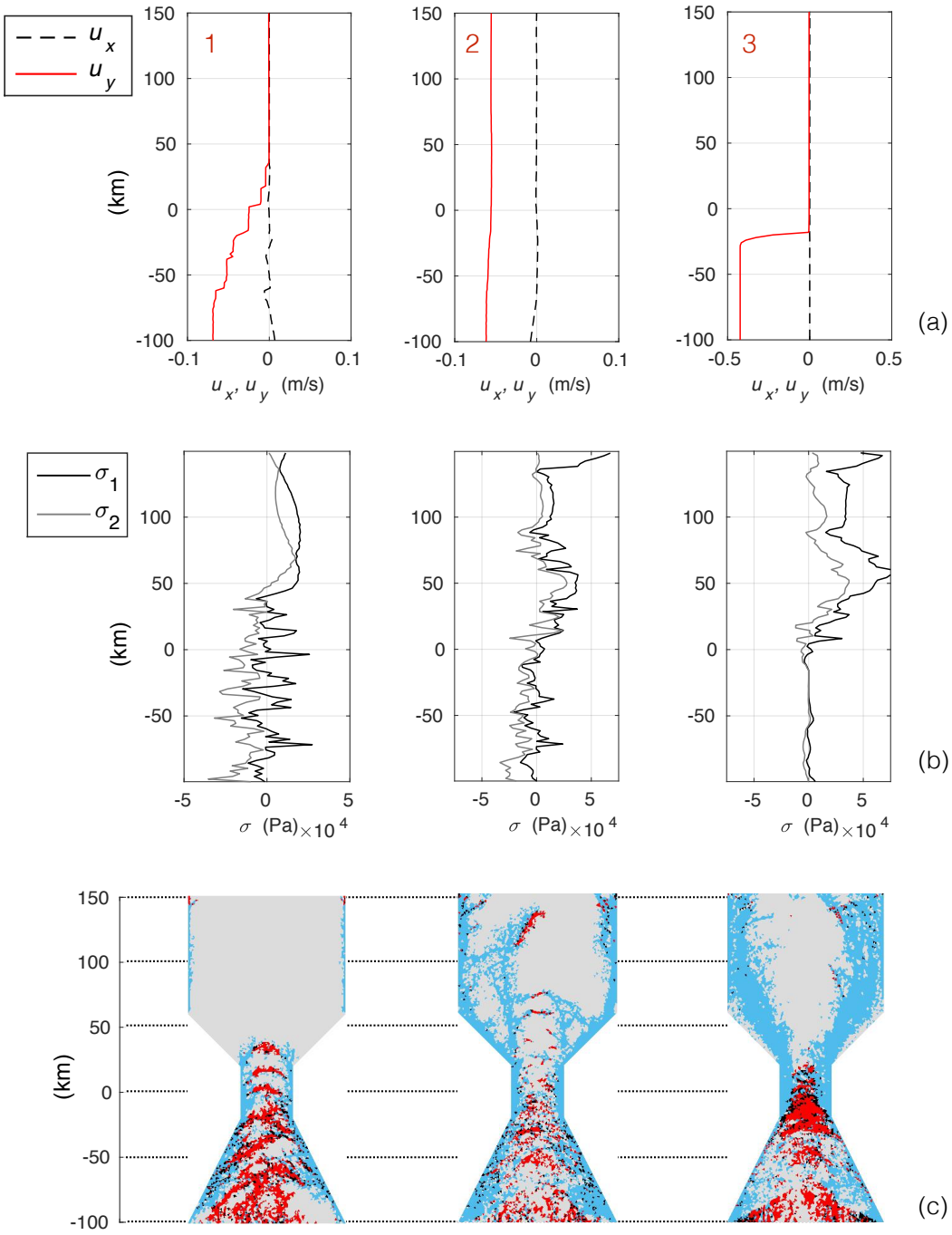

Figure 5. Profiles of (a) the instantaneous $x-$component (dashed curves) and $y-$component (red curves) of the ice velocity and (b) the instantaneous principal stress components σ_1 (black curves) and σ_2 (grey curves) along the central meridional axis of the channel at the three stages indicated on Fig. 4a ($C_{min} = 20$ kPa). (c) Spatial distribution of all the elements that have exceeded the Mohr-Coulomb (blue) the tensile (red) or both (black) damage criteria during the 3 periods of time, between the beginning of the simulation and ~~stages~~ times numbered 1, 2 and 3, ~~as~~ indicated by the red arrows on ~~(~~5a~~)~~.

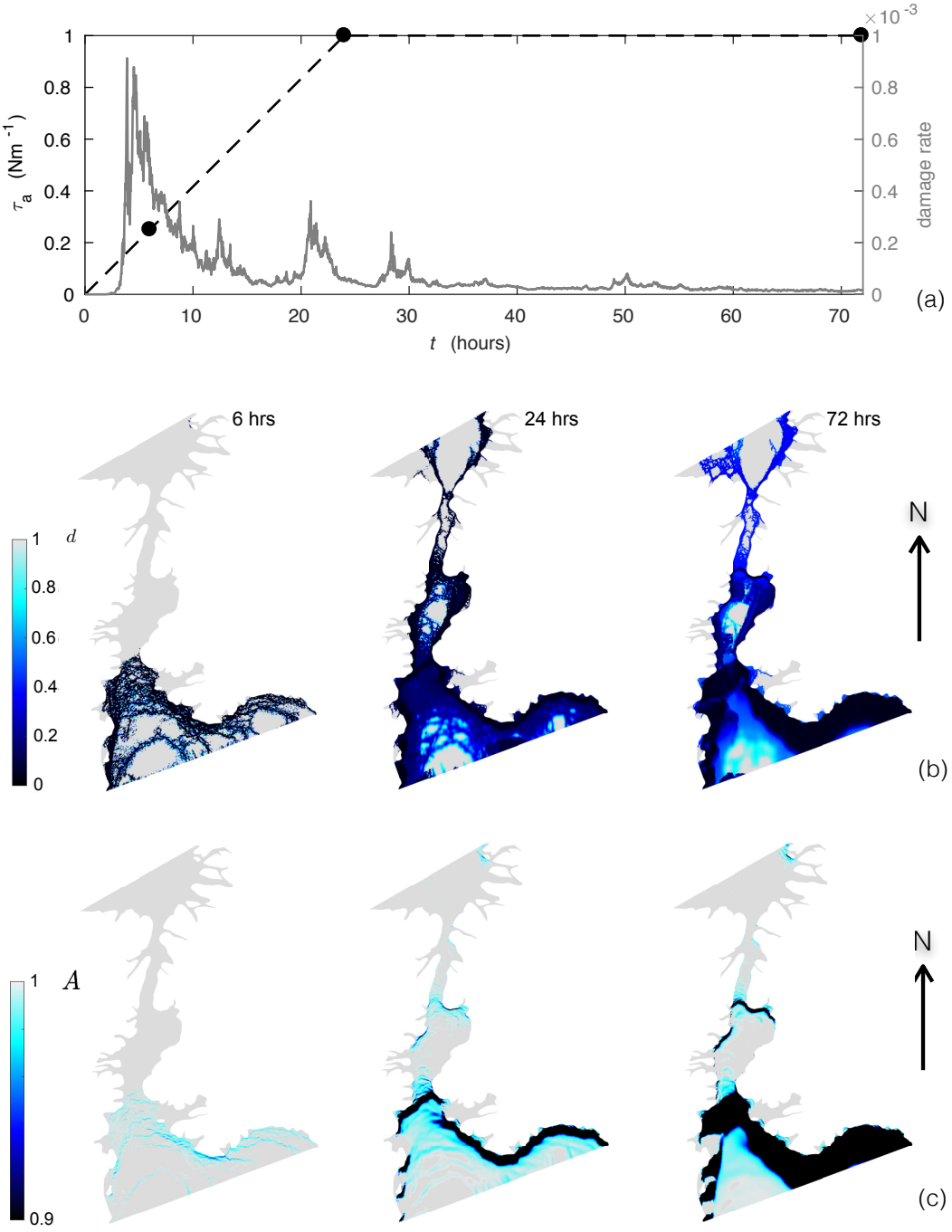

Figure 6. (a) Time series of the wind forcing (dashed curve) and of the damage rate (solid grey curve) over the realistic Nares Strait in a simulation using $C_{min} = 20$ kPa. Instantaneous fields of the simulated (~~a~~b) level of damage and (~~b~~c) ice concentration ~~fields over the realistic Nares Strait~~ at ~~$t = 6, 20$~~ $t = 6, 24$ and 72 hours~~($C_{min} = 20000$ Pa)~~.

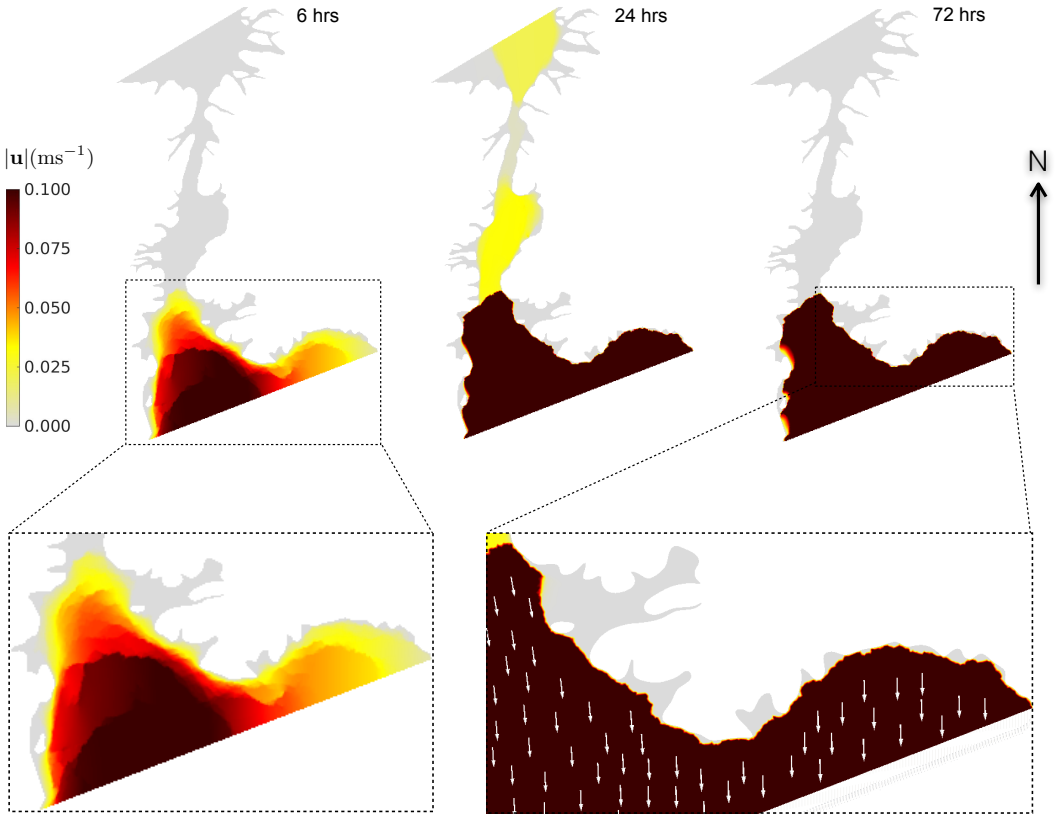

Figure 7. (a) . Instantaneous fields of the simulated ice drift speed over the realistic Nares Strait at ~~$t = 6, 20$~~ $t = 6, 24$ and 72 hours (~~$C_{min} = 20000$ Pa~~$C_{min} = 20$ kPa). The lower panels are zoom-ins of the 6 and 72 hours drift speed fields, showing (left panel) the division of the ice cover downstream of Kane Basin into ice floes with piecewise constant velocities and (right panel) the sharp gradient in ice velocity between free drifting ice and regions of stagnant, landfast ice attached to the coast in narrow fjords and upwind of islands (the white arrows indicate the ~~main ice~~ drift direction at evenly-spaced element nodes).

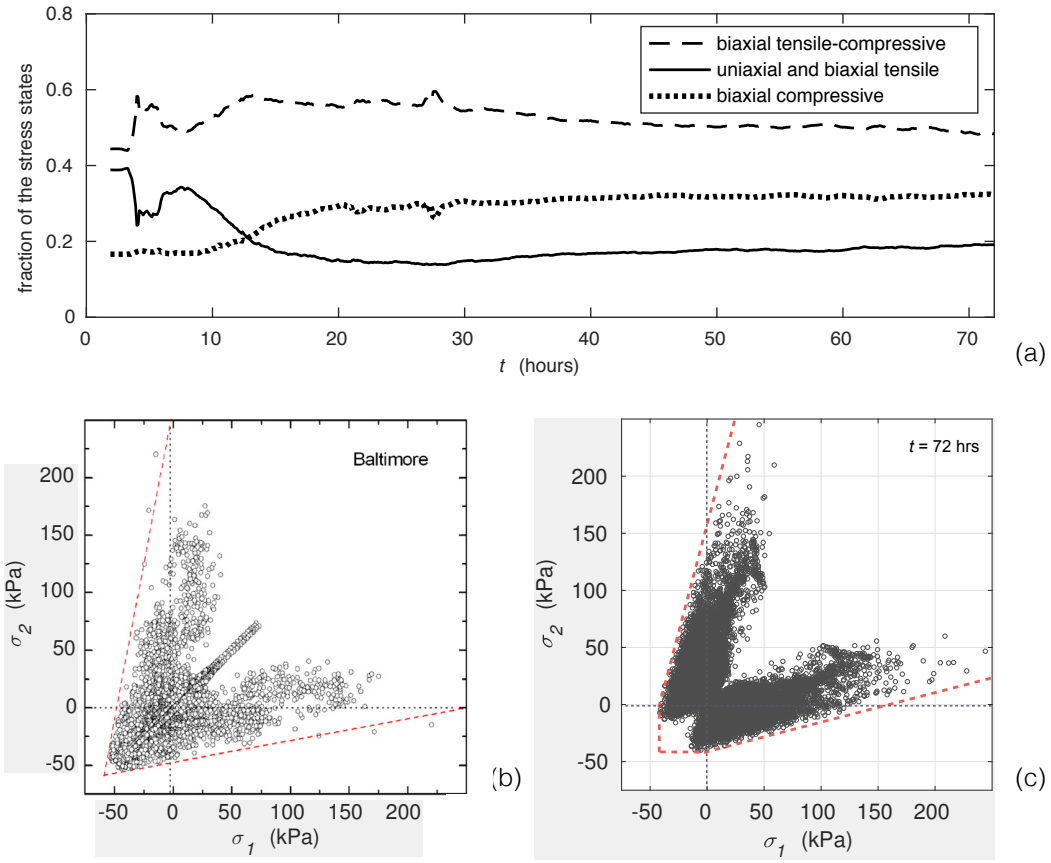

Figure 8. (a) Time series of the proportion of tensile (uniaxial and biaxial, solid curve), biaxial tensile-compressive (dashed curve) and biaxial compressive (dotted curve) stresses over the realistic Nares Strait in the simulation using $C_{min} = 20$ kPa. (~~a~~b) Stress states in principal stress space recorded by one stress-meter (one measurement per hour) during the SHEBA experiment in the Beaufort sea (from mid-October, 1997 to end of June, 1998). The dashed red lines represent the Coulombic branches of a failure envelope for $\sigma_c = 250$ kPa and $\mu = 0.9$. *From Weiss and Schulson (2009).* (~~b~~c) Instantaneous stress states simulated with the Maxwell-EB model using $C_{min} = 20$ kPa after the formation of the stable ice bridge downstream of Kane Basin ($t = 72$ hours). The dashed red lines represent the damage criterion corresponding to the highest value of cohesion over the domain ($\sigma_c \approx 154$ kPa, $\sigma_t = 42$ kPa, $\mu = 0.7$). In both cases, (σ_1, σ_2) and (σ_2, σ_1) are plotted, resulting in symmetry about the axis $\sigma_1 = \sigma_2$.

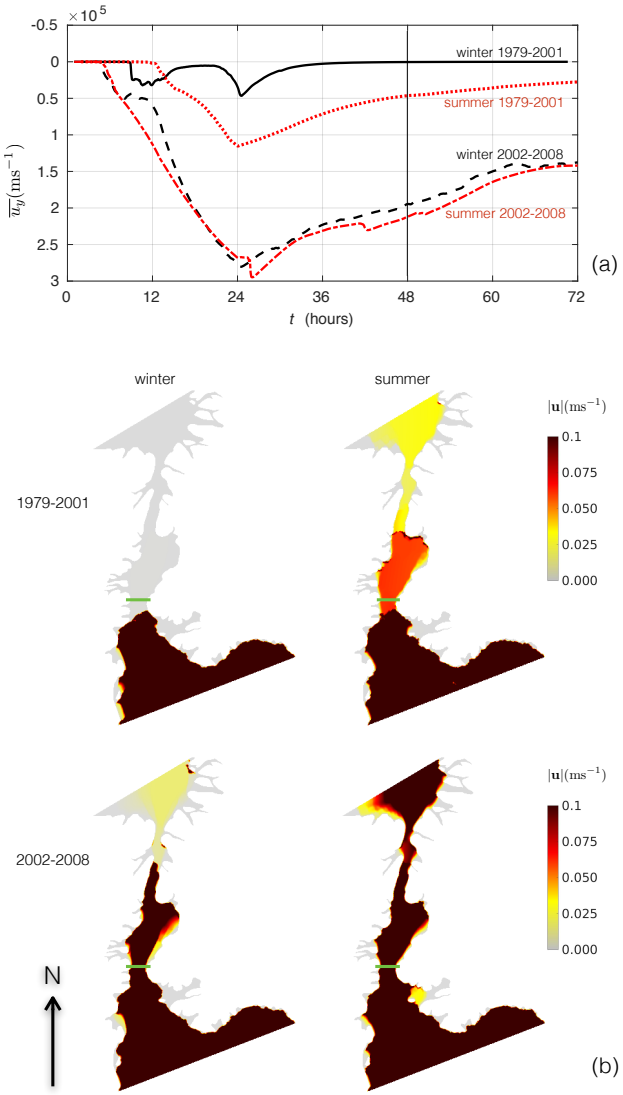

Figure 9. (a) Time series of the meridional component of the simulated ice drift velocity, u_y, averaged zonally across the constriction point between Kane Basin and Smith Sound, in the 1979-2001 (stronger ice cover), 2002-2008 (weaker ice cover) and winter ($t_h \approx 5.7$ days) and summer ($t_h = 365$ days) scenarios. (b) Instantaneous field of the ice drift speed, $|\mathbf{u}|$, over Nares Strait after 48 hours of simulation in the four scenarios. The green lines show the location of the zonal cross-section used for the calculation of $\overline{u_y}$ in (a). Everywhere over the domain and at all times, the drift velocity is dominated by its meridional component and is ~~mostly~~ southward.

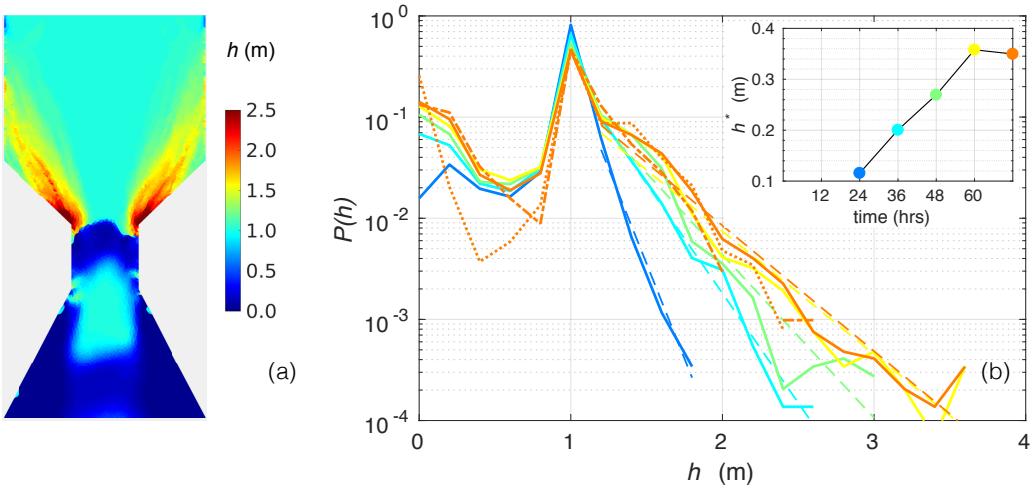

Figure 10. (a) Instantaneous field of the mean ice thickness, h, after 3 days of simulation in an idealized channel simulation. The value of C_{min} is ~~of~~ 10 kPa and self-obstruction to flow (i.e., a stable ice bridge) does not occur. (b) Probability density function of the instantaneous simulated ice thickness $P(h)$ at different times (coloured lines). A bin width of ~~0.1~~ 0.2 m is used. Note the semi-logarithmic axis. The ~~tail of the distribution ($h \geq 1.1$ meters) is fitted using a linear regression to estimate the slope, $-\frac{1}{h^*}$. The temporal evolution of h^* is shown in the insert. The (~~orange) dotted and dotted-dashed lines represents $P(h)$ calculated at ~~$t = 5$~~ $t = 3$ days in simulations using the same idealized domain and boundary conditions ~~and reduced~~ but a decreased spatial resolution of $\Delta x = 4$ km and 8 km respectively. The ~~insert~~ inset shows the values of h^* calculated at different times using a linear regression of $\ln P(h)$ for $h > 1.0$ m.

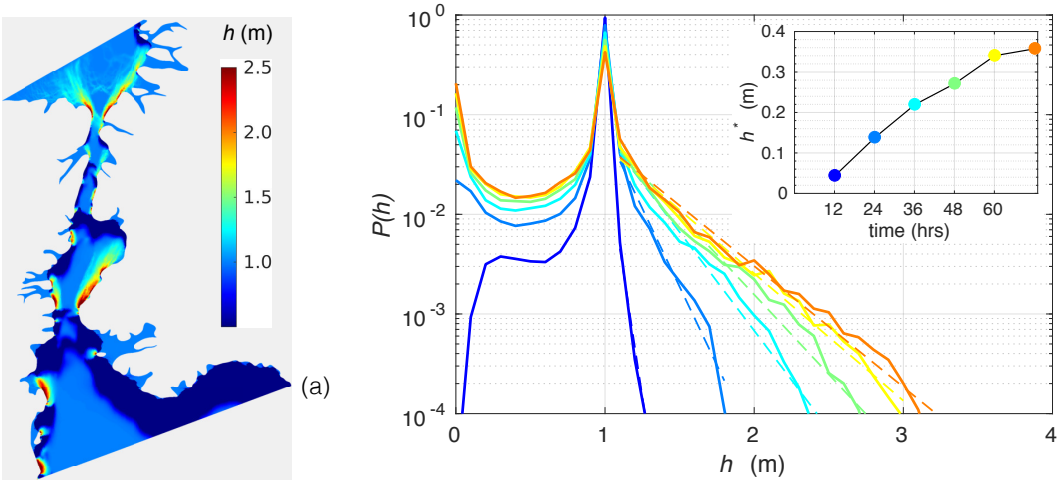

Figure 11. (a) Instantaneous field of the mean ice thickness, h, after ~~2.5~~ 3 days in the realistic simulation of Nares Strait. The value of C_{min} is ~~of~~ 10 kPa and ~~self-obstruction to flow~~ a stable ice bridge does not occur. (b) Probability density function of the instantaneous simulated ice thickness, $P(h)$ at different times (coloured lines). A bin width of ~~0.1~~ 0.2 meters is used. Note the semi-logarithmic axis. The ~~tail of~~ inset shows the ~~distribution ($h \geq 1.1$ meters) is fitted~~ values of h^* calculated at different times using a linear regression ~~to estimate the slope, $-\frac{1}{h^*}$~~ of $\ln P(h)$ for $h > 1.0$ m. The percentage of the variance (R) explained by this fit is $> 95\%$. ~~The insert shows the values of h^* calculated at different times using a linear regression of $\ln P(h)$ for $h \geq 1.1$ m.~~